SURFACE ACTIVATION OF RICE HUSK-DERIVED HYDROCHAR AS AN ADSORBENT FOR ATRAZINE AND AMMONIUM

Miss Kim Anh Phan

จุฬาลงกรณ์มหาวิทยาลัย
CHULALONGKORN UNIVERSITY

A Thesis Submitted in Partial Fulfillment of the Requirements
for the Degree of Master of Science in Hazardous Substance and
Environmental Management
Inter-Department of Environmental Management
GRADUATE SCHOOL
Chulalongkorn University
Academic Year 2020

การกระตุ้นคุณสมบัติพื้นผิวของไฮโดรชาร์จากแกลบข้าว เพื่อเป็นสารดูดซับอาทราซีน และแอมโมเนียม

น.ส.คิม อานห์ พาน

Thesis Title   SURFACE ACTIVATION OF RICE HUSK-DERIVED HYDROCHAR AS AN ADSORBENT FOR ATRAZINE AND AMMONIUM
By   Miss Kim Anh Phan
Field of Study   Hazardous Substance and Environmental Management
Thesis Advisor   Nattapong Tuntiwiwattanapun, Ph.D.
Thesis Co Advisor   Doungkamon Phihusut, Ph.D.

Accepted by the GRADUATE SCHOOL, Chulalongkorn University in Partial Fulfillment of the Requirement for the Master of Science

.... Dean of the GRADUATE SCHOOL
(Associate Professor THUMNOON NHUJAK, Ph.D.)

THESIS COMMITTEE
.... Chairman
(Associate Professor MANASKORN RACHAKARAKIJ, Ph.D.)
.... Thesis Advisor
(Nattapong Tuntiwiwattanapun, Ph.D.)
.... Thesis Co-Advisor
(Doungkamon Phihusut, Ph.D.)
.... Examiner
(Assistant Professor Vorapot Kanokkantapong, Ph.D.)
.... Examiner
(JENYUK LOHWACHARIN, Ph.D.)
.... External Examiner
(Assistant Professor Panida Prarat, Ph.D.)

คิม อานห์ พาน : การกระตุ้นคุณสมบัติพื้นผิวของไฮโดรชาร์จากแกลบข้าว เพื่อเป็นสารดูดซับอาทราซีน และ แอมโมเนียม. (SURFACE ACTIVATION OF RICE HUSK-DERIVED HYDROCHAR AS AN ADSORBENT FOR ATRAZINE AND AMMONIUM) อ.ที่ปรึกษาหลัก : ดร.ณัฐพงศ์ ตันติวิวัฒนพันธ์, อ.ที่ปรึกษาร่วม : ดร.ดวงกมล พิทูสูตร

การหาแนวทางการจัดการอย่างยั่งยืนของการปนเปื้อนอาทรานซีนและปุ๋ยไนโตรเจนในภาคการเกษตรกำลังเป็นที่ ได้รับความสนใจเพิ่มขึ้นจากปัญหาด้านสิ่งแวดล้อมของสารดังกล่าว เป้าหมายของงานวิจัยนี้คือการพัฒนาวัสดุไฮโดรชาร์จาก แกลบข้าว เพื่อดูดซับอาทรานซีนและแอมโมเนียม กระบวนการไฮโดรเทอร์มอลคาร์บอไนเซชั่น โดยการใช้ไมโครเวฟ (Microwave-assisted hydrothermal carbonization; MHTC) จะถูกใช้ปรับปรุงคุณสมบัติทางพื้นผิว ของแกลบข้าวด้วยความร้อนที่ใช้น้ำเป็นตัวเร่งปฏิกิริยาภายใต้อุณหภูมิและความดันสูง ผลของอุณหภูมิ (150 – 200 °C) ระยะเวลา (20 – 60 นาที) และสัดส่วนของเหลวต่อของแข็ง (5:1 – 15:1 มิลลิลิตร/กรัม) ในกระบวนการ MHTC ต่อปริมาณการดูดซับสูงสุดของอาทรานซีนและแอมโมเนียมของวัสดุไฮโดรชาร์ ขั้นต่อมาคือการกระตุ้นพื้นผิวของไฮโดรชาร์ จากแกลบข้าวเพื่อเพิ่มประสิทธิภาพการดูดซับของอาทรานซีนและแอมโมเนียมด้วยโพแทสเซียมไฮดรอกไซด์ (KOH) และ ไฮโดรเจนเปอร์ออกไซด์ (H$_2$O$_2$) ผลการทดลองแสดงให้เห็นว่าอุณหภูมิที่สูงขึ้น ระยะเวลาที่ยาวขึ้น และการใช้สัดส่วน ของเหลวต่อของแข็งที่ต่ำลง มีผลต่อการเพิ่มขึ้นของการดูดซับอาทรานซีนและแอมโมเนียมอย่างมีนัยสำคัญทางสถิติ คุณสมบัติ ทางพื้นผิวของไฮโดรชาร์ได้ถูกวิเคราะห์ด้วยเทคนิค BET FT-IR และ XPS แสดงให้เห็นถึงความเด่นของปริมาณหมู่ ออกซิเจนฟังก์ชั่นในไฮโดรชาร์ ซึ่งส่งผลต่อกลไกการดูดซับของสาร โดยสามารถถูกกระตุ้นเพิ่มขึ้นได้หลังจากการปรับสภาพด้วย KOH จากผลของจุลศาสตร์และไอโซเทอมของการดูดซับอาทราซีนด้วยไฮโดรชาร์จากแกลบข้าวพบว่ามีอัตราการดูดซับ สอดคล้องกับแบบจำลองชนิด Pseudo-second order และมีสมดุลการดูดซับแบบ Freundlich (R^2 > 0.99) มีปริมาณการดูดซึมอาทรานซีนสูงสุดที่ 4.06 มิลลิกรัม/กรัม พบในไฮโดรชาร์ที่มีการกระตุ้นด้วย KOH โดยพบว่าการดูด ซับด้วยพันธะไฮโดรเจนเป็นกลไกการดูดซับหลักของสารดูดซับดังกล่าว แต่สำหรับไฮโดตชาร์ที่มีการกระตุ้นด้วย H$_2$O$_2$ จะมี กลไกในการดูดซับหลักคือ อันตรกิริยาไพ-ไพ (π-π electron donor-acceptor interactions) สำหรับการดูด ซับสารละลายแอมโมเนียมด้วยไฮโดรชาร์พบว่ามีปริมาณการดูดซับที่ต่ำกว่าอาทราซีนมาก ถึงแม้จะถูกกระตุ้นด้วย KOH ซึ่ง ส่งผลต่อการเพิ่มขึ้นของค่าการแลกเปลี่ยนประจุบอก (Cation exchange capacity; CEC) ก็ตาม กล่าวโดยสรุป คือ มีความเป็นไปได้ในการใช้ไฮโดรชาร์จากแกลบข้าวเพื่อเป็นวัสดุดูดซับอาทราซีนในสิ่งแวดล้อม และในอนาคตจะต้องมี การศึกษาการกระตุ้นคุณสมบัติการดูดซับแอมโมเนียมของไฮโดรชาร์เพื่อพัฒนาเป็นวัสดุที่สามารถควบคุมการปลดปล่อยของปุ๋ย (Slow-release fertilizer).

สาขาวิชา	การจัดการสารอันตรายและสิ่งแวดล้อม	ลายมือชื่อนิสิต ....
ปีการศึกษา	2563	ลายมือชื่อ อ.ที่ปรึกษาหลัก ....
		ลายมือชื่อ อ.ที่ปรึกษาร่วม ....

6187599820 : MAJOR HAZARDOUS SUBSTANCE AND ENVIRONMENTAL MANAGEMENT
KEYWOR
D:

Kim Anh Phan : SURFACE ACTIVATION OF RICE HUSK-DERIVED HYDROCHAR AS AN ADSORBENT FOR ATRAZINE AND AMMONIUM. Advisor: Nattapong Tuntiwiwattanapun, Ph.D. Co-advisor: Doungkamon Phihusut, Ph.D.

Due to the agricultural intensity, studies of sustainable solutions for atrazine and nitrogen contamination have attracted more attention. This study is aimed to develop rice husk hydrochar as an adsorbent for atrazine and ammonium adsorption. Effects of microwave-assisted hydrothermal carbonization (MHTC) conditions including temperature (150 – 200°C), residence time (20 – 60 min), and liquid to solid ratio (5:1 – 15:1 mL/g) on the atrazine and ammonium adsorption capacity were investigated. Surface activation of rice husk hydrochar samples was synthesized using potassium hydroxide (KOH) and hydrogen peroxide (H_2O_2) with various concentrations. The results showed that higher MHTC temperature with higher residence time and lower liquid to solid ratio significantly increased the adsorption capacity of these contaminants on rice husk hydrochar. The characterization of pristine and activated hydrochars using BET, FT-IR, and XPS revealed that rice husk hydrochar contained abundant oxygen-containing functional groups, which increased even more after KOH treatment. The results of kinetic and isotherm studies suggested that atrazine adsorption was best fitted with pseudo-second-order and Freundlich models ($R^2 > 0.99$), with the maximum adsorption capacity of 4.06 mg/g for KOH-activated hydrochar. Hydrogen-bonding and π-π electron donor-acceptor interactions played dominant roles for atrazine adsorption of KOH-activated hydrochar and H_2O_2-activated hydrochar, respectively. Compared to atrazine, the ammonium adsorption onto rice husk hydrochar was very low even though the KOH treatment enhanced its CEC values. Therefore, rice husk hydrochar can be considered a promising candidate for atrazine adsorption in the environment, and future studies are recommended to apply this material as a nitrogen slow-release fertilizer.

Field of Study:	Hazardous Substance and Environmental Management	Student's Signature ....
Academic Year:	2020	Advisor's Signature .... Co-advisor's Signature ....

ACKNOWLEDGEMENTS

TABLE OF CONTENTS

LIST OF TABLES

LIST OF FIGURES

Page

จุฬาลงกรณ์มหาวิทยาลัย

CHULALONGKORN UNIVERSITY

LIST OF ABBREVIATIONS

BET	Brunauer Emmett Teller
CEC	Cation Exchange Capacity
π-π EDA	π-π Electron Donor Acceptor
FT-IR	Fourier Transform Infrared Spectroscopy
H_2O_2	Hydrogen Peroxide
HC	Hydrochar
HPLC-UV	High-Performance Liquid Chromatography-Ultraviolet
IARC	International Agency for Research on Cancer
IBI	International Biochar Initiative
KOH	Potassium Hydroxide
MCL	Maximum Contaminant Level
MHTC	Microwave-Assisted Hydrothermal Carbonization
MRL	Maximum Residue Limit
N	Nitrogen
NH_4	Ammonium
RSM	Response Surface Methodology
SSA	Specific Surface Area
US EPA	United States Environmental Protection Agency
WHO	World Health Organization
XPS	X-Ray Photoelectron Spectroscopy

CHAPTER I INTRODUCTION

1.1 Background

Due to recent population growth, agricultural activities have been dramatically intensified by applying chemical pesticides and fertilizers to ensure food security [1]. These activities have posed considerable challenges to environmental quality as well as to human health.

Atrazine, a commonly used herbicide, is applied to control the photosynthetic ability of broadleaf weeds and grasses [2]. Its popularity is because of its practical and no harmful effects on economically useful plants. Therefore, atrazine residue has been commonly detected in sediments, groundwater, and surface water [3]. Atrazine could be transported into the food chain and then causes serious health problems as well as affects other living organisms in the environment [2, 4]. Moreover, this herbicide is difficult to degrade under natural conditions. Atrazine residue has been found in agricultural areas where it was applied 20 years ago [5]. As a result of its persistence, mobility, and toxicity, atrazine removal from contaminated regions has drawn significant interest amongst researchers.

In the case of fertilizers, nitrogen fertilizer (N-fertilizer) is one of the essential nutrient sources for plant growth. Currently, the efficiency with which N-fertilizer application can enrich soil nutrient levels is very low. Significant amounts of N-fertilizer are lost to the environment through nitrate (NO_3^-) leaching due to runoff or irrigation, ammonia (NH_3) volatilization, and nitrous oxide (N_2O) gas emissions [6-8]. Such incidents lead to decreased soil quality and increased greenhouse gas emissions; further, they promote surface water eutrophication [9, 10]. Therefore, reducing the

loss of N-fertilizers from agroecosystems has become a critical aspect of sustainable agricultural development and crop productivity.

Adsorption was applied in this study to prevent atrazine transportation and reduce the loss of N-fertilizer from agroecosystems. Agricultural residues are promising adsorption materials due to their availability and low cost. With proper treatments, these treated-agricultural biomass residues could be effectively increased the contaminant adsorption capacity. Slow pyrolysis has been commonly applied to improve the adsorption abilities of agricultural residues. Nevertheless, the high moisture content in such biomass is a crucial problem in the slow pyrolysis process. Thus, drying agricultural residues are recommended as the pre-treatment. To overcome this problem, an alternative hydrothermal carbonization treatment, which uses wetted biomass under moderate temperature and pressure, was selected in this study. Hydrochar, a solid product of the hydrothermal carbonization of biomass, is considered a promising adsorbent for various applications. The material has attracted attention in recent years because of its low cost and low environmental impact [11]. Hydrochar possesses porous structures with abundant oxygen-containing functional groups on its surface [12, 13]. Therefore, the ability of hydrochar to adsorb organic and inorganic pollutants has been widely investigated [14-17]. In addition, hydrochar can potentially be developed as a sustained-release fertilizer, which could prevent over-application of fertilizers and instead will consistently release nutrients based on crop demand [18, 19].

However, the specific surface area and pore volume of hydrochar are relatively low compared to other adsorbents [20, 21]. Chemical activation has been successfully proven to improve hydrochar physicochemical properties, directly associated with the

enhancement of adsorption capacity [17, 22, 23]. Thus, potassium hydroxide (KOH) and hydrogen peroxide (H_2O_2) solutions were used to modify the physicochemical characteristics of rice husk hydrochar and enhance its adsorption of atrazine and ammonium.

The Box-Behnken method in response surface methodology (RSM) was employed to see the interaction effects between MHTC parameters and adsorption capacity responses. Many studies have suggested that the RSM technique can achieve better performance over the traditional manner by reducing the number of experimental runs, saving time and costs [24, 25].

1.2 Objectives

Developing rice husk hydrochar to adsorb atrazine and ammonium was the main objective of this study.

- To optimize the microwave-assisted hydrothermal carbonization conditions of hydrochar production for atrazine and ammonium adsorption

- To investigate the effect of hydrochar activation using KOH and H_2O_2 on atrazine and ammonium adsorption

- To characterize physicochemical properties of hydrochar and chemical-activated hydrochar

- To determine the desorption behavior of atrazine-adsorbed hydrochar

1.3 Hypotheses

- Specific surface areas and oxygen-containing surface functional groups of hydrochar will be dramatically influenced by the operating temperature

- KOH treatment is expected to increase the porosity and surface area of hydrochar, which will enhance the atrazine and ammonium adsorption capacities of hydrochar

- Enhancing the amount of oxygen functional groups on the hydrochar surface will be achieved using H_2O_2 solution.

- Improvement of physicochemical properties of rice husk hydrochar after activation treatment will enhance atrazine and ammonium adsorption.

- Atrazine will be partly desorbed from the adsorbed material owing to reversible chemical reactions between the contaminant and oxygen-containing functional groups of adsorbent surfaces.

1.4 Scope of study

Herein, the developed rice husk hydrochars were evaluated for their adsorption properties of atrazine and ammonium in the liquid solution. It should be noted that application in soil did not include in this study.

This study can be divided into three main parts, including hydrochar production, activation, and desorption. In the first part, hydrochar was produced at varied MHTC conditions and investigated its adsorption capacity of atrazine and ammonium. In the next part, hydrochar with the highest adsorption capacity of these compounds was activated using KOH and H₂O₂ solutions with different concentrations. These prepared hydrochars were determined adsorption isotherms and adsorption kinetics for atrazine and ammonium. The desorption behaviors from activated hydrochar were conducted later in the last part (**Figure 1**).
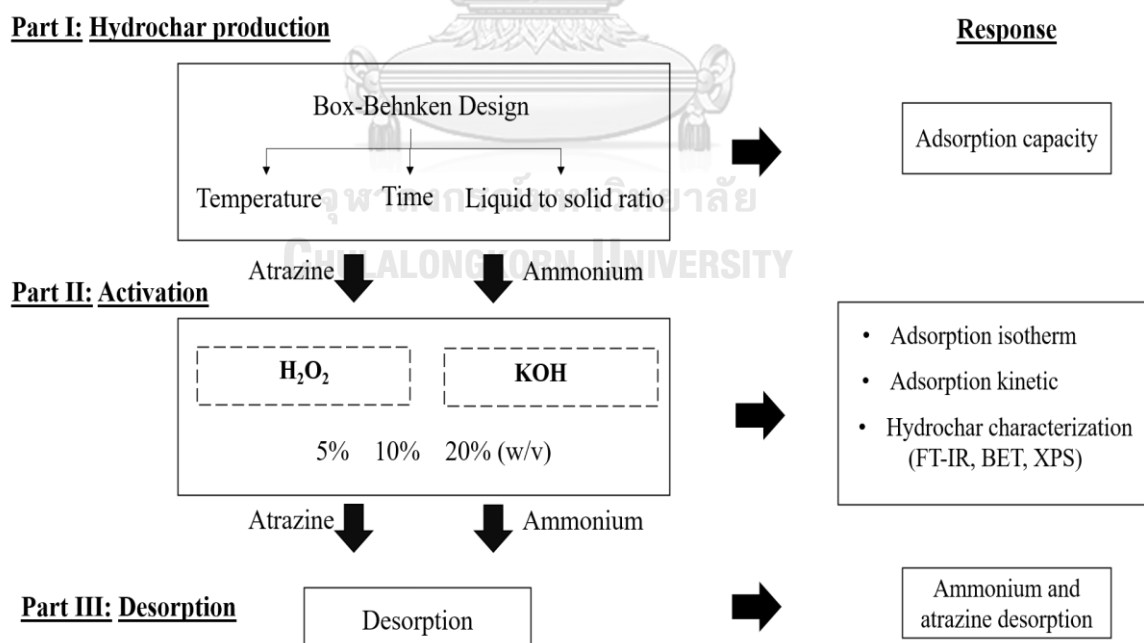
Figure 1. Scope of this current study
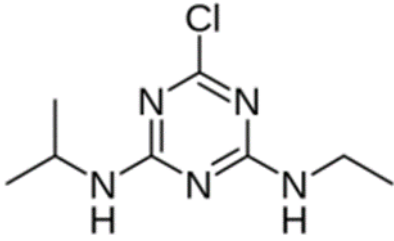
CHAPTER II LITERATURE REVIEW

2.1 Atrazine

2.1.1 Physicochemical properties of atrazine

Atrazine (2-chloro-4-ethylamino-6-isopropylamino-s-triazine) is widely used herbicide in agricultural activities and belongs to the triazine class. It enables to control pre- and post-emergence weeds in various crops such as corn, sugarcane, pineapple, roses, and sorghum [2, 3]. The physical and chemical properties of atrazine are shown in **Table 1** [26]. The maximum contaminant levels (MCLs) of atrazine in drinking water regulated by the US EPA and European Union are 3 ppb and 0.1 ppb, respectively [2, 27]. The maximum residue limit (MRL) for atrazine in agricultural commodities, including sweet corn, baby corn, maize, pineapple, and sugarcane, is 0.1 mg/kg [28]. According to the US EPA, the reference dose for chronic oral exposure to atrazine is 3.5×10^{-2} mg/kg-day [29].

Table 1. Physicochemical properties of atrazine

Properties	Atrazine
Molecular formula	$C_8H_{14}ClN_5$
Molecular weight	215.68
Density	1.23 g/cm^3 (22°C)
Melting point	173 – 175°C
Vapor pressure	2.89×10^{-7} mmHg
pKa	1.68
Log Kow	2.60 – 2.71
Log Koc	1.96 – 3.38
Boiling point	200°C
Henry's law constant	2.96 10^{-1} atm.m^3 mol^{-1}
Solubility in water	33 mg/L at 20°C
Diameter	0.4 – 0.9 nm
Structural formula	

2.1.2 Atrazine application and contamination

Atrazine is ranked the second most widely used pesticide in the world, with an annual

production of about 70,000 – 90,000 tons [30]. For instance, 30,000 tons of atrazine is

applied annually in the United States, which is six times higher than the amount used

in China [2, 31]. Atrazine is in the top ten imported herbicides, insecticides, and fungicides into Thailand by over 4,200 tons in 2013 [32].

Due to such large-scale application of atrazine, this herbicide has been detected not only in terrestrial but also in aquatic ecosystems. According to the Crop Protection Chemicals Reference [33], an average of 200 to 400 mg/m^2 of the active ingredient is typically applied to soil depending upon soil properties, type of crop, temperature, and/or an irrigation program. However, not all field-applied atrazine would be absorbed by crops; approximately 3 percent of that total is lost to freshwater streams from contiguous land [34, 35]. Atrazine showed a low sorption capacity on Ultisols under humid tropical conditions and potentially transport to water bodies [36]. The loss of atrazine would be non-point source contamination causing an increase in herbicide in deeper soil, groundwater, and other water bodies [3]. In Thailand, the average concentration of atrazine present in topsoil is 133.59 µg/kg, which is lower than that in subsoil by 183.23 µg/kg [37].

The transport of atrazine in the environment is strongly dependent on its characteristics, such as its ability to resist microbial decomposition and stability in soil and water. Its half-life ranges from 14 days to 4 years in soil and from 6 months to a few years in aqueous media [38, 39]. In Germany, atrazine was banned in 1991 because of its presence over the threshold regulation limits in drinking and groundwater. Nevertheless, 20 years after this ban, atrazine concentration in groundwater was detected to be close to the threshold value (0.1 µg/L) without any significant decrease [5].

Due to its indiscriminate application and persistence, atrazine has posed a potential threat to ecosystem imbalance and human health. While the International Agency for

Research on Cancer (IARC) has included atrazine in the list of pesticides that are possible carcinogens (Group 2B), the United States Environmental Protection Agency (US EPA) has categorized atrazine as an endocrine-disrupting compound [2, 4]. Besides, it was reported that atrazine exposure has been closely associated with an increase in the risk of intrauterine growth retardation, reduced semen quality, and spontaneous abortions in humans, as well as hermaphroditism and demasculinization in frogs [40-42].

Although atrazine is banned in some European countries because of all aforementioned properties and toxicity, the herbicide is still prevalent in many areas, especially Asia, such as India [43], China [31], Thailand [32, 37]. Therefore, many researchers have stepped up efforts to find more proper solutions to clean up the contaminated areas and prevent atrazine's dispersion into groundwater and surface water.

2.2 Overuse of nitrogen fertilizers

Nitrogen (N) is an essential and irreplaceable nutrient for plant growth and maintains life on earth. When nitrogen fertilizers (N-fertilizers) are applied to soil, the nutrient is absorbed directly by plants or transformed into various forms through oxidation processes. Ammonium (NH_4^+) and nitrate (NO_3^-) are the two main nitrogen types that are easily available for crop absorption [44]. Naturally, nutrients would be synthesized through biogeochemical cycles and are enough for plant growth. In contrast, for degraded soils, nutrients are no longer sufficient to meet the needs of crops, and therefore the application of inorganic fertilizers is required [23]. In approximately 48% of crop cultivation, including maize, rice, and wheat production from 1960 to 2010, nitrogen was supplied through inorganic fertilizers [45].

Moreover, N-fertilizer application in Asia has increased significantly by about 17-folds in the last 40 years [46].

However, excessive application of N-fertilizer beyond plant requirements would result in low acquisition efficiency and environmental issues. According to a study by Donner and Kucharik [47], when N-fertilizer consumption increases by 30%, corn production increases by 4%, but the amount of NO_3^- loss also increases by 53%. This quantity could be lost and transferred into the surrounding environmental phases in many forms, such as NO_3^- leaching, NH_3 volatilization, and N_2O emissions [6-8]. Nitrogen transported into surface water is one of the main drivers of eutrophication of freshwater and estuaries [9, 10].

According to a study in Thailand, 6 out of 11 groundwater samples collected at asparagus farms had NO_3^- concentrations over the drinking water safety limit of 50 mg NO_3^-/L regulated by the World Health Organization (WHO) [8]. The deposition of nitrogen in groundwater is a serious threat to human health because groundwater is an important source of water in developing countries especially where there is no tap water supply system. Although high NH_4^+ concentration does not pose a direct threat to human health, this form of nitrogen can be converted into NO_3^- via nitrification. Exposure to NO_3^- could lead to methemoglobinemia in infants under 6 months of age [48]. Therefore, the US EPA regulates the MCL for NO_3^- in drinking water sources at 10 mg NO_3^--N/L [49]. Total ammonia, including non-ionized (NH_3) and ionized forms (NH_4^+), is regulated below 0.2 mg/L in surface and groundwater by the WHO [50].

Ammonium nitrogen can be present in two forms including ionized (NH_4^+) and nonionized (NH_3) forms depending on pH and temperature of the solution. If solution pH is below 7, ammonium ion is predominantly without considering temperature [51]. NH_3 emissions in the air can cause the formation of light-scattering aerosols, leading to haze and impairment of visibility; it can also cause the formation of inhalable aerosol particles, which directly result in deterioration of human health [6]. In addition, agricultural activities contribute about 60% of N_2O to the annual atmospheric emissions of greenhouse gases [7].

In summary, such negative environmental consequences are directly related to the inefficient use of inorganic fertilizers. It has emphasized the need for the development of technological methods to improve current issues in modern agriculture.

2.3 Current treatment technologies for agricultural contaminants

Due to the development of science and technology, there are many techniques available for atrazine remediation in polluted water, wastewater, and soil. However, these solutions still have several limitations and need to achieve greater efficiencies. These widely known methods include chemical treatment [52], incineration [53], adsorption [54-56], phytoremediation [57], and biodegradation [58]. Photolysis, hydrolysis, dehalogenation, and oxygenation are chemical methods applied to atrazine contaminated environments [59]. The incineration method can destroy over 99.9% of organic pesticides and forms toxic and corrosive gases [53]. Some studies have chosen advanced oxidation processes for atrazine-contaminated soil remediation, and they have shown high and quick removal efficiencies [52]. However, these processes are not economically efficient because of their cost and the formation of unwanted products [60]. Phytoremediation is considered a useful treatment method for the

restoration of contaminated soil because it is cost-efficient, saves land resources, and does not cause secondary pollution. After sowing maize for 60 days, atrazine concentration in sterilized soil was reduced from 1 ppm to 0.09 ppm [57]. Regarding the application of biodegradation methods, the removal percentage of atrazine by *Klebsiella variicola* strain FH-1 under optimal condition (i.e., 25°C, pH 9, and 50 mg/L of initial atrazine concentration) was 81.5% after 11 days [58]. Although phytoremediation and bioremediation can achieve high removal rates of atrazine in contaminated sites, these methods require a long operation time and are susceptible to external environmental factors [14].

In this context, adsorption is a promising effective treatment to prevent atrazine transport in the environment. Adsorption is the process by which molecules of adsorbates are adhered to an adsorbent surface [61]. This process immobilizes contaminants on the surface of adsorbents, which simultaneously reduces their ability to move into the surrounding environment. It also creates favourable conditions for the activity of decomposing organisms. Adsorption has many outstanding advantages over other methods, such as low cost, ease of operation, simplicity of design, and avoidance of harmful by-products [62]. Several studies have investigated the adsorption of atrazine by different types of adsorbents; their results are briefly summarized in **Table 2**.

Table 2. Recent studies on the adsorption of atrazine by different adsorbents

Adsorbent	Feedstock	Activation	Sorption capacity/ Removal percentage	Ref.
Biochar	Dairy manure	-	53 - 77 %	[54]
Iron nanocomposite	Black tea	1-butyl-3-methylimidazolium bromide	11.76 µg/g	[55]
Pyro-hydrochar Hydrochar Biochar	Corn straw	-	1.29 - 3.20 mg/g	[63]
Biochar	Rice husk	-	8.2 mg/g	[56]
Organobentonite	Clay	Nanoscale zero valent iron	63.5 %	[64]
Biochar	*Moringa oleifera* Lam. Seed husks	0.1M CH$_3$OH, 0.1M HNO$_3$	10.32 mg/g	[22]
Biochar	Corn straw	Graphene oxide	67.55 mg/g	[65]
Biochar	Soybean	-	3.05 mg/g	[66]
Biochar	Rice straw	H$_3$PO$_4$	37.5 - 70.7%	[67]
Biochar	Peanut husk	4N H$_2$SO$_4$	0.42 mg/g	[43]

Atrazine removal has been widely studied on various materials such as biochar [22, 43, 54, 56, 65-67], nanocomposite material [55], pyro-hydrochar [63], organobentonite [64], and metal-organic framework [68]. Biochar derived from dairy-manure under 450°C was incubated with atrazine-contaminated soils, which showed effectiveness in immobilizing atrazine as well as reducing its bioavailability to earthworms [54]. The iron composite material was studied about atrazine adsorption ability in contaminated water and achieved 95% of removal efficiency [55]. In recent years, atrazine adsorption capacity has been expanded for novel materials such as pyro-hydrochar, with adsorption capacities ranged 1.29 - 3.20 mg/g [63]. It is proved that adsorption is an effective and practical approach for atrazine contaminated water and soil remediation.

2.4 Solutions for overuse of fertilizers

Due to the negative consequences of excessive application of fertilizer, it is necessary to study technologies that can tackle this problem. Smart fertilizer has been proposed as a sustainable solution that can meet all current requirements to improve fertilization strategies.

Smart fertilizer with controlled nutrient release promises to be a sustainable solution because of its ability to increase food production and ensure environmental quality compared to conventional fertilizer practices. According to Trenkel (1997), slow/controlled-release fertilizers may delay the availability of nutrients or steady supply for plant uptake with a longer time than the conventional nutrient fertilizer [69]. The rate of nutrient release is slowed down, leading to an adequate response to plant growth and reduced loss to the environment [11].

Various materials have been studied to act as carrier matrices for nutrients in the development of smart fertilizer such as clays and nanoclays [70], nondegradable and degradable polymers [71, 72], and agricultural residues [73-75]. However, the issues of cost, toxicity, and potential environmental impacts are major factors that are always considered for materials used for smart fertilizers. Biomass-based char has the potential to be an effective carrier or coating material for the smart fertilizer because of its cost efficiency and limited environmental impacts [11].

Due to the physicochemical properties of biochar, it has exhibited the potential in slow-release and reducing the loss of fertilizers such as ammonium [73], phosphate [74], nitrate [75]. For instance, Cai et al. investigated the potential application of corn cob, pomelo peel, and banana stalk obtained biochars for nitrogen fertilizer sustained-release materials. These biochars exhibited excellent performance in capturing NH_4^+ over 90% after 21 days, which were attributed to the presence of abundant oxygen-containing functional groups on the material surfaces [73]. Hagemann et al. reported the ability of biochar derived from three different feedstocks to prevent nitrate loss into the ecosystems and develop as slow-release fertilizers in agricultural activities [76]. In addition to the above benefits, biochar also is capable of retaining water and carbon sequestration. However, the effectiveness of this material is particularly dependent on feedstock and production conditions [77].

2.5 Adsorption mechanisms of organic and inorganic contaminants

Adsorption is an effective method for the removal of organic and inorganic contaminants. The adsorption mechanisms are strongly dependent on physiochemical properties of contaminants and adsorbents and environmental conditions. It is

necessary to understand the behaviors of atrazine and ammonium onto adsorbents, which allows to predict the efficiency of these adsorbents in the practical application.

Partitioning

Bio-based materials includes carbonized fractions (i.e., graphene and crystalline-like fractions) and uncompleted carbonized fractions (i.e., organic carbon, noncrystalline, amorphous fractions). The partitioning of organic solutes occurs on the amorphous fractions of adsorbents containing aliphatic and polyaromatic compounds [78]. It may play an important role in the organic contaminant adsorption to the adsorbent produced at low temperature where the non-carbonized fractions present more prominent [79]. For instance, corn stalk hydrochar produced at 250 and 200°C exhibited a high organic phase, which suggested the dominance of atrazine partitioning [17].

Pore filling

Pore filling mechanism is the diffusion of contaminants into pores of the carbonized fractions of biomass-derived materials [56]. This mechanism is driven by the presence of micropore (<2 nm) and mesopore (2 – 50 nm) systems on the adsorbent surface and contaminant molecule's size. Moreover, it is a dominant mechanism for the adsorption of organic contaminants at low concentration [80]. At higher contaminant concentration, micropores of adsorbents are easily saturated, and no more adsorption can happen at these sites [81].

Due to the moderate molecular diameter of atrazine (0.43 – 0.89 nm), it is likely to access microporous and mesoporous areas of carbonaceous materials [56]. The importance of the pore-filling mechanism in atrazine adsorption to various materials has been reported in several previous studies. The study of Hao et al. [82]

demonstrated that corncob biochar produced at the higher temperature (350 – 650°C) showed higher atrazine adsorption, which was attribute to its higher pore volume. It suggested that pore filling was contributed to the adsorption of atrazine. Pig manure-obtained biochar was applied to remove atrazine and carbaryl in the aqueous environment and better atrazine adsorption efficiency was reported because of its smaller molecular size [83].

π - π electron donor acceptor interaction (EDA)

EDA describes the interaction between the aromatic contaminant and the aromatic surface of the adsorbent's carbonized fraction. A carbonaceous material produced at low temperature (< 500°C) can act as an electron acceptor due to the high contents of electron-withdrawing groups. In contrast, that material produced at a higher temperature may act as an electron donor [82, 84]. Therefore, the importance of π - π EDA interaction is controlled by the aromaticity and polarity of the adsorbent.

It is able to occur π - π EDA interaction between carbonaceous materials and atrazine because of the presence of an aromatic ring in atrazine molecule [85, 86]. For example, the FT-IR result of corncob biochar showed more aromatic carbon with higher pyrolytic temperature. It suggested the interaction between π-electron acceptor of the aromatic material and π-electron donor of atrazine [82]. π - π EDA interaction was a dominant mechanism responsible for the adsorption of atrazine to corn stalk biochar [17].

Hydrophobic interaction

Hydrophobic interaction is non-specific adsorption occurring between a hydrophobic organic molecule and the hydrophobic surface of an adsorbent [87]. It means that both adsorbate and adsorbent have to present hydrophobicity. Typically, biomass-based

adsorbents produced at high temperature have low polarity (low O:C ratio) and high aromaticity (low H:C ratio). It is therefore suggested more hydrophobic effects [56]. The higher hydrophobicity of organic compounds enhances their adsorption to the adsorbents through hydrophobic interaction [88].

Hydrogen bonding

Hydrogen bonding is the reaction between an O or N atom of a molecule and a H atom bonded to an O or N atom of another molecule [66, 89]. It is likely to bind contaminants strongly compared to hydrophobic effects [73]. Due to atrazine is a weak base (pK_a 1.68), it can form H bonds to clay surface or carboxyl groups via its heterocyclic N atoms, as shown in **Figure 2** [83]. Figure demonstrated atrazine molecule could act simultaneously as H bond donor and acceptor [90].
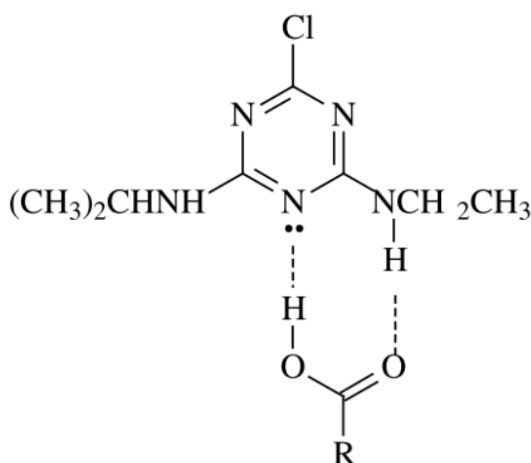
Figure 2. Hydrogen bonding between atrazine and carboxyl group

The changes in carboxyl (-COOH) and carbonyl (C=O) after adsorption of corn stalk biochar have concluded the contribution of hydrogen bonding in atrazine adsorption [17]. Similar findings were also found in the atrazine adsorption to modified *Moringa oleifera* Lam. Seed biochar produced at 300°C [22]. Several studies have proved that hydrogen bonding plays a more critical role than hydrophobic effects in atrazine adsorption [56, 87]. For instance, sludge-derived biochar possessing low polarity exhibited lower atrazine adsorption efficiency than the material with higher polarity [87].

Adsorption of atrazine to biomass-derived materials can be the combination of different interactions. However, the dominance of adsorption mechanisms is dependent on physiochemical properties of adsorbents and contaminants and environmental conditions. Therefore, it is necessary to understand the removal mechanisms, which help predict the effectiveness of the adsorbent.

2.6 Utilization of agricultural wastes

A tremendous amount of agricultural organic waste is annually generated due to strategies to enhance agricultural production worldwide. In 2008, approximately 661 million tons of rice grain was produced throughout the world, and rice husk accounted for 20 – 25 % of the total rice grain weight [20]. The copious amount of rice husk is regularly burned openly or dumped in landfills [20, 91]. These improper disposal techniques have resulted in adverse environmental impacts. Hence, it has raised an interesting research topic of effectively using harvesting residues as a potential resource. Recent studies have applied biological and thermochemical pre-treatment processes such as pyrolysis, torrefaction, gasification, hydrothermal carbonization, anaerobic digestion, and compost to enhance the combustion efficiency of biomass

[92, 93]. Thermochemical treatments are more common than biological methods because they require a shorter reaction time and higher conversion performance [94]. Many researchers have studied using agricultural residues, such as green wastes [10], corn straw [65, 95], rice straw [67], and rice husk [56], as precursors of adsorbents. Due to their lignocellulosic structure, agricultural residues have many functional groups such as aldehydes, alcohols, carboxylic acids, ketones, ethers, and phenolics, which are suitable for biosorption [96]. Therefore, biomass-based materials are considered the most suitable choices that coincide with sustainable development goals worldwide.

In this study, rice husk was developed as an adsorbent for atrazine and N-fertilizer. The composition of rice husk is 35% cellulose, 30% hemicellulose, 18% lignin, 13% silica, and 4% miscellaneous components [97]. This feedstock is available abundantly and is very cheap or even free cost. It can reduce the production cost [56]. Several previous studies related to rice husk-derived materials have been done and proved the efficiency of this feedstock in the adsorption application. For instance, under a similar pyrolysis condition (600°C), rice husk biochar showed better atrazine removal efficiency (11.8 – 42.6%) than eucalyptus bark biochar (23.4 – 40.1%), corn cob biochar (18 – 30.4%), and bamboo chip biochar (12.3 – 26.9%) [67]. In another study, rice husk biochar produced under 550 and 700°C had atrazine adsorption capacities of 6.9 and 8.2 mg/g, respectively [56]. With all the benefits mentioned above, rice husk is a very promising precursor to produce adsorbents.

2.7 Hydrochar

2.7.1 Hydrothermal carbonization and hydrochar

Among the available technologies for the valorization of agricultural wastes, hydrothermal carbonization has gained significant attention because of its outstanding advantages. Hydrothermal carbonization refers to the thermochemical conversion of biomass surrounded with water at a mild temperature or under over-saturated pressure [98]. This method is considered a safe, simple, effective, and environmentally friendly solution to solve current environmental issues [20, 99]**.**

Hydrothermal carbonization can convert wet biomass into carbonaceous products without the requirement of pre-drying feedstocks [98]. The hydrothermal temperature is much lower than that used in other conventional carbonization methods such as pyrolysis and gasification; therefore, this method achieves economic efficiency and is less energy-intensive [20]. Heavy metals detected in orange pomace hydrochar are below the European biochar certificate; besides, there was no detection of polyaromatic hydrocarbon compounds [100]. The liquid phase in hydrothermal carbonization has facilitated the solid product with abundant surface functional groups, established rich pore structure and dissolves some off-gases leading to a reduction of air pollutants [16, 20]. After completing the hydrothermal carbonization process, this liquid fraction can be separated and reutilized effectively.

The liquid fraction from the hydrothermal carbonization process contains many valuable substances, such as phenols, carboxylic acids, and monosaccharides. Therefore, various technologies such as chemical separation, anaerobic digestion, and bio-electrochemical systems have been developed for energy recovery as well as the recovery of valuable chemicals from this liquid fraction [101].

Hydrochar is a carbonaceous product of hydrothermal carbonization. Due to the low cost and less energy consumption of this process, hydrochar has been investigated for its application in multidisciplinary areas such as solid fuel, soil amendment, and adsorbents [20, 98, 99].

2.7.2 Hydrochar application

Hydrochar has abundant functional groups and forms aromatic structures on its surface that make it an alternative adsorbent [16]. Hydrochar obtained from cellulose and hemicellulose via a series of reactions during the hydrothermal carbonization presents a polyaromatic structure with polyfuranic rings [99]. Furthermore, hydrochar's surface contains a high concentration of oxygen-containing functional groups such as -OH, -C=O, and -COOH, as shown in **Figure 3** [98]. These characteristics of hydrochar have made it an excellent potential adsorbent for various inorganic and organic contaminants [15-17].
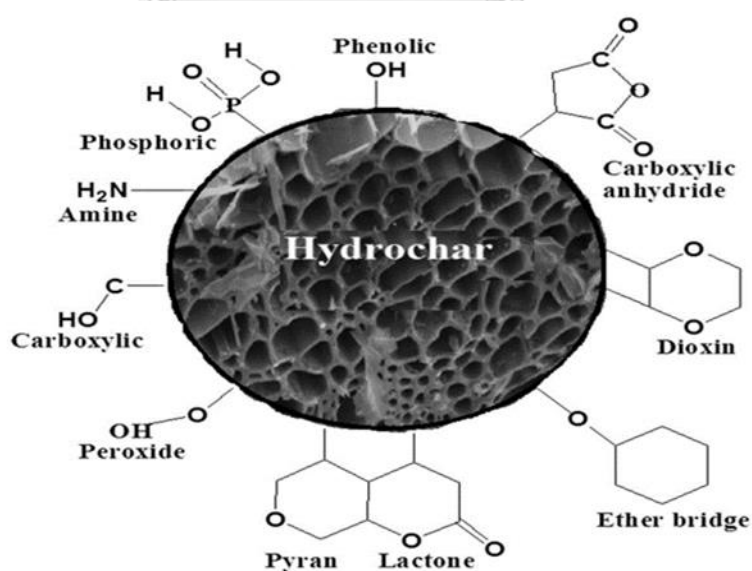
Figure 3. Various functional groups on the surface of hydrochar

For instance, hydrochar obtained from male oil palm flower showed a maximum adsorption capacity of 42.92 mg/g for methyl blue at 30°C [15]. Hydrochar derived from pinewood and rice husk were proven to be quite effective for lead removal with capacities of 4.25 and 2.40 mg/g, respectively [16]. Liu et al. reported the removal efficiency of atrazine to corn stalk hydrochar produced at 250°C higher than at 200°C because of its higher C content [17]. Similarly, corn straw-derived hydrochar generated under 200°C exhibited atrazine removal, with the adsorption capacity of 1.30 mg/g, but it was lower than that of biochar produced at 500°C [63]. To improve the performance of hydrochar, corn straw-obtained hydrochar was chemically activated using potassium oxalate and achieved fast removal of atrazine with an adsorption efficiency of 93.6% [95].

In addition to the studies about organic adsorption, hydrochar has attracted attention to develop as a slow-release fertilizer. Zhang et al. reported that a high content of ammonium nitrogen in compost leachate was absorbed by KOH-activated hydrochar of 260°C, with the maximum adsorption capacity of 140 mg/g. This saturated adsorbed hydrochar was proposed to apply as an ammonium-rich fertilizer [102]. In another study, KOH-activated hydrochar successfully captured ammonium from digestate (108.57 mg/g) owing to the interaction between ammonium and oxygen-containing functional groups on the surface of the studied material. Following five interval extractions, the total ammonium nitrogen released from the saturated hydrochar was upto 12.06 mg N/g at pH 8.5, which suggests the potential to be an ammonium slow-release fertilizer [103]. Significant ammonium adsorption was exhibited by oak-obtained hydrochar at 250°C compared to oak-based biochar at 450°C and 650°C [104].

So far, only a few studies have investigated the removal of atrazine for rice husk-derived hydrochar and develop this adsorbent as nitrogen-show-release fertilizer. Hydrochar is a promising adsorbent as it is cheap and eco-friendly; thus, more studies are required to thoroughly understand the adsorbent's properties before it is introduced to practical application.

2.7.3 Hydrochar and biochar

According to the International Biochar Initiative (IBI) guidelines, biochar is defined as "a solid material obtained from the thermochemical conversion of biomass in an oxygen-limited environment." The physicochemical properties of biochar strongly depended on feedstocks and production conditions. Therefore, to ensure the quality of biochar, the contaminant contents of the feedstock have lower than 2% by dry weight [105].

While hydrochar is produced in slurry conditions (a mixture of biomass and liquid) via hydrothermal carbonization, biochar is made in a dry carbonization condition like pyrolysis [106, 107]. Moreover, hydrothermal carbonization of biomass typically operates at a lower temperature (150 – 350°C) compared to the pyrolysis condition (300 - 650°C) [77, 99]. It has resulted in the significantly different physicochemical properties of chars produced from these processes.

To distinguish biochar from other materials, the molar $H:C_{org}$ ratio is typically used because it is related to the degree of carbonized completion of feedstock to form aromatic ring structures. Biochar possesses the below $H:C_{org}$ of 0.7 and greater fused aromatic ring formations. Feedstocks that have not been thermochemically altered or partially thermochemically altered would be upper 0.7 of the $H:C_{org}$ ratio [105].

Biochar has been studied for many applications such as energy production, agriculture, carbon sequestration, wastewater treatment, and bio-refinery [77]. In terms of adsorption application, biochar derived from various biomass such as peanut husk [43], corn straw [63, 65], rice husk [56] has been found to be an effective adsorbent for atrazine removal. Although hydrochar has shown potential absorbent for the contaminant removal, a few studies have been done (**Table 2**). In terms of the production process, hydrochar produced by hydrothermal carbonization offers some benefits over biochar produced by pyrolysis for economic efficiency. In particular, the hydrothermal carbonization treatment to produce hydrochar can eliminate the requirement for pre-drying feedstock.

Moreover, the contents of alkali and alkaline earth and heavy metal in hydrochar are lower than these of biochar under the same operating temperature. It is attributed to the formation of acetic acid during the hydrothermal carbonization process, which can solubilize and leach out these inorganic elements [108, 109]. Interestingly, the adsorption efficiency of hydrochar has been illustrated higher than that of biochar in some studies. For example, hydrochar derived from the greenhouse and municipal wastes under 250°C had the ammonium nitrogen adsorption capacity of 121.7 and 146.4 mg N/g, respectively. Meanwhile, biochar obtained from these feedstocks under 600 – 650°C achieved the ammonium nitrogen adsorption of 99.3 – 128.3 mg N/g [10]. Finally, the benefits of hydrochar over biochar have drawn an opportunity to consider an alternative adsorbent for removing atrazine and as ammonium-based fertilizer.

2.8 Microwave-assisted hydrothermal carbonization (MHTC)

2.8.1 Effects of hydrothermal carbonization conditions on hydrochar properties

The thermochemical conversion of biomass is to cleavage the rigid structure of biomass into smaller and less complex molecules. The effectiveness of this process depends on the reaction time, temperature, and liquid to solid ratio (L-S). Jain et al. reviewed and plotted trends of oxygen functional groups as a function of temperature, residence time and biomass concentration [99], as shown in **Figure 4**.
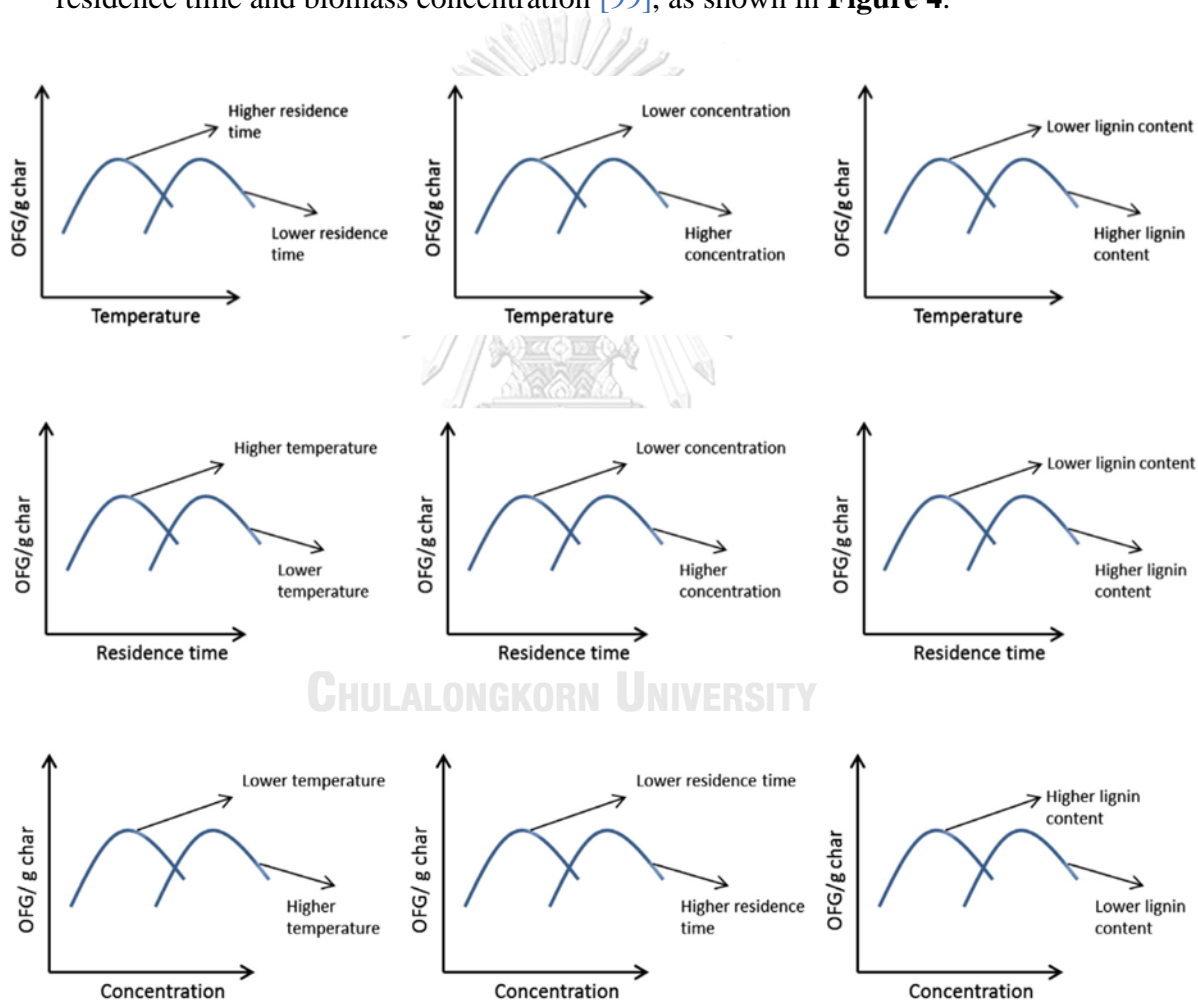
Figure 4. Trends of oxygen-containing functional groups versus temperature, residence time and biomass concentration with various parameters

Temperature

The operating temperature in hydrothermal carbonization plays a vital role in governing the thermochemical conversion of biomass and the formation of products for different applications [99]. Firstly, the hydrothermal carbonization temperature can prevail the dehydration and condensation of hydrochar. For example, Liu et al. confirmed a reduction in the O/C and H/C atomic ratios with an increase in temperature of hydrothermal carbonization treatment from 200 to 250°C [17]. This result is consistent with that of Zhang et al., who reported that the decrease in O/C and H/C atomic ratios of corn cob derived hydrochar was happened with the increase in synthesis temperature from 230 to 260°C [103]. Therefore, higher temperature has resulted in extensive dehydration and condensation of hydrochar.

Secondly, the different compositions of each feedstock have been recognized their effects on the decomposition of hydrochar. Falco et al. reported the presence of cellulose signals of rye straw hydrochar obtained lower than 200°C, whereas these signals were disappeared at 200°C. It was explained by the presence of lignin in the starting biomass, which limited the disintegration of cellulose at lower temperature [110]. In another study by Kang et al., the decrease in ion exchange capacity is attributed to an increase in hydrothermal carbonization temperature from 225 to 265°C for woodmeal, lignin, cellulose, and D-xylose [111].

According to the prediction of Jain et al., higher hydrothermal carbonization temperatures can facilitate higher oxygenated functional groups with lower residence times, higher biomass to liquid ratio and greater lignin content (**Figure 4**) [99]. These factors directly influence on the reaction rate of the decomposition of lignocellulosic biomass in the synthesis process.

Residence time

Although the temperature is the dominant factor governing hydrothermal carbonization, the properties of hydrochar simultaneously depend on other factors such as residence time. There was a decrease in the contents of oxygen-containing functional groups with an increase in residence time [99, 112, 113]. It was attributed to the immoderate dehydration or carbonization or the formation of gaseous products [114]. For instance, there was a drop in oxygen contents of beech wood-obtained hydrochar from 27.99 to 24.98 wt.% as residence time increased from 2 to 17 h under 220°C [112]. Longer residence time has resulted in more condensed products (i.e., low O/C and H/C atomic ratios) because of excessive hydrolysis and polymerization or the conversion of oxygen-containing functional groups to stable oxygen groups [113].

As shown in **Figure 4**, greater oxygenated functional groups can be achieved at higher residence time with higher biomass concentration. It is the results of better reaction performance and the production of secondary solid product [99]. In addition to the contribution of temperature and biomass concentration, higher contents of lignin of starting feedstock can generate higher amount of oxygenated function groups because longer exposure. Nevertheless, it is only achieved if hydrothermal carbonization temperature is sufficient to degrade the lignin structures.

L-S ratio

The L-S ratio refers to the liquid to biomass ratio or biomass concentration in the synthesis process. This ratio can prevail the cross-reactions of the species in the hydrothermal carbonization, especially the polymerization process. It can be seen in **Figure 4**, higher biomass concentration can produce higher oxygenated functional

groups combined with higher temperature, residence time and fewer lignin content. Because these conditions can facilitate the hydrolysis is conducted easily [99].

2.8.2 Microwave-assisted hydrothermal carbonization (MHTC)

Microwave technology has been widely studied because of its energy efficiency compared to conventional heating methods. It is suggested that this technology offers selective, fast, and homogeneous heating, which helps to reduce operating time and bring cost efficiency [115, 116]. In the study of Elaigwu and Greenway [117], *Prosopis Africana* shell hydrochars were prepared by microwave-assisted and conventional hydrothermal carbonizations at 200°C. Hydrochar produced by MHTC for 20 min showed a comparable degree of decomposition pattern made by conventional hydrothermal carbonization for 240 min. A similar result is found in a study about hydrothermal carbonization of cellulose [118]. Hydrochar produced by MHTC with equivalent energy properties can be generated 5 – 10 times faster in reaction time than the conventional hydrothermal carbonization. The maximum rice straw hydrochar (57.9%) was obtained by MHTC at 180°C for 20 min [119]. Additionally, the conventional treatment generates high heat loss and heat transfer resistance, resulting in damage to the reactor [120].

2.9 Chemical activation

Although hydrochar has the potential to capture contaminants present in the environment, its surface area and porosity are relatively moderate compared to those of other materials such as biochar and zeolite [20, 21]. For instance, the specific surface area of corn straw-derived hydrochar (6.37 m^2/g) was much lower than that of corn straw biochar (327.7 m^2/g) [63]. Liu et al. demonstrated the moderate specific surface area of corn stalk-obtained hydrochar by 3.8 m^2/g [17]. Numerous studies

have proven that these limitations can be tailored using chemical and physical activation [75, 121-123]. Chemical activation is a favourable method because it enhances the material performance, can be conducted at a lower temperature and produces less amount of burn-off char than the physical method does [124]. Various chemical activating agents such as KOH, NaOH, H_3PO_4, and H_2O_2 have been widely studied for their effects on the characteristic of biomass-derived hydrochar [99].

Potassium hydroxide (KOH) is a popular activating agent to improve the properties of adsorbents [121-123]. In this process, potassium from the activating chemical separates the lamellae of crystallites that establishes the carbon structure. After washing the activated adsorbent, potassium is washed away and leaves behind high surface area and porosity [121, 122]. The improvement of the physical properties of materials has resulted in the highly efficient application. Cornstalk biochar produced at 500°C was activated by 2M KOH with the solid to liquid ratio of 1:250 (g/mL) for 4h; then, the atrazine removal efficiency of KOH activated biochar was increased by 46.4% compared to that of the pristine biochar. It can be attributed to the higher specific surface area of the material from 32.9 to 59.2 m^2/g [123]. Hydrochar from green waste treated with a 2:1 KOH/char (w/w) showed good mesoporosity and adsorbed 385 mg/g of methylene blue [122]. Mesoporous is considered a critical factor influencing atrazine adsorption; higher mesopore volume results in higher removal efficiency [123]. For ammonium adsorption, alkali modification has shown promising performance [102, 103, 125]. A high amount of ammonium (140.3 mg/g) was successfully adsorbed on KOH-activated hydrochar, and increased hydroxyl and carboxyl groups on the hydrochar surface was responsible for bonding and coordination with pollutants. In this study, hydrochar obtained from corn cob at

260°C was activated by 3M KOH with the solid to liquid ratio of 1:20 (g/mL) for 3h at room temperature [102]. The successful improvement of the material performance after chemical activation in some recent studies is summarized in **Table 3**.

Table 3. Activation of adsorbents and their adsorption capacities

Feedstock	Adsorbent	Activating agent	Adsorbate	Adsorption capacity (mg/g)		Surface area (m²/g)		Ref.
				Initial	Modified	Initial	Modified	
Green waste	Hydrochar	KOH	Methylene blue	244	385	-	-	[122]
Corn straw	Biochar	KOH	Atrazine	1.94	2.84	32.85	59.23	[123]
Corn stalk	Hydrochar	H_2O_2	Atrazine	4.3	8.5	3.8	6.4	[17]
Walnut shell	Hydrochar	H_2O_2	Methylene blue	50.56	173.92	-	-	[126]
Corn cob	Hydrochar	KOH	Ammonium	106.6	140.26	3.79	5.26	[102]
Grape pomace	Hydrochar	KOH	Pb^{2+}	27.8	137	-	-	[127]
Corn cob	Hydrochar	KOH	Ammonium	70.77	103.53	2.3	4	[103]

H_2O_2 solution has been widely used as an oxidizing agent to increase the quantity of oxygen functional groups on hydrochar surfaces [17, 126]. Xue et al. confirmed that the oxygen concentration on peanut hull-derived hydrochar surface was improved from 16.4% to 22.3% after 10% H_2O_2 modification [128]. Enhancing surface oxides after activation by H_2O_2 can facilitate contaminant capture performance [124]. Liu et al. [17] showed that corn stalk-derived hydrochar was synthesized at 200°C and 250°C were able to adsorb atrazine in the aqueous environment. After oxidizing with H_2O_2, atrazine adsorption on hydrochar increased, while biochar efficiency decreased. It proved that oxidation with 5% H_2O_2 could increase oxygenated functional groups on hydrochar surface. This change promotes atrazine partitioning into the organic phase, which is the dominant adsorption mechanism [17], as shown in **Figure 5**. Wang et al. [129] explored that peanut shell biochar oxidized by 2M H_2O_2 was achieved a greater ammonium adsorption capacity (123.23 mg/g) in an aqueous environment.

Figure 5. Mechanism of atrazine adsorption on aged hydrochar

Besides using heat to activate materials, cold activation is also of interest to scientists in recent years because of its outstanding economic efficiency. Jelena et al. have reported that the removal of Pb^{2+} using KOH-modified grape pomace hydrochar was increased approximately 5 times in comparison to untreated hydrochar. The KOH activation was conducted by mixing hydrochar, and 2M KOH for 1h at room temperature, which increased surface area by removing impurities blocked pores and possessed more oxygen-containing functional groups than the untreated hydrochar [127]. Switchgrass hydrochar activated using 2N KOH solution for 1h at room temperature achieved approximately 100% of copper and cadmium removal efficiencies [130]. KOH-cold activation efficiency was also proved by the 2 – 3 times increase in cadmium sorption capacity of sawdust, wheat straw, and corn stack hydrochar [131]. A similar result of these studies is an increase in aromatic and oxygen-containing functional groups on surfaces of KOH-treated hydrochar. Cold activation has applied not only KOH but also other activating agents like H_2O_2. Xue et al. activated peanut hull hydrochar by 10% H_2O_2 solution at room temperature for 2h. The considerable increase in the oxygen-containing functional groups on the hydrochar surfaces has resulted in a 20-time rise in lead sorption compared to un-treated hydrochar [128]. Therefore, in this current work, hydrochar activation using KOH and H_2O_2 at room temperature was performed to improve physicochemical properties that are preferable for contaminant adsorption.

2.10 Response surface methodology

Response surface methodology (RSM) is one of the common statistical and mathematical methods to figure out the interaction between independent parameters and target responses. Its results can help develop a predicted model for achieving a

maximum value of the responses [132]. The conventional method to analyze the interaction between parameters is changing one factor at a time. Compared to this traditional method, the RSM method suggests outstanding benefits such as fewer experimental runs, less time consuming, and less experimental cost [25]. Besides, it was reported that the single factor experiment is incapable of providing the effects of process parameters on the target responses as well as crucial information about the experimental process [24]. Also, the RSM includes ANOVA results to evaluate the adequacy of the developed models [25]. Box-Behnken and central composite designs are the two common experimental designs applied in RSM [24, 25, 132].

Due to its benefits mentioned above, RSM has been widely applied in many studies to optimize the thermochemical conversion process. For example, [132] used this method to optimize pyrolysis conditions for rice husk biochar production with maximum yield, fixed carbon contents, and minimum ash content. RSM was successfully applied to optimize the vanadium (IV) extraction from stone coal leaching solution using an emulsion liquid membrane [25]. Moreover, this tool was also used to optimize hydrothermal carbonization conditions (i.e., reaction temperature, reaction time, and biomass to water ratio) to achieve maximum palm shell hydrochar yield [133]. Similarly, [134] optimized these MHTC process parameters for maximum calorific value of green waste hydrochar to develop this material as a fuel source and an adsorbent material.

Although the RSM has been successfully applied in many previous studies, no optimization studies have been done about rice husk hydrochar, with a view to generating absorbent with maximum atrazine and ammonium adsorption capacities.

CHAPTER III MATERIALS AND METHODS

3.1 Chemicals

Atrazine (analytical grade, $\geq$ 97% purity) and NH_4Cl (analytical grade, $\geq$ 99.5% purity) were used as adsorbates in this study. Potassium hydroxide (KOH), hydrogen peroxide (H_2O_2, 30%) and acetonitrile were analytical grades without further purification. Deionized (DI) water (18.2 MΩ.cm) was used throughout all experiments.

3.2 Hydrochar production

Rice husk was received from a rice mill in Nan province, Thailand and then washed with deionized (DI) water twice to remove impurities and dirt. The feedstock was dried at 105°C in an oven for 12 h. The dried rice husk was fractionated using a 35 mesh to get a uniform size (lower than 0.5 mm) and then stored in a polypropylene plastic bag for further use.

The ground rice husk and DI water were added to reaction vessels at the liquid to solid (L-S) ratio of 5:1, 10:1 and 15:1 (mL/g). These vessels were tightly sealed and placed in a microwave oven (Ethos Easy, Milestone) operated at a power of 980W. The samples were heated to 150, 175 and 200°C and held at a specified temperature for 20 - 60 min. After completing the reaction, the system was fan-cooled down to 25 ± 0.5°C for 30 min. The carbonized solid was separated from liquid fraction using Whatman filter paper 41 and rinsed several times with DI water. The filtered hydrochar was finally dried at 105°C in an oven for 12 h. The prepared hydrochar was stored in polypropylene plastic bags and placed in a desiccator for future studies.

3.3 MHTC optimization for atrazine and ammonium adsorption

The MHTC process parameters for hydrochar production were optimized using Box-Behnken design. Three input variables, including temperature, time and L-S ratio, and their values are presented in **Table 4**.

Table 4. Experimental values of MHTC parameters used in Box-Behnken design

Factor	Unit	Low value	Center value	High value
Temperature	^{o}C	150	175	200
Time	min	20	40	60
L-S ratio	mL/g	5:1	10:1	15:1

With these three input variables, 15 experimental runs were suggested to optimize MHTC process parameters for maximum atrazine and ammonium adsorption capacities using STATISTICA software (version 10). The complete design matrix for the MHTC variables and the responses are given in **Table 5**.

Regression analysis was employed to develop a polynomial equation for predicting the atrazine and ammonium adsorption capacity (q), as presented in **Equation (1)**:

$$p=b_0+b_1A+b_2B+b_3C+b_{11}A^2+b_{22}B^2+b_{33}C^2+b_{12}AB+b_{23}BC+b_{13}AC \tag{1}$$

where p is the response value (mg/g); A, B, C are the values of temperature, residence time and L-S ratio, respectively; b_0 is the coefficient at the center, b_1,b_2,b_3 are the linear coefficients, b_{11},b_{22},b_{33} are the quadratic coefficients, b_{12},b_{23},b_{13} are the interaction coefficients.

The ANOVA analysis and goodness of fit for the predicted data also conducted using STATISTICA software.

3.4 Preliminary atrazine and ammonium adsorption

The preliminary adsorption was conducted to determine atrazine and ammonium adsorption capacities of 15 different hydrochars and then contributed to optimizing MHTC conditions. This process was completed as follows: 0.1 g of hydrochar was mixed with 25 mL of atrazine or ammonium and then placed on an orbital shaker at 200 rpm; after 24 h, the supernatant was withdrawn and filtered through a 0.45-µm nylon filter; the filtrate subsequently analyzed for atrazine or ammonium concentration. The initial concentration of atrazine or ammonium nitrogen applied in this step was 20 mg/L.

The amount of atrazine or ammonium nitrogen adsorbed per unit mass of the adsorbent was calculated using **Equation (2)**:

$$q_e = \frac{(C_o - C_e)V}{m} \tag{2}$$

where q_e is the amount of atrazine or ammonium nitrogen adsorbed per unit mass of adsorbent (mg/g) at equilibrium; C_o and C_e are the initial and equilibrium concentration of adsorbates (mg/L), respectively; V is the volume of aqueous solution (L) and m is the mass of hydrochar used (g).

3.5 Hydrochar activation

Two types of hydrochar were selected from 15 kinds of hydrochar generated previously corresponding to the highest adsorption capacity of atrazine and ammonium were activated using H_2O_2 and KOH solutions.

To make the H_2O_2-activated hydrochar, 1 g of hydrochar was placed into 25 mL of H_2O_2 solution (i.e., 5%, 10%, 20%) and shaken for 1h at room temperature. The mixture was filtered by the Buchner funnel, and the solid was retained. The H_2O_2-

treated hydrochar was rinsed with DI water until reaching a neutral pH. To complete the activation step, treated hydrochar was dried in the oven under 105°C for overnight and then stored in the desiccator for later studies. The prepared H_2O_2-activated hydrochars at 5%, 10%, or 20% H_2O_2 were labelled as 5HHC, 10HHC, or 20HHC, respectively.

KOH-activated hydrochar was produced similarly with various concentrations of the activating agent. The obtained KOH-activated hydrochars at 5%, 10%, or 20% KOH were labelled as 5KHC, 10KHC, or 20KHC, respectively.

3.6 Adsorption kinetic and isotherm studies

3.6.1 Preliminary atrazine and ammonium adsorption

This preliminary adsorption was performed to select the chemical-activated hydrochars with the most efficient removal of atrazine or ammonium. For atrazine adsorption, there were 6 types of chemical-activated hydrochar. The 0.1 g of each activated hydrochar was added into 25 ml of atrazine solution (20 mg/L). The mixtures were shaken at room temperature using the shaker for 24 h. The supernatant was withdrawn and analyzed to determine the adsorption capacity of atrazine for each activated hydrochar.

Similar adsorption conditions were repeated for ammonium with the initial concentration of 500 mg N/L. The adsorption capacity of ammonium for each hydrochar was measured. Following the comparison of atrazine or ammonium adsorption capacity between different adsorbents, the activated hydrochar with the highest removal of atrazine or ammonium was chosen for adsorption kinetic and isotherm studies.

3.6.2 Adsorption kinetics

Regrading to atrazine adsorption kinetics, 0.1 g of each hydrochar was mixed with 25 mL of 20 mg/L atrazine in 40 ml glass vials. The vials were closed tightly and shaken at 200 rpm at room temperature. The supernatants were then collected at different time intervals ranged from 1 – 24 h and passed through 0.45 µm syringe filters.

Kinetic studies for ammonium adsorption were conducted in similar conditions for atrazine, but the initial concentration was 500 mg N/L.

The experimental data of adsorption kinetics was fitted to the pseudo-first-order model, pseudo-second-order model, and intraparticle diffusion given by **Equation (3)**, **(4),** and **(5)**, respectively.

$$\text{Pseudo-first-order model: } q_t = q_e \left[1 - e^{-k_1 t} \right] \tag{3}$$

$$\text{Pseudo-second-order model: } q_t = \frac{k_2 q_e^2 t}{1 + k_2 q_e t} \tag{4}$$

$$\text{Intraparticle diffusion: } q_t = k_3 t^{1/2} + C \tag{5}$$

where q_t (mg/g) is the amount of adsorbed contaminant at time t (min); q_e is the amount of adsorbed contaminant at equilibrium (mg/g); k_1 (1/min), k_2 (g/(mg.min)), and k_3 are the pseudo-first-order, pseudo-second-order, and intraparticle diffusion rate constants, respectively; C is a constant represented for the thickness of the boundary layer (mg/g).

The values of q_e and k_1 for the pseudo-first-order model were calculated from the intercept and the slope of the linear plot of log (q_e – q_t) versus t, respectively. The linear plot of t/qt versus t for the pseudo-second-order model allowed to calculate q_e and k_2.

3.6.3 Adsorption isotherms

To study atrazine adsorption isotherms, 0.1 g of each hydrochar was transferred into 25 mL aqueous solution with varying concentrations of atrazine (2 - 30 mg/L). All samples were shaken for 24 h at 200 rpm using the orbital shaker at room temperature. After shaking, the supernatant was collected using 0.45 µm syringe filters.

Regarding ammonium adsorption isotherms, hydrochar was mixed with the same ratio as atrazine adsorption and shaken for 48 h at room temperature. The initial concentration of ammonium was varied from 30 – 3000 mg N/L. When the adsorption process was completed, the supernatant was withdrawn using 0.45 µm syringe filters and analyzed.

The experimental isotherms were fitted using two isotherm models (i.e., Freundlich and Langmuir models) given by **Equation (6)** and **(7)**, respectively.

Freundlich model: $q_e = K_F C_e^{1/n}$ (6)

Langmuir model: $q_e = \dfrac{q_m K_L C_e}{1 + K_L C_e}$ (7)

where q_e (mg/g) represents the sorption number of pollutants at equilibrium; q_m (mg/g) is the maximum sorption capacity; K_L (L/mg) is the Langmuir constant; K_F is the Freundlich constant; n is the empirical parameter depend on the degree of heterogeneity of adsorbing sites.

3.7 Atrazine and ammonium determination

To ascertain accuracy of the results, all atrazine adsorption experiments were conducted triplication and ammonium experiments were run in duplicate. Then the average values and standard deviation were reported for the experimental results.

Atrazine concentration in the filtrates was analyzed by a high-performance liquid chromatography-ultraviolet (HPLC-UV, Agilent) [135]. The last filtrate (2 mL) was injected into a vial ready for the HPLC analysis using a C18 hypersil column (5 µm, 250×4 mm). Operating conditions were as follows: 60:40 (v/v) of the acetonitrile to DI water ratio, 1 mL/min of flow rate, 25°C of a column temperature, 20 µL of injection volume, and 220 nm of detection wavelength. The retention time for atrazine was 4.5 min.

Ammonium concentration was analyzed using Kjeldahl nitrogen in an automated distillation unit (Buchi, Switzerland).

3.8 Hydrochar characterization

The specific surface area was measured by N_2 adsorption using the Brunauer - Emmett-Teller (BET) method (Thermo Finnigan, USA). The functional groups presented on hydrochar surfaces were determined by Fourier Transform Infrared (FT-IR) Spectroscopy (Perkin Elmer, USA) recording in the region of 4000 to 400 cm^{-1} and analyzed by X-ray photoelectron spectroscopy (XPS) (Kratos, USA). Cation exchange capacity (CEC) was analyzed by the saturation exchange sites with 1M ammonium acetate (NH_4OAc) at pH 7.0 [136].

3.9 Desorption

Desorption of atrazine from hydrochar was studied. Following adsorption, the atrazine-adsorbed hydrochar was filtered and dried at 60°C in the oven. The atrazine-adsorbed hydrochar was mixed with DI water with the ratio of 1:250 (g/mL) and shaken for 24 h. Finally, atrazine concentration was determined in the supernatant.

Hysteresis (H) for atrazine desorption was calculated as **Equation (8)**:

$$H = n_{Fads}/n_{Fdes} \qquad (8)$$

where n_{Fads} and n_{Fdes} represent the nonlinearity factor of Freundlich models for adsorption and desorption, respectively [67].

3.10 Statistical analysis

SPSS (version 20) was used to implement the ANOVA test and compare the means of the adsorption capacity at 95% confident interval.

CHAPTER IV RESULTS AND DISCUSSION

4.1. Effect of MHTC conditions on atrazine and ammonium adsorption of hydrochar

The adsorption efficiency of biomass-derived adsorbents to organic and inorganic pollutants depends dramatically on their physicochemical properties controlled by the MHTC conditions. In this study, the impact of MHTC process parameters (i.e., temperature, residence time, and L-S ratio) on atrazine and ammonium adsorption capacities of hydrochar was determined.

4.1.1 Atrazine and ammonium adsorption capacities of hydrochar

Thirteen hydrochars produced under different MHTC conditions were designed by the Box-Behnken method, as illustrated in **Table 5**. These rice husk hydrochars were, in turn, adsorbed atrazine and ammonium for 24h in the single-solute system.

Table 5. Experimental matrix by Box-Behnken design and corresponding responses

Run	Temperature (°C)	Time (min)	L-S ratio (mL/g)	Adsorption capacity	
				Ammonium (mg N/g)	**Atrazine** (mg/g)
1	150	20	10	0.08 ± 0.23	0.41 ± 0.02
2	200	20	10	0.30 ± 0.45	1.23 ± 0.01
3	150	60	10	0.45 ± 0.35	0.53 ± 0.01
4	200	60	10	0.89 ± 0.43	1.37 ± 0.01
5	150	40	5	0.25 ± 0.34	0.39 ± 0.01
6	200	40	5	0.07 ± 0.19	1.07 ± 0.00
7	150	40	15	-0.63 ± 0.44	0.43 ± 0.02
8	200	40	15	0.54 ± 0.35	0.95 ± 0.02
9	175	20	5	0.57 ± 0.22	1.40 ± 0.01
10	175	60	5	0.18 ± 0.24	1.85 ± 0.04
11	175	20	15	-0.27 ± 0.45	0.19 ± 0.01
12	175	60	15	-1.57 ± 0.25	0.55 ± 0.01
13	175	40	10	-1.02 ± 0.75	0.95 ± 0.00
14	175	40	10	-0.53 ± 0.32	0.60 ± 0.01
15	175	40	10	-0.54 ± 0.13	0.74 ± 0.00

4.1.1.1 The atrazine adsorption capacities of different rice husk hydrochars

The results showed that the adsorption capacities of thirteen rice husk hydrochars to atrazine ranged from 0.19 to 1.85 mg/g. Rice husk hydrochar with the highest atrazine adsorption performance was produced at 175°C for 60 min with the L-S ratio of 5:1 (mL/g). The atrazine adsorption to the material can be controlled by the physicochemical properties of the adsorbent. Previous studies suggested that organic contaminant sorption to adsorbents produced at the low temperature is attributed to the partitioning mechanism [137, 138].

The atrazine partitioning shows a positive relation to the aliphatic polymer fraction of adsorbents [17, 137]. Cao et al. observed better atrazine adsorption of biochar produced at 200°C compared to that made at 350°C, which was attributed to a reduction in its aliphatic fraction. The organic phase of the adsorbent changed from a flexible aliphatic phase (H/C ratio of 1.32) to a rigid and condensed aromatic structure (H/C ratio of 0.79) [137]. Moreover, a decrease in the specific surface area of corn stalk hydrochar was determined when increasing the operating temperature from 200 - 250°C, with the reduction of 4.9 to 3.8 m^2/g, respectively [17]. It can be proved for the higher atrazine adsorption capacity of hydrochar produced at 175°C compared to that obtained at 200°C. However, the physicochemical properties of hydrochar are also influenced by other MHTC parameters such as residence time and the L-S ratio.

4.1.1.2 The ammonium adsorption capacities of different rice husk hydrochars

While all produced hydrochars showed atrazine adsorption abilities, nine out of them absorbed ammonium, with the adsorption capacity ranging from 0.07 to 0.89 mg N/g. The most moderate ammonium adsorption was hydrochar produced at 200°C for 40 min with the L-S ratio of 15:1 (mL/g); Meanwhile, hydrochar with the highest

ammonium adsorption capacity was generated under 200°C for 60 min with the L-S ratio of 10:1 (mL/g). Similarly, in the study of Yao et al. [139], there were nine of the thirteen biochars recorded ammonium sorption abilities with removal rate ranged 1.8 - 15.7%. According to Qu et al., rice husk contains 0.68% nitrogen of total elemental compositions [140]. The hydrothermal carbonization treatment has been widely applied to convert organic or insoluble nitrogen of digestate [103] and compost leachate [102] to inorganic or soluble nitrogen form. Therefore, the increase in ammonium concentration after adsorption can be explained by the nitrogen element in rice husk and ammonium formation attributed to the hydrothermal carbonization.

4.1.2 Optimization of atrazine adsorption capacity

The results of ANOVA analysis for atrazine adsorption capacity of hydrochar were shown in **Table 6**. The temperature had a significant effect on the atrazine adsorption capacity of hydrochar ($p < 0.05$), while residence time and L-S ratio did not significantly affect the adsorption capacity ($p > 0.05$). Furthermore, the atrazine adsorption capacity was significantly affected by the interaction effect of temperature and L-S ratio ($p < 0.05$).

Table 6. ANOVA results for atrazine adsorption capacity of hydrochar

Factor	Sum of squares	DF	Mean square	F value	p-value
Temperature (A)	1.03	1	1.03	35.09	0.03*
Time (B)	0.09	1	0.09	2.93	0.23
L-S ratio (C)	0.35	1	0.35	12.00	0.07
Temperature (A^2)	0.03	1	0.03	0.90	0.44
Time (B^2)	0.16	1	0.16	5.34	0.15
L-S ratio (C^2)	0.003	1	0.003	0.10	0.78
AB	0.0002	1	0.0002	0.01	0.95
AB^2	0.03	1	0.03	0.94	0.43
A^2B	0.04	1	0.04	1.28	0.38
AC	0.006	1	0.01	0.21	0.69
A^2C	0.74	1	0.74	25.18	0.04*
BC	0.002	1	0.002	0.07	0.82
Error	0.06	2	0.02		
Total SS	3.07	14			

p-value < 0.05

The predicted equation of atrazine adsorption capacity of hydrochar was generated using the MHTC process parameters and the observed atrazine adsorption capacity of each hydrochar, as follows:

Atrazine adsorption capacity (mg/g) = -53.6971 + 0.6085A – 0.0016A^2 – 0.2029B – 0.0015B^2 + 5.8773C + 0.0011C^2 + 0.0029AB – 0.0684AC + 0.0002A^{2}C – 0.0002BC

(9)

where A, B and C denote the coded values of temperature (°C), residence time (min), and L-S ratio (mL/g), respectively.

The quadratic polynomial model passed the goodness-of-fit test (p-value = 0.99 from Chi-Square test), which had a coefficient of determination (R^2 = 0.98) and adjusted determination coefficient (R^2_{Adj} = 0.87) at the 95% confidence interval. It is observed that there were synergistic effects between the atrazine adsorption capacity of hydrochar and temperature and L-S ratio. At the same time, residence time showed an antagonistic effect on the adsorption ability of hydrochar. Moreover, the interactive effect of temperature and L-S ratio on atrazine adsorption capacity was significant (p < 0.05), which had a synergistic effect.

The three-dimensional response surface plots exhibit the effect of the L-S ratio and temperature with varying residence times on the atrazine adsorption capacity, as shown in **Figure 6**. The atrazine adsorption capacities of rice husk hydrochar increased with the increase in residence time of the MHTC process ranged from 20 to 60 min. Higher atrazine removal (q > 1.2 mg/g) was found in the operating temperature ranges of 175 – 200°C, lower L-S ratio and higher residence time. As illustrated in **Figure 6(b,c)**, the atrazine adsorption capacity of hydrochar at higher the L-S ratio with the residence time of 40 and 60 min was greatly decreased. When the

operating temperature was lower than 160°C, the atrazine adsorption capacity (q < 0.6

mg/g) was significantly reduced without considering the L-S ratio.

Figure 6. The response surface plots showing the effects of temperature and L-S ratio on atrazine adsorption capacity with varying residence time (a) 20 min, (b) 40 min, (c) 60 min

4.1.3 Optimization of ammonium adsorption capacity

The ANOVA analysis results for ammonium adsorption capacity on hydrochar produced at various MHTC conditions are given in **Table 7**. Like the atrazine adsorption capacity, the temperature of MHTC significantly affected the ammonium adsorption capacity of hydrochar ($p < 0.05$). However, there was no significant influence of other factors of MHTC on the adsorption ability to ammonium.

Table 7. ANOVA results for ammonium adsorption capacity of hydrochar

Factor	Sum of squares	DF	Mean square	F value	*p*-value
Temperature (A)	0.27	1	0.27	3.39	0.21
Time (B)	0.003	1	0.003	0.03	0.87
L-S ratio (C)	0.59	1	0.59	7.37	0.11
Temperature (A^2)	1.96	1	1.96	24.56	0.04*
Time (B^2)	0.58	1	0.58	7.32	0.11
L-S ratio (C^2)	0.003	1	0.003	0.03	0.87
AB	0.01	1	0.01	0.16	0.73
AB^2	0.01	1	0.01	0.17	0.72
A^2B	0.88	1	0.88	10.99	0.08
AC	0.46	1	0.46	5.76	0.13
A^2C	0.60	1	0.60	7.50	0.11
BC	0.21	1	0.21	2.59	0.25
Error	0.159	2	0.08		
Total SS	6.265	14			

*p-value < 0.05

The ammonium adsorption capacity of each hydrochar produced at different MHTC conditions was applied to develop the quadratic polynomial model presented in **Equation 10**, which had an R^2 of 0.97 and an adjusted R^2_{Adj} of 0.82.

Ammonium adsorption capacity (mg N/g) = $-74.4054 + 0.9106A - 0.0027A^2 + 1.4083B + 0.0024B^2 + 4.8211C + 0.0011C^2 - 0.0178AB + 0.0001A^2B - 0.0585AC + 0.0002A^2C - 0.0023BC$ (10)

where A, B, and C denote the coded value of temperature (°C), residence time (min), and L-S ratio (mL/g), respectively.

This equation passed the goodness of fit between observed and predicted data (*p*-value = 0.99). Based on the predicted equation, there are synergetic effects between ammonium adsorption capacity and the particular impacts of MHTC process parameters. In contrast, the combined effects of temperature, time, and L-S ratio were antagonistic to the ammonium adsorption capacity of hydrochar.

The response surface plots showing the effects of temperature and L-S ratio on ammonium adsorption capacity with varying residence time are illustrated in **Figure 7**. With the residence time of 20 min in **Figure 7a**, high ammonium adsorption capacities (q > 0.4 mg N/g) were found in two different conditions as follows: low temperature (160 – 180°C) combined with low L-S ratio or higher temperature (200°C) with greater L-S ratio (>10:1 mL/g). Meanwhile, when increasing the residence time to 40 and 60 min (as shown in **Figure 7b** and **c**, respectively), hydrochar produced at the higher temperature and lower L-S ratio achieved better ammonium adsorption capacity (> 1 mg N/g).

According to Takaya et al., the surface functionality may play a crucial role in ammonium adsorption capacities of various biomass-derived hydrochars produced at

250°C and biochars generated at 400 – 450°C and 600 – 650°C than their surface area and porosity. In addition, there was a positive relationship between the number of functional groups, CEC and ammonium adsorption in that study [10]. However, this result did not coincide with the findings of Zhang et al. Corn cob-derived hydrochars were produced at 230 and 260°C, the material at higher synthesis temperature with higher specific surface area achieved higher ammonium adsorption capacity (7.2 and 7.4 mg N/g, respectively). Although the higher specific surface area caused by higher synthesis temperature has resulted in the different ammonium adsorption capacity of these hydrochars, abundant oxygen functional groups (C═O, C─O bonds) acts as a proton donor and significantly interact with ammonium ions [103]. Thus, the presence of oxygen-containing functional groups has high impacts on the ammonium removal of biomass-obtained materials controlled by the synthesis temperature, residence time and L-S ratio. According to the prediction of Jain et al., the lower L-S ratio can facilitate higher oxygen-containing functional groups combined with higher temperature and residence time because the hydrolysis can easily occur under this condition [99]. This is consistent with the effects of MHTC process parameters on ammonium adsorption capacities in this study.
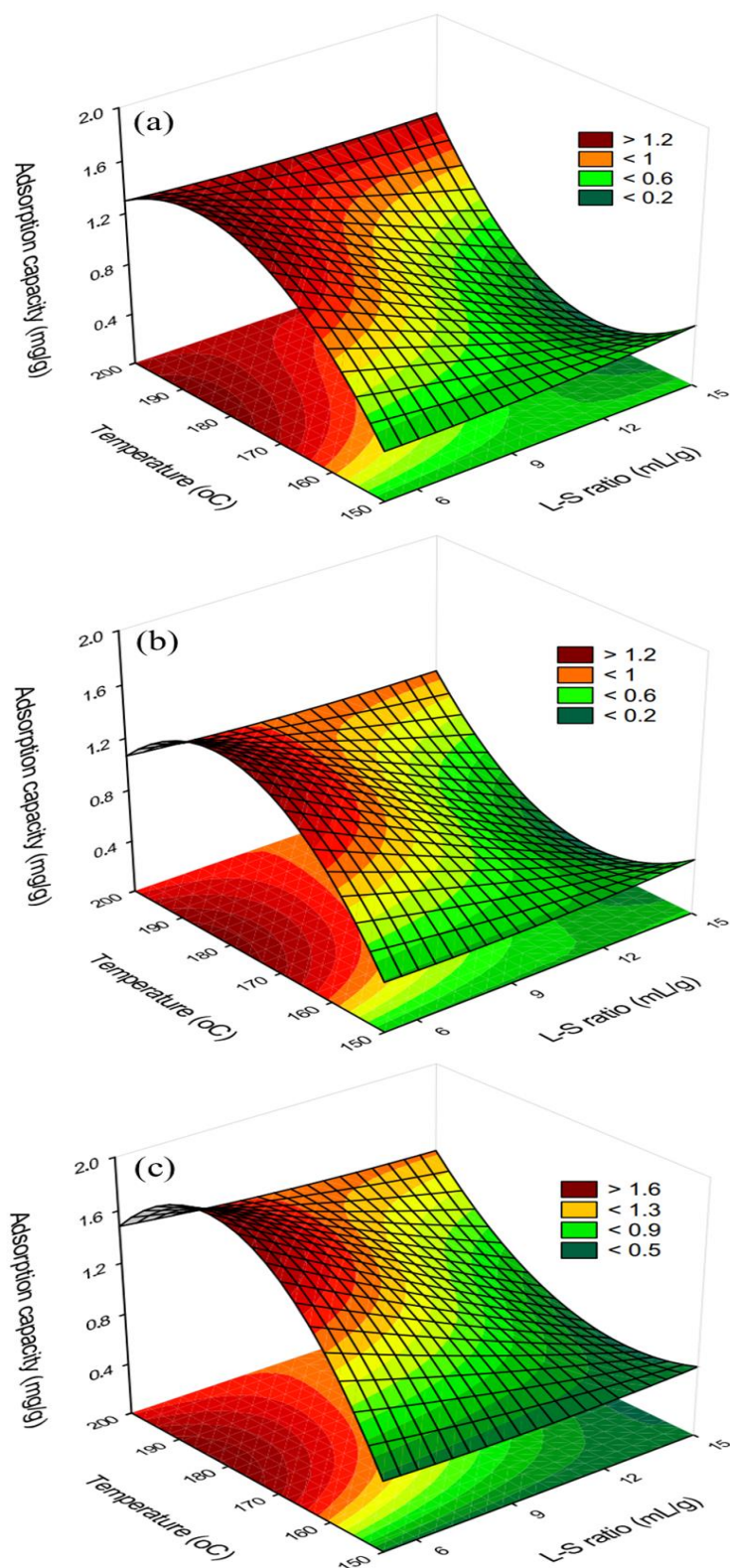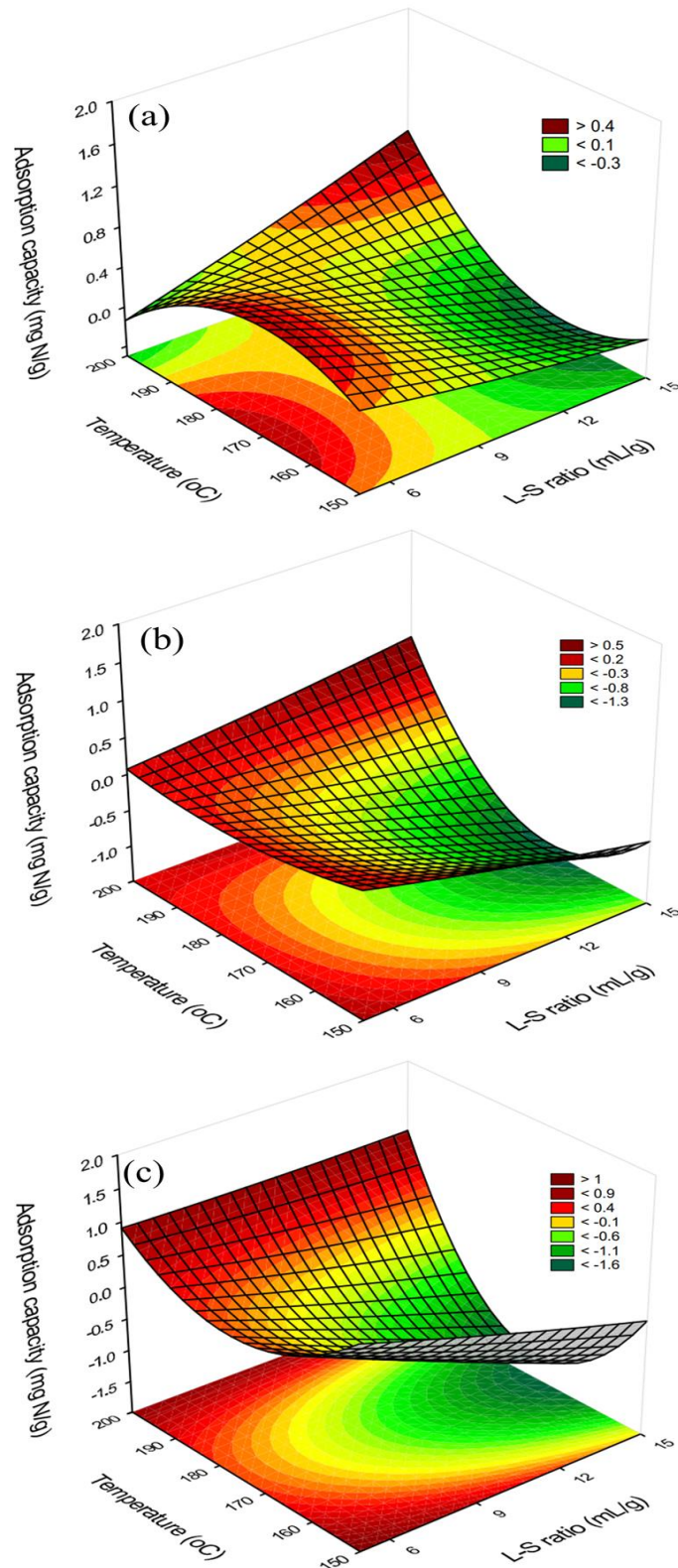
Figure 7. The response surface plots showing the effects of temperature and L-S ratio on ammonium adsorption capacity with varying residence time (a) 20 min, (b) 40 min, (c) 60 min

4.2 Effects of surface activation of rice husk hydrochar on adsorption capacity

Based on the above results, two types of rice husk hydrochar corresponding with the best atrazine and ammonium adsorption performance were chosen for chemical activation. Hydrochar used for the atrazine study was made under 175°C for 60 min with the L-S ratio of 5:1 (mL/g). Another hydrochar produced under 200°C for 60 min with the L-S ratio of 10:1 (mL/g) for ammonium adsorption. The effect of activating agent concentration on the adsorption efficiency was considered.

4.2.1 Atrazine adsorption of activated rice husk hydrochar

The atrazine adsorption capacity of rice husk hydrochar before and after activation using different concentrations of H_2O_2 and KOH solutions is shown in **Figure 8a**. Prior to activating, the adsorption capacity of atrazine onto rice husk hydrochar (HC) was 1.51 ± 0.05 mg/g. There was an enhancement in hydrochar performance for atrazine removal after chemical activation. It is notable that the concentration of activating agents influenced the atrazine adsorption of each hydrochar. When the concentration of H_2O_2 solution was varied from $5 - 20\%$, rice husk hydrochar activated using 10% H_2O_2 solution (10HHC) was exhibited the most effective for atrazine adsorption (1.63 ± 0.06 mg/g). However, the similar pristine hydrochar activated by 20% KOH solution (20KHC) had a higher atrazine adsorption capacity (1.68 ± 0.08 mg/g). The effectiveness of H_2O_2 treatment in the activation of corn stalk hydrochar showed an increase in atrazine adsorption (3.98 mg/g), which was caused by an increase in oxygen-containing functional groups. However, H_2O_2 oxidant was believed a cause of reduction of atrazine adsorption to corn stalk biochar obtained at 500 and 650°C (the adsorption capacity of 2.02 and 2.10, respectively). Because this oxidant reduced aromatic compounds on biochar, the bonds between atrazine and

biochar through π-π electron donor acceptor decreased [17]. Tan et al. investigated the maximum adsorption capacity of corn straw to atrazine after KOH treatment. Its capacity increased to 2.84 mg/g, resulting from a higher BET surface area after activation [123]. Consequently, H_2O_2 and KOH treatments enhanced atrazine adsorption of rice husk hydrochar, and the effectiveness of these treatments was varied between the studies.
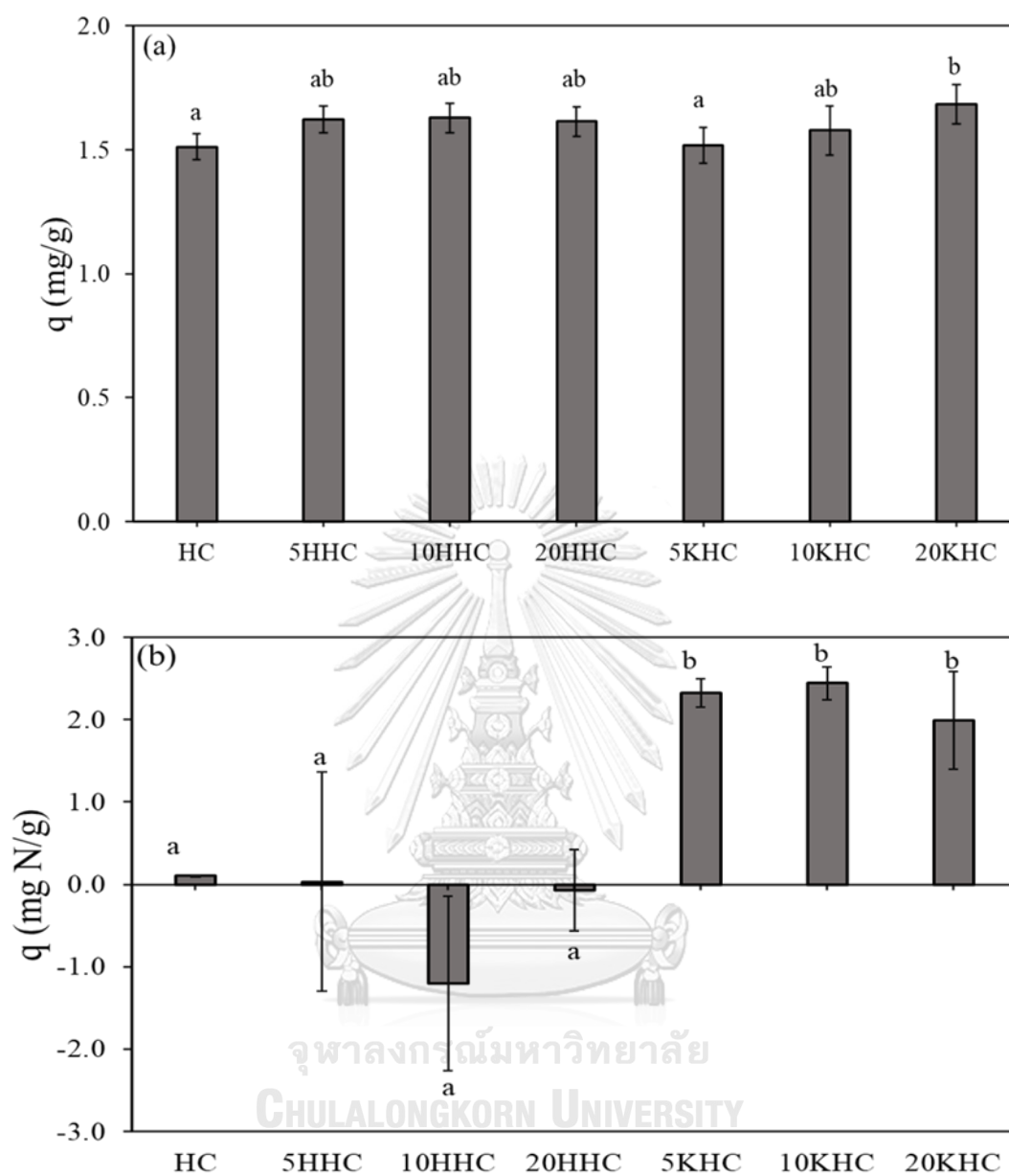
Figure 8. The adsorption capacity of pristine and chemical-activated hydrochars for

(a) atrazine and (b) ammonium at 24h

Means in each bar graph followed by the same letter are not significantly different (p

< 0.05)

The result of statistical analysis showed that there was no significant statistical difference in the atrazine adsorption capacity between 10HHC and 5HHC. Similarly, there was no significant difference in the atrazine adsorption for 20KHC and 10KHC. It is considered about the economic efficiency of the material production, so 5HHC and 10KHC were selected for further atrazine adsorption in this study.

4.2.2 Ammonium adsorption of activated-rice husk hydrochar

Pristine and chemical-activated hydrochars under different concentrations of KOH and H_2O_2 solutions were adsorbed ammonium at 500 mg N/L for 24h. The ammonium adsorption capacity of pristine and activated hydrochars ranged from 0.03 to 2.44 mg/L, as showed in **Figure 8b**. There was a significant improvement in the ammonium adsorption efficiency after KOH treatment, which is approximately 24 times higher than the efficiency of the pristine hydrochar (0.1 ± 0.0 mg N/g). Especially, 10KHC showed the highest ammonium adsorption capacity with 2.44 ± 0.2 mg N/g for 24h. The effect of KOH activation in improving ammonium absorption has been reported in previous studies. For example, corn cob hydrochar activated using 3M KOH achieved ammonium adsorption from digestate about two times higher than hydrochar without activation [103]. The effectiveness of ammonium adsorption from the compost leachate using KOH-activated hydrochar was proven [102]. These studies are in general agreement with an increase in oxygen contents of the adsorbents after KOH activation. This facilitates the adsorption of ammonium because oxygen-containing functional groups can act as proton donors.

Nevertheless, the chemical activation of rice husk hydrochar using H_2O_2 solution did not show a promising result in ammonium adsorption. There was a considerable reduction in the ammonium adsorption capacity of H_2O_2-activated hydrochar.

Especially, 10HHC and 20HHC released 1.20 ± 1.1 and 0.07 ± 0.5 mg N/g, respectively. It was reported that activation could disrupt N-containing compounds present in carbonaceous materials, which has resulted in an increase in N contents in the solution [104]. According to the study of Teng et al., rice husk hydrochar produced under 180°C contained 0.8% of the nitrogen content [141]. Thus, it may cause a slight increase in ammonium concentration after mixing H_2O_2-activated hydrochar and contaminated solution.

Takaya et al. figured that there was no significant difference in either increase or reduction in ammonium adsorption of oak-based hydrochar and biochar after KOH, H_2O_2, H_2SO_4, H_3PO_4 treatments. There was an apparent decrease in ammonium adsorption of KOH and H_2O_2-treated hydrochar and biochar, although these materials possessed high cation exchange capacity (CEC). They concluded that CEC is not a major drive to absorb ammonium onto the material [104]. The same conclusion was drawn in the methylene blue adsorption study [142].

In this study, HC and 10KHC were ultimately selected to investigate more about ammonium adsorption kinetic and isotherm models.

4.3 Kinetic adsorption studies

4.3.1 Kinetic adsorption of atrazine

The time-dependence of atrazine adsorption onto HC, 10KHC, and 5HHC is shown in **Figure 9**. The atrazine adsorption capacity of these prepared absorbents was generally increased over time. These absorbents exhibited rapid increases in atrazine adsorption in the first 2.5 h and the following lower adsorption rates until reaching the final equilibrium state. Notably, 10KHC showed substantially faster increases in atrazine adsorption in the first 45 min than 5HHC and HC do. When the material reaches the

equilibrium state, there is no notable fluctuation in its adsorption capacities. It is explained by the decrease in available active sites on the adsorbent over time, which prevents the diffusion of a new molecule into pores as well as the adsorption of this molecule [143].
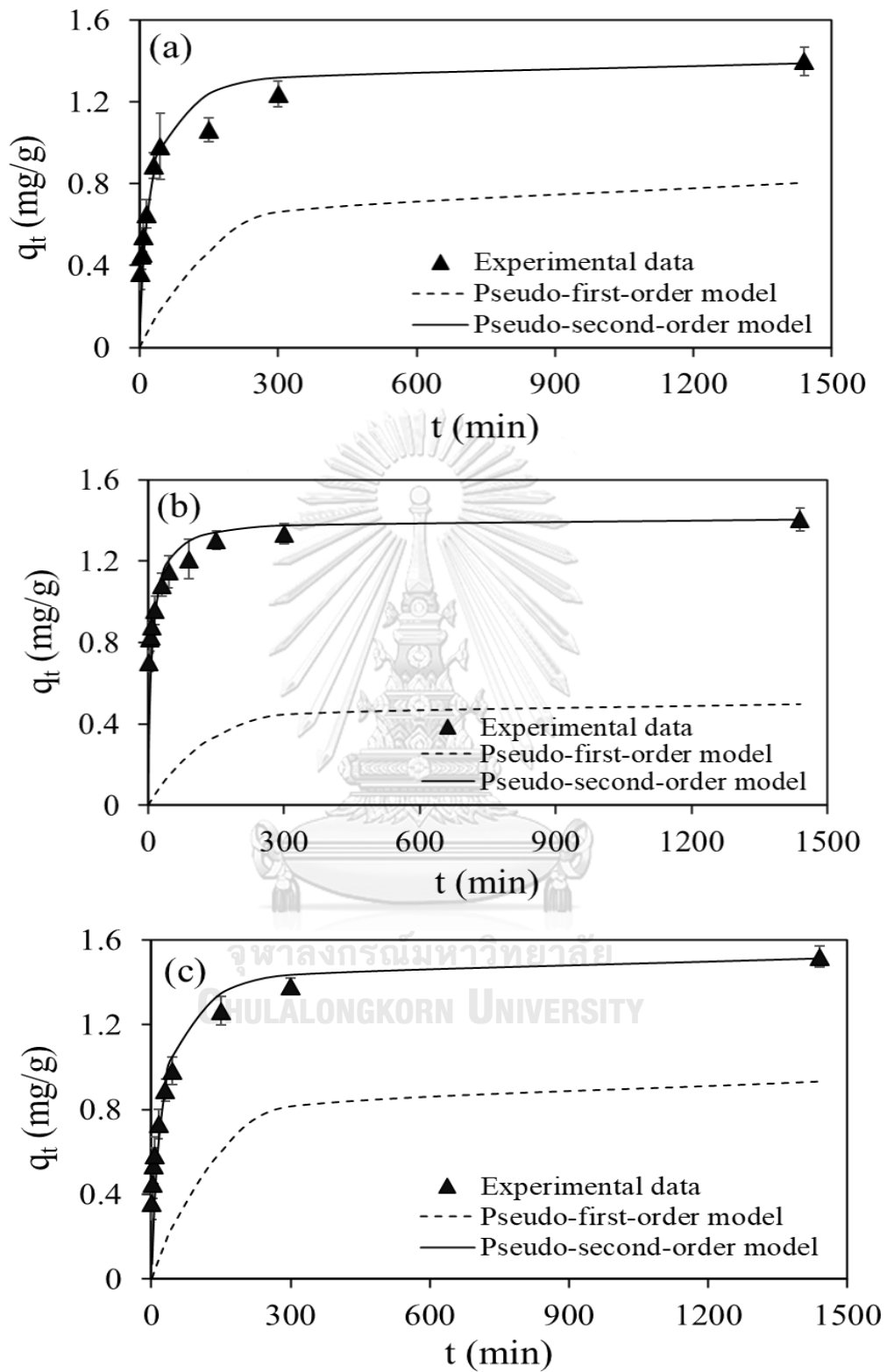
Figure 9. Adsorption kinetic fitting results of pseudo-first-order and second-order

models for atrazine onto (a) HC, (b) 10KHC and (c) 5HHC

At the equilibrium state, atrazine adsorption capacities of HC, 10KHC, and 5HHC were 1.40 ± 0.06, 1.41 ± 0.06, and 1.52 ± 0.05 mg/g, respectively. The performance of 5HHC in atrazine adsorption was better than that of HC and 10KHC. The adsorption capacity of 5HHC at equilibrium was higher than some materials that were evaluated before. For instance, chemical-activated peanut husk biochar produced at 300°C achieved the atrazine adsorption capacity of 0.42 mg/g at the equilibrium state [43]. In the study of Liu et al., corn straw hydrochar generated at 200°C was applied to absorbed atrazine in an aqueous solution for 137h, with the capacity of 1.29 mg/g [63]. Biochars derived from six different feedstocks, including soybeans, corn stalks, rice stalks, cattle manure, and pig manure, at 450°C had the atrazine adsorption capacity of 1.42, 1.04, 1.33, 1.25, and 0.99 mg/g at the equilibrium stage, respectively [66]. Moreover, hydrochar produced in this study showed higher adsorption efficiency at the equilibrium than iron-nanocomposite material (11.4 µg/g) [55].

The plots of atrazine adsorption kinetics with the pseudo-first-order and pseudo-second-order models are illustrated in **Figure 9**, with the calculated kinetic parameters showing in **Table 8**. The adsorption of atrazine onto pristine and chemical-activated hydrochars was best fitted with the pseudo-second-order model with the coefficient of determination (R^2) in the range of 0.9987 to 0.9998. The experimental and calculated values of the adsorption capacity at the equilibrium were 1.40 and 1.39 mg/g for HC; 1.41 and 1.41 mg/g for 10KHC; 1.52 and 1.54 mg/g for 5HHC, respectively. Due to the highest values of R^2 (> 0.99) and the closeness of calculated and experimental adsorption capacity values, the pseudo-second-order kinetic was suitable for the predicted kinetics and chemisorption can be a predominant mechanism controlling atrazine adsorption on both pristine and activated hydrochars. In addition, the

adsorption rate constants (k_2) of atrazine to 10KHC ($k_2 = 0.09$ g mg^{-1}min^{-1}) were higher than that of HC and 5HHC ($k_2 = 0.03$ g mg^{-1}min^{-1}). This result is consistent with atrazine adsorption on various absorbents such as H$_3$PO$_4$-activated corn straw biochar [144], pyro-hydrochar [63]. The aromaticity of carbonaceous material is positively related to the organic contaminant adsorption through π-π electron donor-acceptor interaction. In which, atrazine can act as a π-electron donor and aromatic carbon can act as π-electron donor or π-electron acceptor [63, 66]. Additionally, oxygen-containing functional groups on the adsorbent material can bind with atrazine via H-bonding interaction and electrostatic interaction [17, 56].

Table 8. Kinetic parameters of atrazine adsorption on pristine and activated hydrochars

Absorbents	$q_{e, exp.}$ (mg/g)	Pseudo-first-order model			Pseudo-second-order model		
		$q_{e, cal.}$ (mg/g)	k_1 (1/min)	R^2	$q_{e, cal.}$ (mg/g)	k_2 (g mg^{-1}min^{-1})	R^2
HC	1.40	0.81	0.01	0.8689	1.39	0.03	0.9987
10KHC	1.41	0.50	0.01	0.8654	1.41	0.09	0.9998
5HHC	1.52	0.93	0.01	0.9312	1.54	0.03	0.9989

NB: $q_{e, exp.}$ – $q_{e, experimental}$; $q_{e, cal.}$ – $q_{e, calculated}$

The intra-particle diffusion model was applied to determine the diffusion of atrazine onto three adsorbents (**Figure 10** and **Table 9**). There were two linearity correlations, which means that the adsorption process can include two consecutive processes. In the first linear process, the R^2 values of the three absorbents were higher than 0.98, which indicates a strong interaction between adsorbate and adsorption sites on both pristine and activated hydrochars. It assumes that the boundary layer diffusion rate is faster than intraparticle diffusion in this first process. The active sites on the outside layer are all occupied; thus, atrazine would move into the inside pores and deeper. It is known as intra-particle diffusion. However, the R^2 value of the second process was relatively high ($R^2 > 0.87$). It is also recommended that atrazine is absorbed to the deeper pores and controlled by the intraparticle diffusion process [144]. The C constants of the two linearities were larger than zero; hence, there was not only a single rate-limiting process. Finally, intraparticle diffusion and boundary layer diffusion also affect the adsorption process [43, 145, 146].
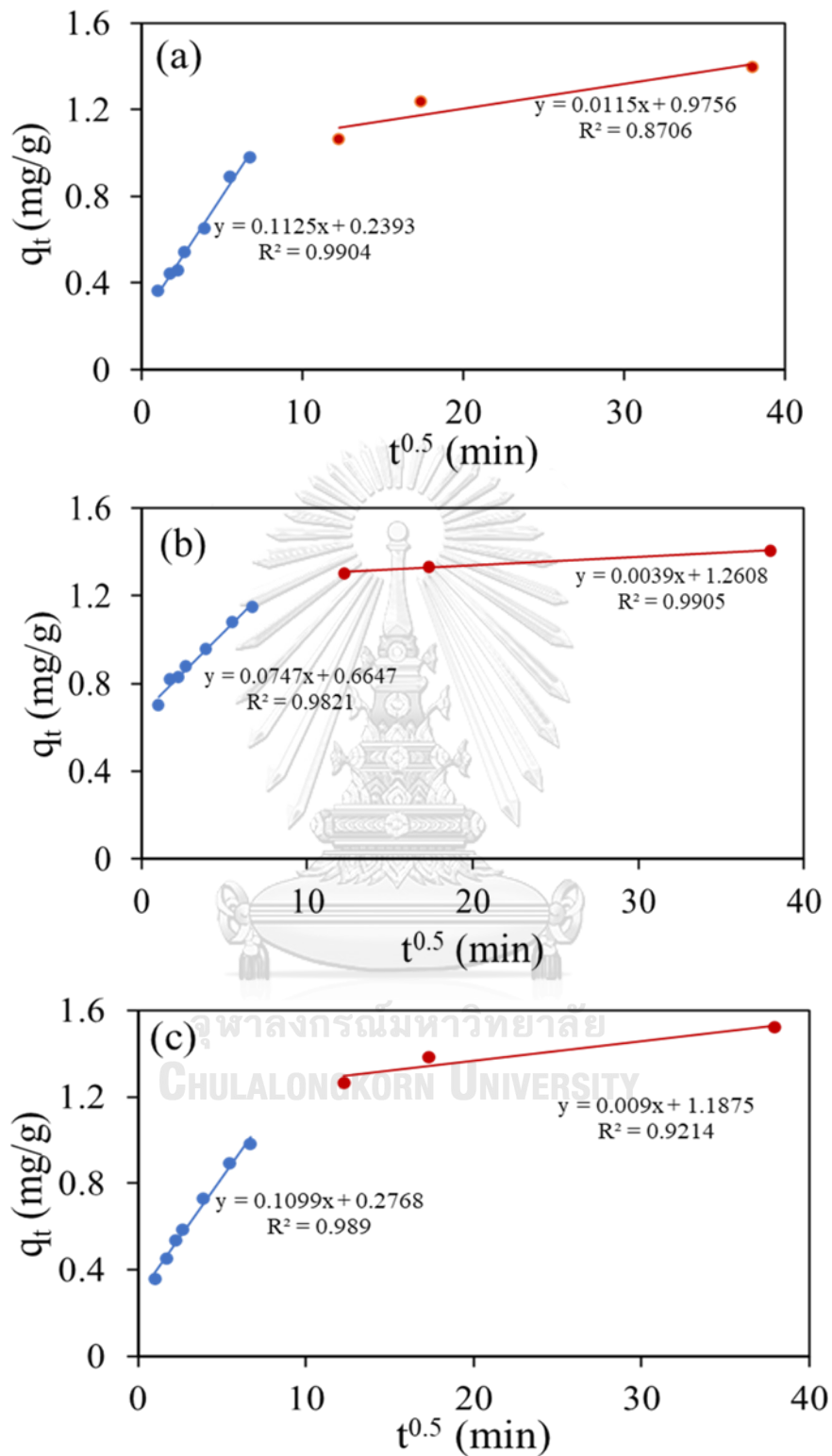
Figure 10. Adsorption kinetic fitting results of intraparticle diffusion (Weber-Morris)

model onto (a) HC, (b) 10KHC and (c) 5HHC

Table 9. Kinetic parameters of the intra-particle diffusion model for atrazine adsorption on HC and activated HC

	Instantaneous adsorption stage			Slow adsorption stage		
	k_{p1}	C_1	R^2	k_{p2}	C_2	R^2
HC	0.1125	0.2393	0.9904	0.0115	0.9756	0.8706
10KHC	0.0747	0.6647	0.9821	0.0039	1.2608	0.9905
5HHC	0.1099	0.2768	0.989	0.009	1.1875	0.9214

4.3.2 Ammonium adsorption kinetics

Ammonium adsorption to HC and 10KHC was obtained at different time intervals ranged from 0 – 24h with the initial concentration of 500 mg N/L, as illustrated in **Figure 11**. The adsorption capacities of ammonium to HC and 10KHC generally increase over time. However, there was no adsorption of ammonium to these adsorbents for the first 15 min. The ammonium concentration in the solution then began to decrease and remained constant at approximately 24h. Takata et al. observed that many biochars derived from oak wood and greenhouse wastes released ammonium rather than adsorbed at initial concentrations lower than 400 mg N/L. However, when the initial ammonium concentration was increased up to 1000 mg N/L, oak wood-based biochars produced at 450 and 650°C released ammonium by 6.2 and 11.9 mg N/g, respectively. It concluded that the lower initial ammonium concentrations did not be a reason because biochar can absorb ammonium at low concentrations [10]. Therefore, it can be deduced that the ammonium release from HC and 10KHC in the first 15 min took place faster than adsorption did.
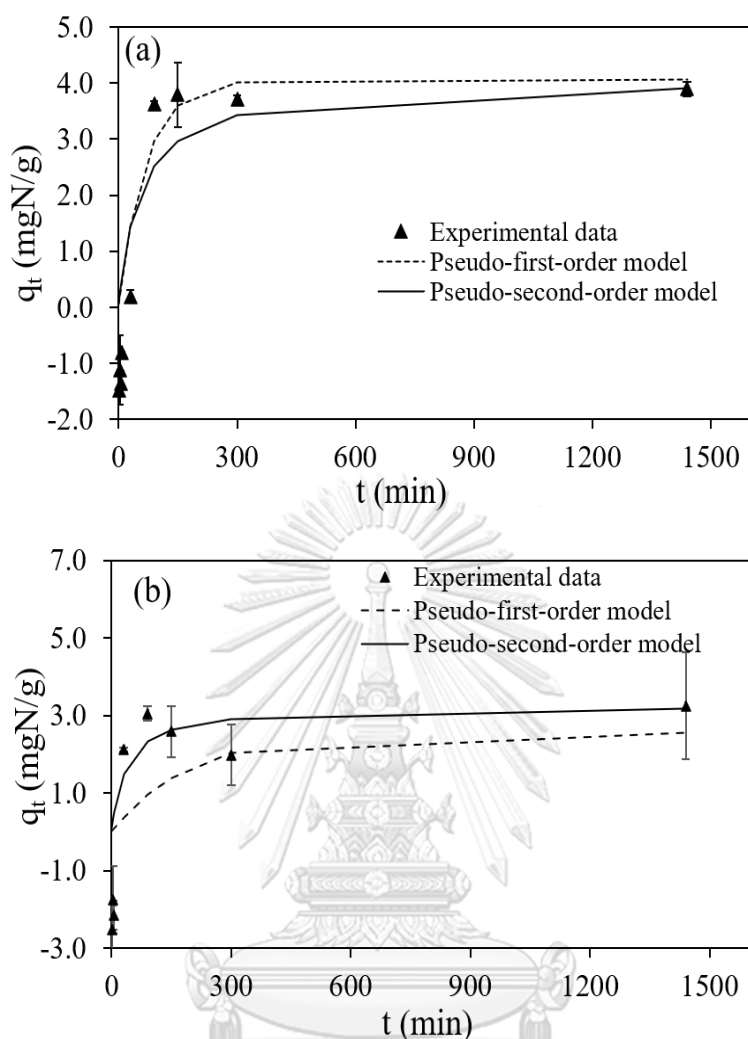
Figure 11. Ammonium adsorption kinetics of HC (a) and 10KHC (b) at 500 mg N/L

for 24h

At the equilibrium time, the adsorption capacity of HC (3.89 mg N/L) was more

effective than that of 10KHC (3.25 mg N/g). The comparison of ammonium

adsorption capacity between various materials was summarized in **Table 10**. The

ammonium adsorption capacity of the two adsorbents in this study was comparable

with other adsorbents such as pine sawdust biochar (1.27 – 4.66 mg/g) and wheat

straw biochar (0.82 mg/g) [147], and corn straw biochar (2.3 mg N/g) [148].

Nevertheless, several studies exhibited dramatically higher ammonium adsorption

capacities of other adsorbents compared to those of this study. For instance, Zhang et al. reported ammonium adsorption capacities of KOH-activated corn cob hydrochar produced at 230 and 260 °C to be 11.3 and 11.6 mg N/g, respectively [103]. Hydrochar derived from oak wood and greenhouse wastes under 250°C showed the ammonium adsorption capacity of 65.8 and 48.1 mg N/g, respectively [10].

Table 10. Ammonium adsorption capacities of various materials

No.	Absorbent	Feedstock	Activation	Qe (mg N/g)	Ref.
1	Hydrochar	Corn cob	KOH	11.3 – 13.6	[103]
2	Hydrochar	Oak wood	-	Hydrochar: 48.1 – 65.8	[10]
	Biochar	Greenhouse wastes		Biochar: 0 – 18.4	
3	Biochar	Pine sawdust	-	1.27 – 4.66	[147]
		Wheat straw		0.82	
4	Hydrochar	Corn cob	KOH	8.4 – 8.9	[102]
5	Biochar	Rice straw	Potassium iron	12.8 – 19.3	[23]
6	Biochar	Corn straw	-	2.3	[148]
7	Biochar	Cotton stalk	NaOH	93.4	[125]
8	Brown coal		NaOH	0.55	[149]
9	Hydrochar	Rice husk	KOH	3.25 – 3.89	This study

Kinetic parameters of the pseudo-first-order and pseudo-second-order models for ammonium adsorption were presented in **Table 11**. The coefficients of determination obtained from the pseudo-second-order model for HC and 10KHC (R^2 = 0.84 and 0.96, respectively) were higher than the pseudo-first-order model (R^2 = 0.68 and 0.21, respectively). The calculated ammonium adsorption capacities using the pseudo-second-order model for HC ($q_{e,cal}$ = 4.06 mg N/g) and 10KHC ($q_{e,cal}$ = 3.26 mg N/g) were consistent with their corresponding experimental data. Thus, the pseudo-second-order model represented ammonium adsorption kinetic better than the pseudo-first-order model in this study. This finding is consistent with many previous studies about ammonium adsorption on various materials such as corn cob hydrochar [102, 103], pine sawdust and wheat straw biochars [147].

Table 11. Kinetic parameters of ammonium adsorption on HC and 10KHC

Absorbents	$q_{e, exp.}$ (mg/g)	Pseudo-first-order model			Pseudo-second-order model		
		$q_{e, cal.}$ (mg/g)	k_1 (1/min)	R^2	$q_{e, cal.}$ (mg/g)	k_2 (g mg^{-1}min^{-1})	R^2
HC	3.89	4.06	0.015	0.6871	4.06	0.004	0.8426
10KHC	3.25	2.55	0.005	0.2148	3.26	0.008	0.9672

It suggested that chemical reaction was the rate-limiting step for ammonium adsorption to HC and 10KHC. It can suggest ion exchange and electrostatic interactions between the material and the functional groups on the adsorbent surface [150]. According to the result of the pseudo-second-order kinetic model, adsorption rate (k_2) of 10KHC (0.008 g.mg^{-1}.min^{-1}) was slightly higher than that of HC (0.004 g.mg^{-1}.min^{-1}).

4.4 Isotherm adsorption studies

4.4.1 Atrazine adsorption isotherms

The adsorption of HC, 10KHC, and 5HHC was evaluated at different initial concentrations of atrazine ranged from 2 – 30 mg/L for 24h. Adsorption efficiency corresponding with each adsorbent significantly increased with the increase in initial atrazine concentration, as illustrated in **Figure 12**. 10KHC with the atrazine adsorption capacity ranges of 0.21– 2.21 mg/g was higher than pristine hydrochar (HC) with the capacity ranges of 0.19 – 2.05 mg/g. The positive relation between the atrazine removal performance of the adsorbents and initial contaminant concentration was attributed to the concentration gradient driving force [140]. It can be seen that the atrazine adsorption capacities of these adsorbents have not reached the plateau stage. Due to atrazine's low water solubility (33 mg/L), the maximum initial concentration used in this study was 30 mg/L. 10KHC showed the best performance of atrazine adsorption, with the adsorption capacity of 2.21 ± 0.15 mg/g. It is followed by HC and 5HHC, with the adsorption capacities of 2.05 ± 0.13 and 2.04 ± 0.09 mg/g, respectively.
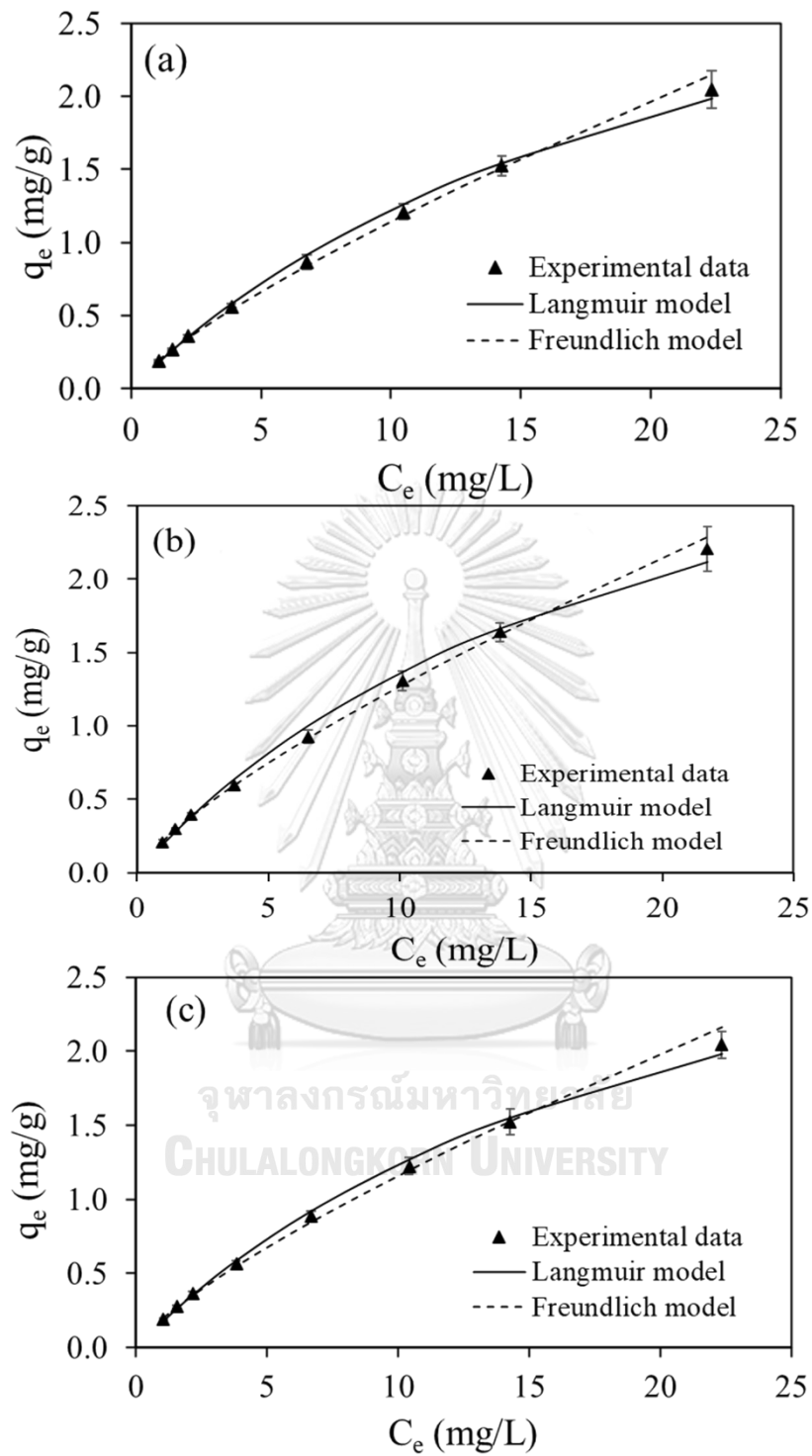
Figure 12. Adsorption isotherm fitting results of Langmuir and Freundlich models

for atrazine onto (a) HC, (b) 10KHC and (c) 5HHC

Freundlich and Langmuir models were applied to consider the interaction between absorbents and atrazine at different initial concentrations. As shown in **Figure 12** and **Table 12**, the Freundlich model was better fitted with experimental data for all three types of adsorbents ($R^2 > 0.99$). It assumes that the adsorption of atrazine onto these adsorbents are the multilayer adsorption onto heterogeneous active sites. This finding is in agreement with many previous studies such as P-doped corn straw biochar [144], β-cyclodextrin functionalized rice husk-based cellulose [140], and H_2O_2-oxidized corn stalk biochar [17]. The nonlinearity factors (n) of HC, 10KHC, and 5HHC were 1.28, 1.32, and 1.29, respectively. It reveals that atrazine adsorption was a ready and favorable process [17, 55]. Therefore, hydrophobic partitioning, pore filling, and surface adsorption may be responsible for the adsorption of atrazine onto hydrochar and activated hydrochar. The surface sorption includes hydrogen bonding and π-π electron donor-acceptor interaction [151, 152].

Moreover, it was notable that HC, 10KHC, and 5HHC displayed a linear isotherm model ($R^2 > 0.98$). It implies the presence of solute partitioning in atrazine adsorption mechanisms. It is suggested the primary sorption mechanism of organic contaminants onto materials produced at the low temperature [17, 137]. The sorption isotherm results of atrazine onto corn cob biochar showed a combined effect of linear and nonlinear adsorption. This corn cob biochar produced at different operating temperatures (350 – 650°C), which was not completely carbonized. Thus, corn cob biochar includes the carbonized and non-carbonized fractions characterized by non-linear and linear adsorption, respectively [82].

Table 12. Fitting parameters of sorption isotherms of atrazine onto pristine and activated hydrochar by Langmuir and Freundlich models

Sample	Linear			Langmuir			Freundlich		
	Slope	Intercept	R^2	q_m (mg/g)	K_L (L/mg)	R^2	n	K_F (mg/g)(L/mg)$^{1/n}$	R^2
HC	0.09	0.19	0.9837	4.03	0.04	0.9732	1.28	0.19	0.9986
10KHC	0.09	0.20	0.985	4.06	0.05	0.9518	1.32	0.22	0.9992
5HHC	0.09	0.20	0.9817	3.89	0.05	0.9792	1.29	0.19	0.998

The fit of experimental data to the Langmuir model ($R^2 > 0.95$) was lower than those of the linear and Freundlich models. The Langmuir model suggests monolayer adsorption to finite homogenous active sites. 10KHC achieved the highest maximum adsorption capacity of atrazine ($q_m = 4.06$ mg/g), followed by HC ($q_m = 4.03$ mg/g) and HHC ($q_m = 3.89$ mg/g).

The results of atrazine adsorption capacity in this study are compared with other available materials, as illustrated in **Table 13**. Many materials have been studied to remove atrazine in the aqueous environment as well as the development of treatments to improve their efficiency. In general, the efficiency of rice husk-derived hydrochar and chemical-activated hydrochar exhibited quite comparative with some biochars produced at the higher temperature. For example, the maximum adsorption capacity of atrazine onto peanut husk biochar produced at 300°C for 2h was 1.44 mg/g [43]. However, the efficiency of hydrochar achieved in this work is relatively moderate compared to H_3PO_4-activated biochar [144], graphene oxide biochar [65].

Table 13. Adsorption capacities of several materials for atrazine

No.	Absorbent	Feedstock	Activation	Qe (mg/g)	Qm (mg/g)	Ref.
1	Biochar	Peanut husk	CH$_3$OH, H$_2$SO$_4$	0.42	1.44	[43]
2	Biochar	Soybean	-	1.42	-	[66]
		Cornstalk		1.06		
		Rice stalk		1.33		
		Cattle manure		1.25		
		Pig manure		0.99		
3	Hydrochar	Corn straw	-	1.30	-	[63]
	Biochar			1.99		
	Pyro-hydrochar			3.20		
4	Iron nanoparticle	Black tea	1-Butyl-3-methylimidazolium	0.11	0.12	[55]
5	Biochar	Corn straw	H$_3$PO$_4$	-	26.64	[144]
6	Biochar	Corn stalk	H$_2$O$_2$	-	2.02	[17]
	Hydrochar			-	3.98	
7	Cyclodextrin	Rice husk	β-cyclodextrin	98.62	152.39	[140]
8	Biochar	Corn straw	Graphene oxide	68.12	72.18	[65]
9	Hydrochar	Rice husk	KOH and H$_2$O$_2$	1.40 – 1.52	3.89 – 4.06	This study

4.4.2 Ammonium adsorption isotherms

The effects of initial ammonium concentration on the adsorption of HC and 10KHC were investigated for 48h, as presented in **Figure 13**. The results showed that the adsorption capacity of these adsorbents followed a different pattern. Ammonium release happened in rice husk hydrochar (HC) with the release range of 0.41 – 6.39 mg N/g. Meanwhile, the adsorption capacity of 10KHC climbed up with the increasing ammonium concentration owning to higher initial concentration gradients. However, the removal of ammonium using 10KHC only remained to a certain point. Specifically, the adsorption capacity of 10KHC increased from 1.24 to 1.94 mg N/g with initial concentrations ranging from 30 – 500 mg N/L; However, these capacities dropped to 0.41 and 0.35 mg N/g at the initial concentration of 1000 and 1800 mg N/L, respectively. Takaya et al. reported results similar to those in this study. The ammonium adsorption capacity of oakwood hydrochar and greenhouse waste biochar increased with an increase in initial concentration. However, when the initial concentration reached 1100 mg N/L, the adsorption capacity of these two materials simultaneously decreased sharply. The author has not given a specific explanation of this phenomenon. In another study, there was a decrease in ammonium adsorption capacity of NaOH-treated corn stalk biochar when initial concentrations exceeded 400 mg/L [125].
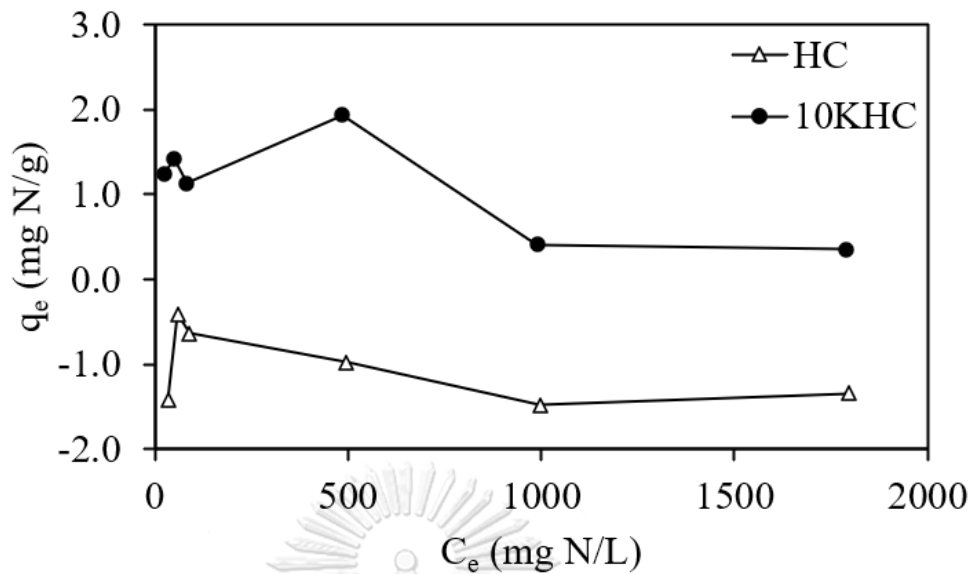
Figure 13. Effect of initial ammonium concentration on adsorption of HC and

10KHC for 48h

The adsorption efficiency of ammonium using different adsorbents is strongly defended on many factors, generally categorized into aspects: preparation conditions and adsorption conditions [153]. In terms of preparation conditions, it encompasses many factors such as types of feedstock and thermochemical parameters that significantly affect the effectiveness of adsorbents. For instance, in the study of Takaya et al., the ammonium adsorption capacity of oak wood hydrochar decreased when the initial concentration was over 800 mg N/L. At the same time, that of greenhouse waste hydrochar was continuously increased. Moreover, the influence of pyrolysis temperature on the ammonium removal efficiency of greenhouse waste biochar was clearly shown in this paper [10]. The effectiveness of the material in removing pollutants depends not only on its physicochemical properties but also on the influence of environmental conditions. The removal efficiency of adsorbent decreased once higher ammonium initial concentration [10, 154]. Higher ammonium

removal efficiency (70 – 80%) was achieved using rice husk and biochars under medium range concentration (250 – 1000 mg N/L) and dropped to 50% once over 1000 mg N/L of the initial concentration [154]. It can be attributed to the low adsorption capacity of biochar [153].

Moreover, pH plays a vital role in the ammonium adsorption capacity of each adsorbent. In the study of Liu et al., the optimum pH for this adsorption was neutral (pH = 7) [125]. There was a lower ammonium removal efficiency at the lower or higher optimum pH ranges. When pH is larger than 7, most ammonium can be converted to $NH_3.H_2O$, resulting in the reduction of ammonium adsorption [155]. Conversely, when the pH solution is very low, the competition between ammonium ions and hydrogen ions for adsorption sites occurs in the aqueous solution that has resulted in less effectiveness of the adsorption process [125]. The influence of specific surface area of the adsorbent on ammonium adsorption has not been answered clearly and consistently. For instance, Takaya et al. found a similar ammonium adsorption capacity onto presscake and commercial oak biochars, although their specific surface areas were very different (2.5 and 280 m^2/g, respectively) [10]. Meanwhile, Kizito et al. reported the important role of larger specific surface area to higher ammonium adsorption of wood biochar over rice husk biochar [154].

Therefore, the decrease in adsorption capacity with the overloading of ammonium concentration in this study is probably because of its moderate adsorption capacity. It can be attributed to the chemical composition of rice husk and MHTC conditions. Or it could be a combination of the effect with the pH leading to a deterioration of the effectiveness of the adsorbent.

The linearized Freundlich isotherm model did not fit the experimental data for HC and 10KHC, but the Langmuir model can better present this study. The plot of Langmuir isotherm of ammonium adsorption onto HC and 10KHC is shown in **Figure 14**, and the corresponding parameters are presented in **Table 14**.
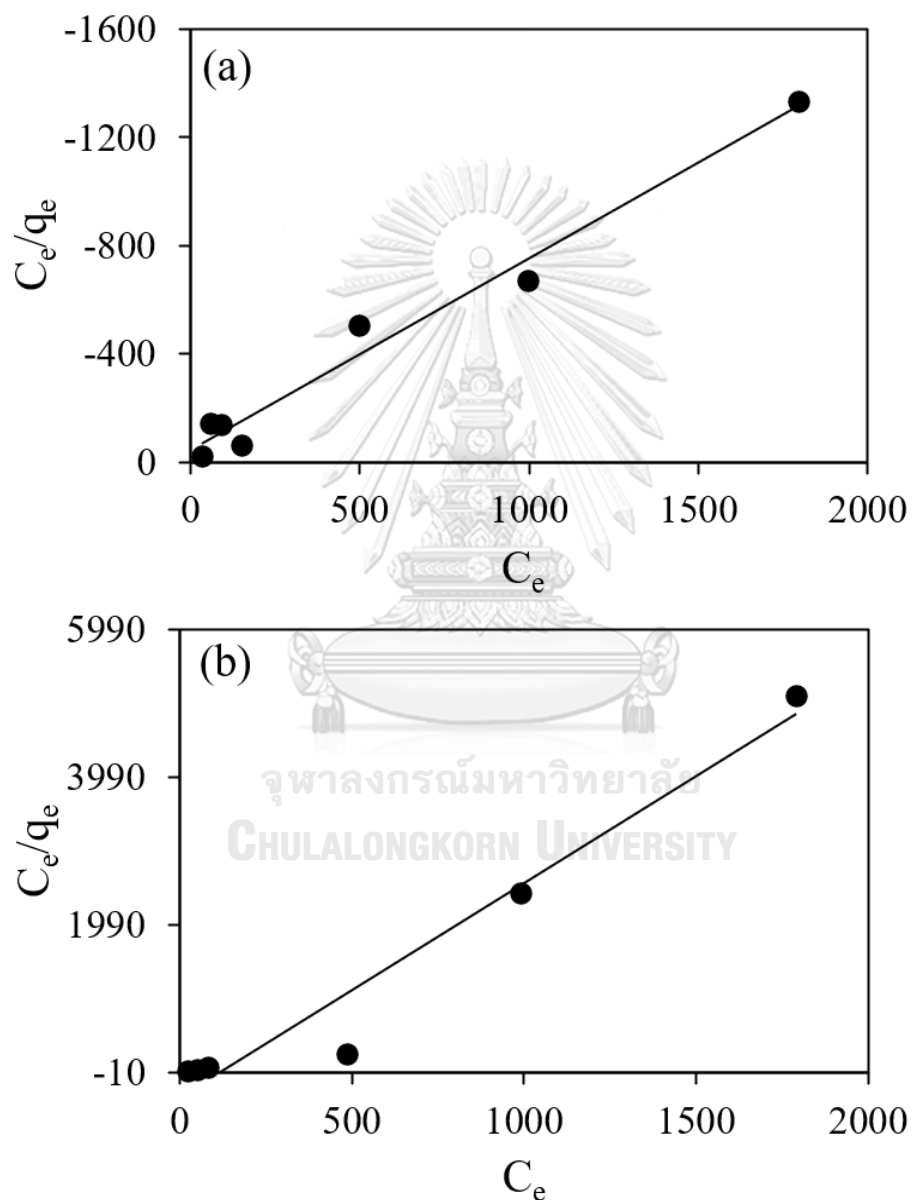
Figure 14. Langmuir model for ammonium adsorption of (a) HC and (b) 10KHC

The ammonium adsorption was better fitted with the Langmuir isotherm model, with R^2 values of HC (0.98) and 10KHC (0.96). It is suggested that there was a monolayer formation between the contaminant and a homogenous surface area [103, 156]. The maximum adsorption capacity of 10KHC (q_m = 0.35 mg N/g) calculated from the Langmuir model was lower than the observed experimental data. It can be the result of the lower adsorption capacity of ammonium at the higher initial concentration (greater than 500 mg N/L). The study of Shin et al. reported the better fit with the Langmuir model for ammonium adsorption onto biochar, with the R^2 value of 0.93 [156]. Similarly, the sorption of ammonium onto the oakwood and greenhouse waste hydrochar obtained under 250°C was best fitted to the Langmuir model with the R^2 values of 0.97 – 0.99. However, the maximum ammonium adsorption capacity of these adsorbents was negative [10]. Nazari et al. showed the increase of Na^+ and K^+ contents in solution after ammonium adsorption by Victorian brown coal, by 0.1 to 49.2 mg/L and 5.2 to 57.2 mg/L, respectively [157]. It can be deduced that ion exchange is the dominant adsorption mechanism to eliminate ammonium by the adsorbent in the aqueous environment.

Table 14. Ammonium adsorption parameters of HC and 10KHC fitting to Langmuir model

Sample	Langmuir		
	q_m (mg N/g)	K_L (L/mg)	R^2
HC	-1.14	0.015	0.9761
10KHC	0.35	-0.0088	0.9581

4.5 Hydrochar characterization

4.5.1 Surface properties

Physical properties of the adsorbent play a critical role in controlling the behavior of the prepared materials in the adsorption process. The specific surface area, total pore volume and pore diameter of pristine hydrochar and chemical-activated hydrochar are shown in **Table 15**.

Table 15. Surface properties of chemical-treated and untreated rice husk hydrochars

Sample	SSA (m^2/g)	Total pore volume (cm^3/g)	Pore diameter (nm)
HC	13.09	0.033	11.43
10KHC	5.16	0.016	12.66
5HHC	11.51	0.037	11.39

The activation of rice husk hydrochar changed in its porous properties depended on the catalysts. The specific surface of rice husk hydrochar (HC) produced at 175°C for 60 min with the L-S ratio of 5:1 (mg/L) was 13.09 m^2/g. Notably, this hydrochar produced under moderate temperature showed a higher specific surface area than other materials such as corn stalk hydrochar (produced at 250°C, 3.8 m^2/g) [17], rice husk biochar (produced at 600°C, 6.1 m^2/g) [67]. After activation using H$_2$O$_2$ and KOH solutions, the specific surface areas of 10KHC and 5HHC were decreased down to 5.16 and 11.51 m^2/g, respectively.

The average pore diameters of HC, 10KHC, and 5HHC were 11.43, 12.66, and 11.39 nm, respectively. It showed that mesopores were dominant in these three adsorbents. The total volume of HC was 0.033 cm^3/g, which was higher than that of 10KHC

(0.016 cm^3/g) and slightly lower than that of 5HHC (0.037 cm^3/g). Due to the molecular diameter of atrazine (0.4 – 0.9 nm), the presence of mesopores in the adsorbents is facilitated the atrazine diffusion into the inner pores, which enhances the adsorption ability of the materials [123].

Jaramillo et al. observed similar changes in the porous properties of cherry stone-derived biochar after activation using the H$_2$O$_2$ solution. Notably, while the specific surface area of originated biochar decreased from 604 to 591 m^2/g after H$_2$O$_2$ treatment, its total mesopore volume increased from 0.069 to 0.087 cm^3/g. It concluded that H$_2$O$_2$ oxidant did not work effectively than HNO$_3$, O$_2$ and O$_3$ [158]. The decrease in specific surface area of H$_3$PO$_4$-activated rice straw biochar (192.3 m^2/g) was reported, which was attributed to the increase in functional groups inside its pores [67]. However, the specific surface area of corn stalk biochar was dramatically increase after H$_2$O$_2$ treatment (169.8 m^2/g) [17]. Therefore, the differences in the effectiveness of activation treatment between studies varied by types of feedstocks or catalyst concentrations [17, 158].

4.5.2 Surface functional groups

FT-IR spectra of untreated and treated hydrochars before and following atrazine adsorption is illustrated in **Figure 15**. The results showed that many peaks represented aromatic and oxygen-containing functional groups were observed on the surfaces of HC, 10KHC, and 5HHC. The peak at 1100 – 1000 cm^{-1} was assigned to the antisym stretching of Si–O–Si [159, 160]. A broadband peak was presented for both untreated and treated hydrochar at around 3400 – 3300 cm^{-1} exhibited the –OH stretching vibration [119]. This group has obtained either alcohol from cellulose, hemicellulose, lignin, carboxylic acids, silanol group (Si–OH), or the water adsorbed by rice husk

throughout the MHTC [161]. Peaks at around 1275 and 800 cm^{-1} were represented to aliphatic C─H stretching and aromatic C─H stretching, respectively [66]. The C═O vibration of the esters, ketones, and aldehydes in hemicellulose was observed at around 1726 cm^{-1} [162]. The peak around 1603 and 1382 cm^{-1} were attributed to the C═C stretching vibration and ─COOH, respectively [17, 163]. It can be observed that the surface functional groups had not been dramatically changed between untreated hydrochar and KOH or H_2O_2-activated hydrochar.

The adsorption of atrazine onto both treated and untreated hydrochars has resulted in changes in some vibration peaks. The C═O peak became less intense and flatter for hydrochar and H_2O_2-activated hydrochar after atrazine adsorption. This result is in accordance with the results of atrazine-adsorbed biochar produced from different feedstocks [66]. Besides, the presence of the polar groups such as ─COOH, C═O, ─OH on both untreated and treated hydrochar has suggested the contribution of H-bonding interactions. In this case, atrazine can act as an H-bond donor and H-bond acceptor [85]. Aromatic peaks were observed on the surfaces of three materials. The presence of the aromatic groups can affect the hydrophobicity of the materials, which simultaneously influences atrazine adsorption via π-π electron donor-acceptor [85, 86].
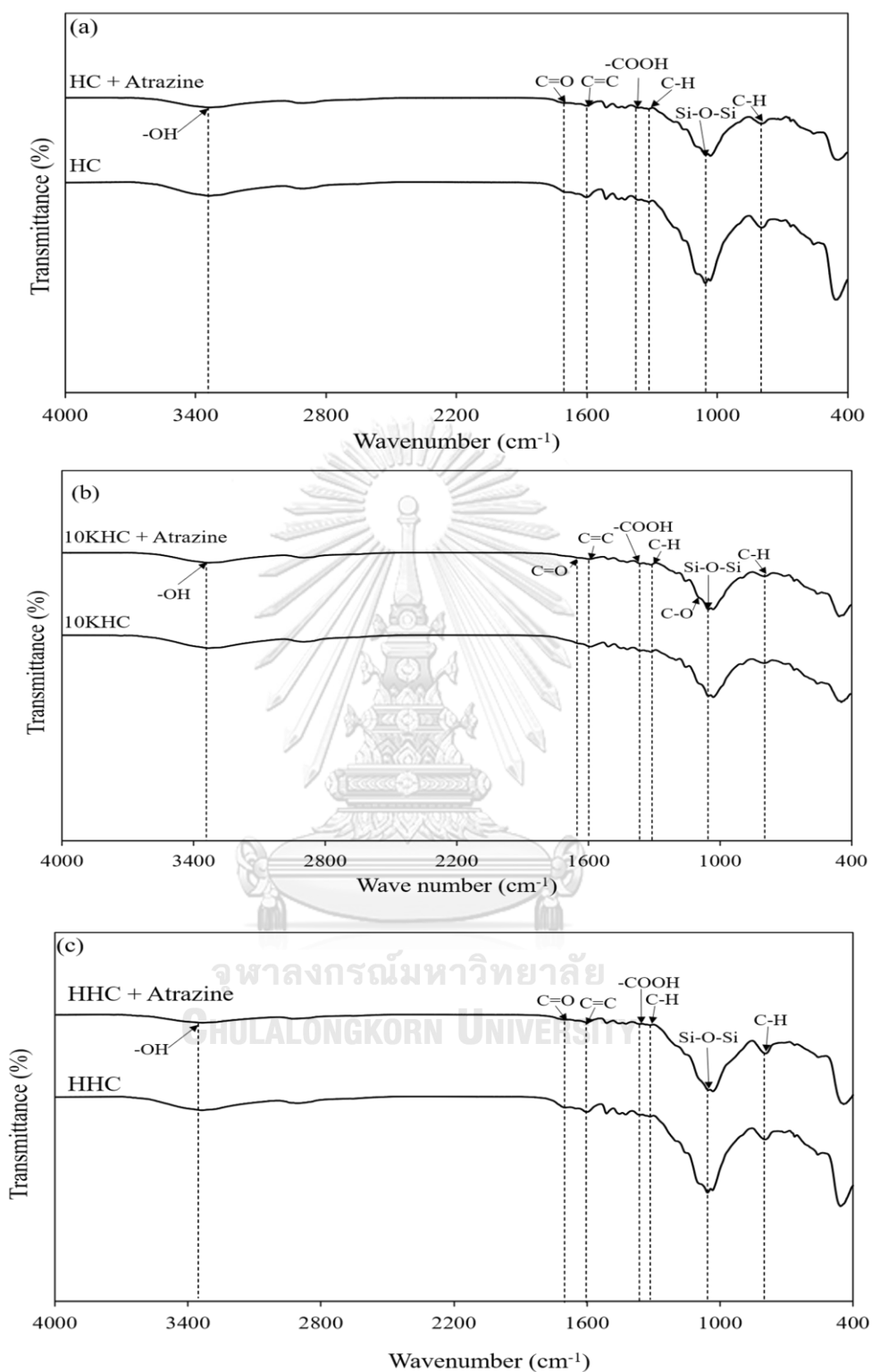
Figure 15. FT-IR spectra of (a) HC, (b) 10KHC, and (c) 5HHC before and after

atrazine adsorption

4.5.3 XPS analysis

The results of FT-IR have indicated the presence of various functional groups on the surface of adsorbents which could be quantitatively investigated using XPS. The C1s core level of HC, 10KHC and 5HHC before and after atrazine adsorption could be deconvoluted into four different peaks, as illustrated in **Figure 16** and **Table 16** [17, 63, 66, 164].

Table 16. Binding energy of functional groups for C1s

Functional groups	Binding energy
C=C, CH$_x$ and C—C	284.7 ± 0.2 eV
C—OR	285.7 ± 0.2 eV
C=O, O=C—O	288.0 ± 0.2 eV
—COOR	289.2 ± 0.2 eV

The chemical compositions of the rice husk hydrochar had been differently changed after activation treatment using KOH and H$_2$O$_2$ treatment, as illustrated in **Figure 16 (a,b,c)**. With pristine hydrochar, the total contents of aromatic compounds and oxygen-containing functional groups were 54.6% and 45.4%, respectively. There was a remarkable increase in the content of oxygen-containing functional groups after KOH treatment. The total abundance bonds of C—OR, C=O (C=O—O), and —COOR increased from 34.4 to 56.1%, 7.8 to 10.7%, and 3.3 to 5.2% between HC and 10KHC, respectively. The corresponding decrease in the carbon contents (C=C, CH$_x$ and C—C) occurred from 54.6 to 28.0% of HC after KOH treatment. With the similar performance of KOH treatment, the content of C=C, CH$_x$ and C—C bonds in 5HHC (53.3%) was slightly lower than that of HC (54.6%). Simultaneously, there was an

increase in ─COOR bonds from 3.3% to 4.8% between 5HHC and HC. Thus, the changes in the contents of functional groups on the adsorbents after the activation treatments could affect the atrazine removal.
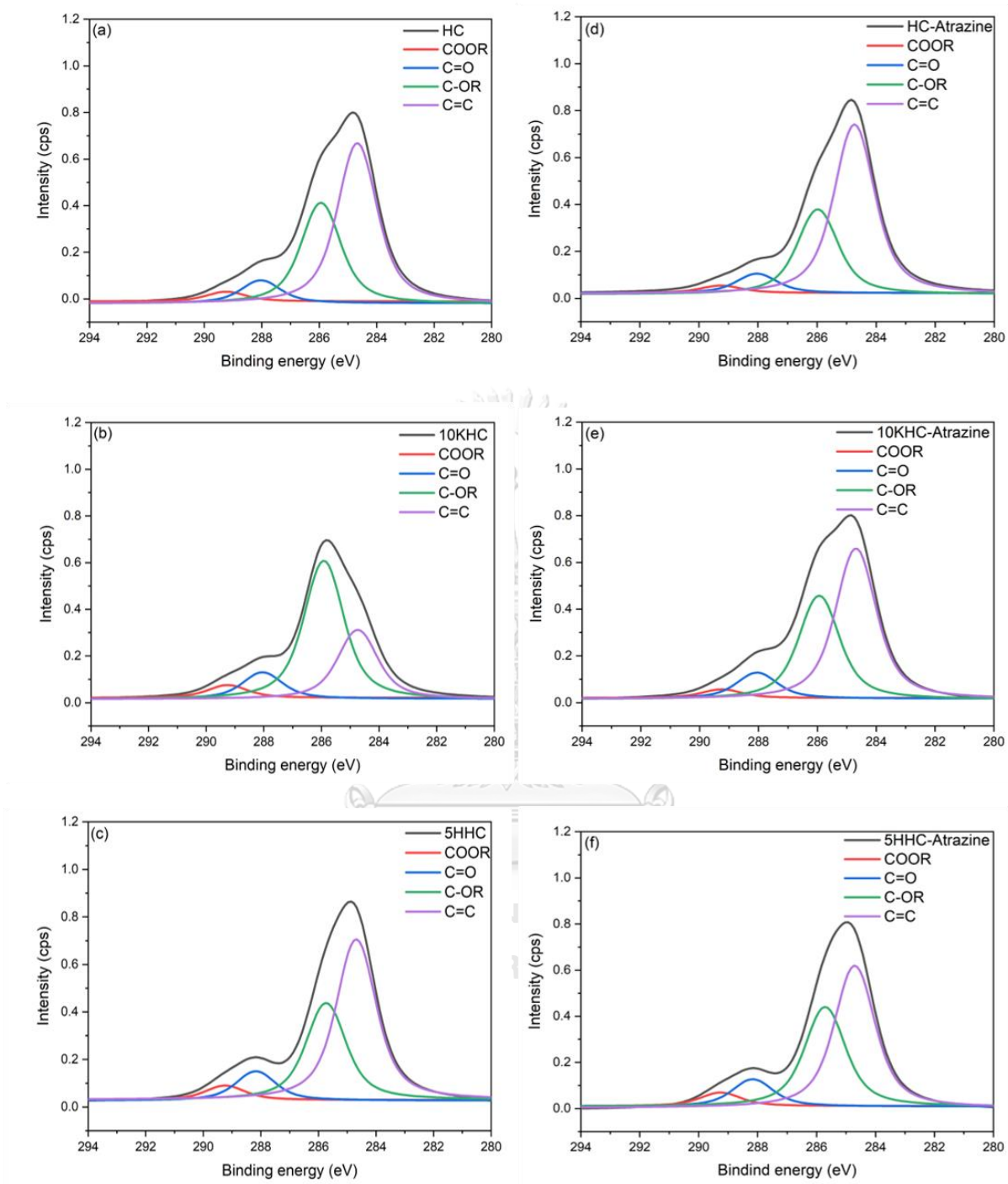
Figure 16. XPS survey spectrum of (a,d) HC, (b,e) 10KHC and (c,f) 5HHC before

and after atrazine adsorption

The quantitative contents of surface functional groups of the pristine and activated hydrochar before and after atrazine adsorption were shown in **Figure 17**. There was a significant decrease in oxygen-containing functional groups of the pristine hydrochar after atrazine adsorption for 24h, from 34.4 to 30.2% for C─OR groups, 7.8 to 6.9% for C═O groups, and 3.3 to 2.6% for ─COOR groups. A similar reduction of these functional groups was found in 10KHC after atrazine adsorption. The contents of C─OR, C═O, and ─COOR groups were diminished from 56.1 to 35.9%, 10.7 to 9%, and 5.2 to 3.0%, respectively. It indicated that oxygen-containing functional groups played a crucial role in atrazine adsorption of HC and 10KHC. Meanwhile, the decrease in carbon compounds (C═C, CH_x and C─C) and C═O occurred in 5HHC from 53.3 to 50.3% and 9.8 to 9.7%, respectively. Therefore, the presence of oxygen-containing functional groups plays a vital role in atrazine adsorption onto HC and 10KHC, but aromatic compounds (C═C, CH_x and C─C) significantly enhanced this adsorption performance of 5HHC.
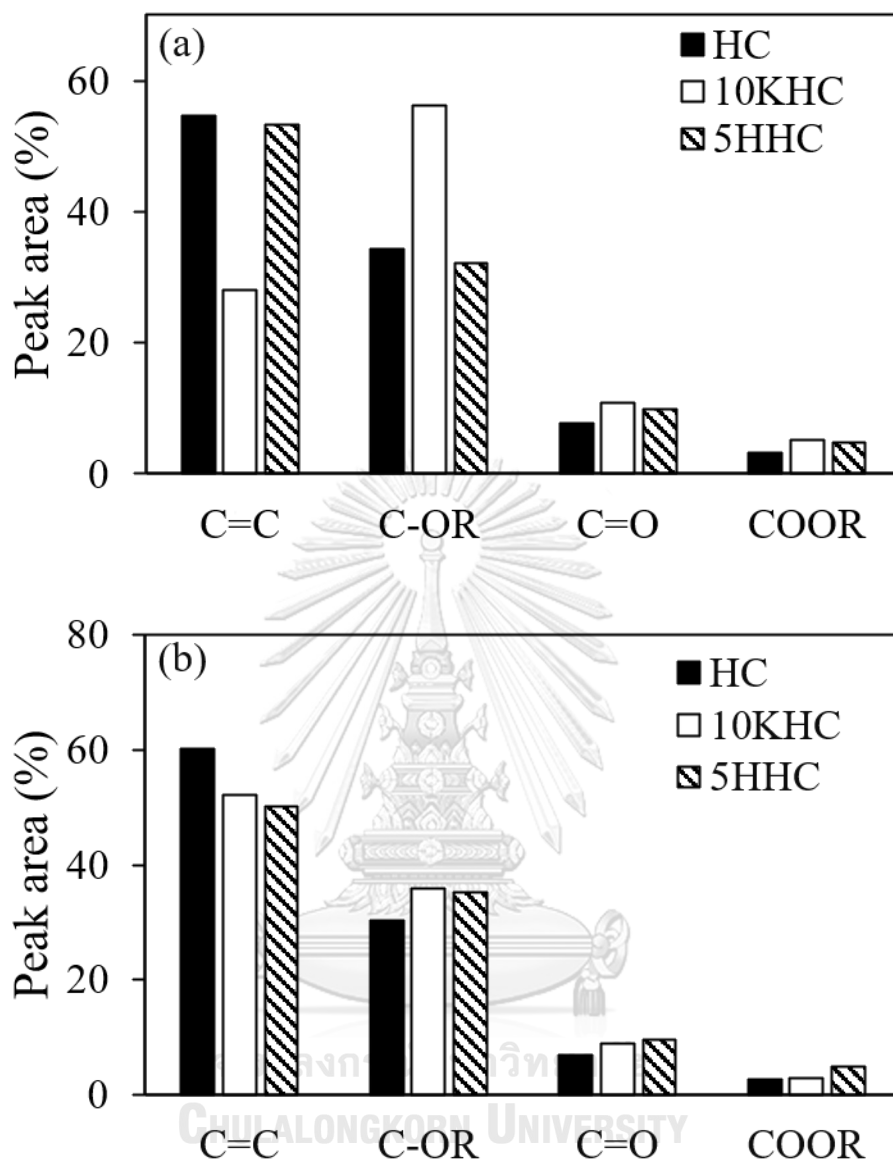
Figure 17. Integrated areas of functional groups on pristine and activated hydrochar

before (a) and after (b) atrazine adsorption

4.5.4 Cation exchange capacity (CEC)

CEC analysis was investigated with two rice husk hydrochars (i.e., HC and 10KHC)

used in the ammonium adsorption kinetic and isotherm studies, as presented in **Table**

17. The CEC value of rice husk hydrochar after KOH treatment was increased over

two-time than that of the original material. Although KOH treatment substantially improved CEC of rice husk hydrochar, this value is still lower than other available materials. For instance, hydrochar derived from oak wood, greenhouse waste, municipal waste, and presscake from anaerobic digestate under 250°C had the CEC values of 88.3, 83.1, 44.5, and 62.6 cmol/kg, respectively [10]. The CEC values of biochar obtained from pine sawdust and wheat straw biochars under 550°C were 29.0 and 30.5 cmol/kg, respectively [147]. It was reported that negative surface charge of the adsorbent had a greater role than the specific surface area in ammonium adsorption [10]. The effectiveness of cation adsorption has a positive relation to CEC values [10, 137, 147].

Table 17. CEC of pristine and KOH-activated hydrochar

Sample	CEC (cmol/kg)
HC	8.11
10KHC	16.38

4.6 Implication of adsorption mechanisms

4.6.1 Possible atrazine adsorption mechanisms

The effectiveness of the carbonized material in the adsorption application is generally controlled by many factors such as large specific surface area and numerous surface functional groups [63]. The atrazine adsorption mechanisms on pristine and chemical-activated rice husk hydrochar are presented in **Figure 18**. According to the XPS data, KOH treatment significantly enhanced the contents of oxygen-containing functional groups on the 10KHC. The decrease in these compounds (C─OR and C═O (C═O─O)) after atrazine adsorption has proven their crucial role in the 10KHC

performance. Although HC and 5HHC possessed a comparative specific surface area (13.09 and 11.51 m^2/g, respectively), the atrazine adsorption capacity of 5HHC was slightly better than that of HC. It can be explained by the presence of aromatic compounds like C═C, CH_x, and C─C, which can act as π-electron acceptor and atrazine acts as π-electron donor. The formation of new bonds between atrazine and aromatic compounds of 5HHC enhanced the atrazine removal. In general, both the oxygen-containing functional groups and aromatic groups contribute to the atrazine adsorption of the material. However, the atrazine removal of KOH-activated hydrochar was slightly effective than the other prepared hydrochar. It means that these oxygen-containing functional groups predominate in the chemical reaction to atrazine.

Besides, these rice husk hydrochars were produced under low temperature, which has resulted in the existence of non-carbonized fractions. It is possibly deduced that atrazine can partly partition into this fraction [17, 137].
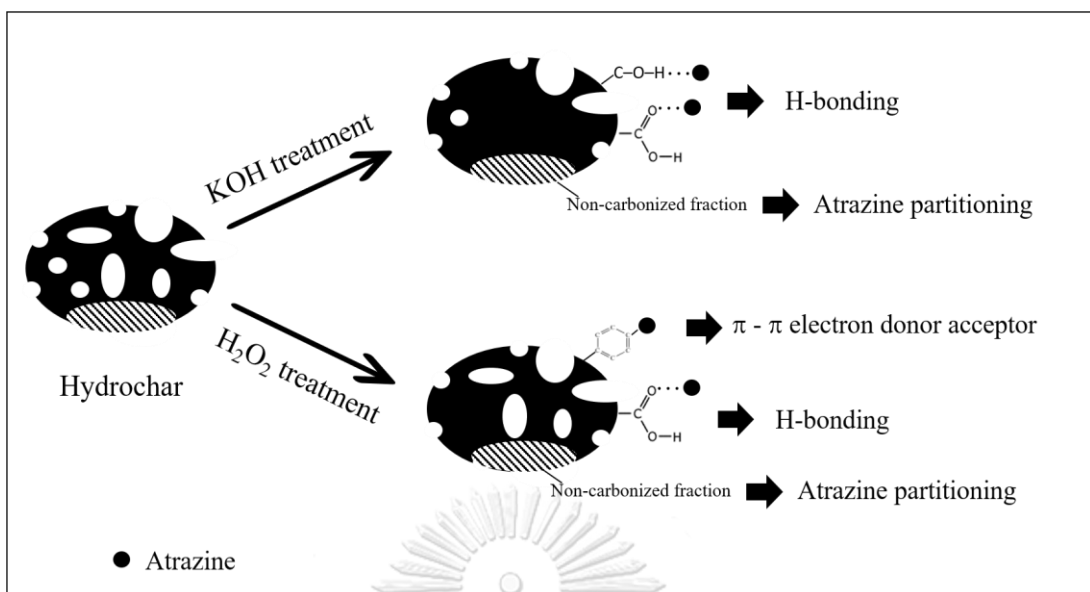
Figure 18. A schematic diagram of atrazine adsorption mechanisms on pristine and chemical-activated rice husk hydrochar

4.6.2 Possible ammonium adsorption mechanisms

According to Tan et al., the ammonium adsorption mechanisms can encompass electrostatic attraction, ion exchange and physical adsorption [165]. In this study, the ammonium adsorption of these hydrochars was fitted with the pseudo-second-order kinetic model. It is suggested that chemisorption was a predominant mechanism for ammonium sorption. In addition, ammonium adsorption capacities of pristine and KOH-activated hydrochars were positively related to CEC. Therefore, ion exchange can be the main reaction between ammonium and rice husk hydrochars. It is consistent with the adsorption mechanism between ammonium and wheat straw biochar [147] and corn cob hydrochar [103].

4.7 Atrazine desorption

The atrazine desorption capacity from rice husk hydrochar was from 0.09 – 0.82 mg/g after 24h, as presented in **Table 18**. According to Maldal et al., the amount of atrazine desorption depends on the adsorbent properties and the pollutant concentration [67].

Table 18. The Freundlich isotherm parameters of atrazine desorption from hydrochar

	Freundlich			q_{des}	H
	K_{Fdes}	$1/n_{Fdes}$	R^2	(mg/g)	$[(1/n_{Fdes})/(1/n_{Fads})]$
HC	0.248599	0.9987	1	0.09 – 0.82	1.27

The experimental data exhibited a good fit with the Freundlich model ($R^2 = 1$), with the Freundlich constant ($1/n_{Fdes}$) of hydrochar smaller than 1, as shown in **Table 18** and **Figure 19**. The hysteresis (H) for atrazine desorption from hydrochar was calculated based on the Freundlich constants of adsorption and desorption. When H value is larger than 1, the hysteresis is negative. In contrast, positive hysteresis occurs when the H value is smaller than 1. In this study, the desorption of atrazine from hydrochar was negative hysteresis (H = 1.27). Atrazine adsorption showed the best fitted with the Freundlich model, which suggested the multilayer atrazine adsorption onto the heterogeneous surfaces. This similar result was reported in the study of atrazine desorption from biochars derived from bamboo chips (H = 1.16), corn cob (H = 1.09), eucalyptus bark (H = 1.09), and rice straw (H = 1.14) [67]. The positive hysteresis of pollutant desorption is attributed to irreversible interaction or sequestration of pollutant and organic carbon content of the adsorbent [166] and/or the capture of this pollutant in meso- and micro-pores of the adsorbent [167].

However, it is difficult to point out which one more prominent contribution to the hysteresis of the adsorbent.
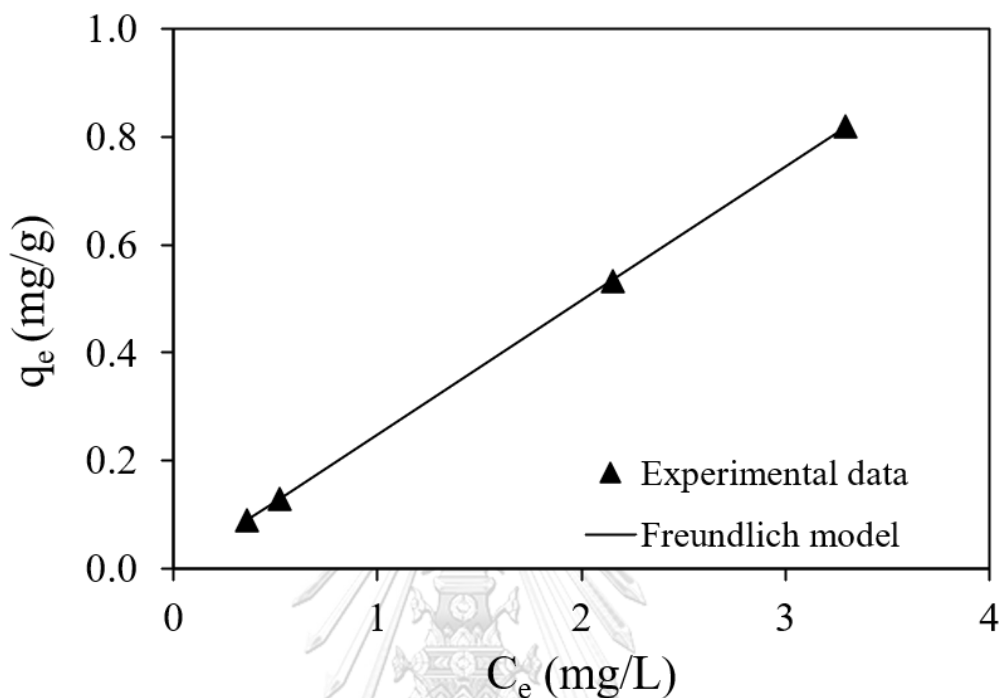
Figure 19. Freundlich isotherm for atrazine desorption from hydrochar

To develop a biomass-based material into nitrogen slow-release fertilizer, the desorption study is required. However, the prepared adsorbents in this study had low ammonium adsorption capacity (by 3.25 - 3.89 mg N/g) compared with materials available on the market. For example, cotton stalk biochar was activated using 1M NaOH extremely adsorbed ammonium with 93.4 mg N/g [125], or KOH-activated corn cob hydrochar had the ammonium adsorption capacity at the equilibrium time by approximately 9 mg N/g [102]. Therefore, the desorption study for ammonium-adsorbed hydrochar was not performed in this study.

4.8 Comparison of atrazine adsorption between hydrochar and biochar

The atrazine adsorption capacity of pristine and activated rice husk hydrochar was compared with that of commercial biochar (BC), as illustrated in **Figure 20**. This

biochar was purchased from the farmer who produced it from various agricultural residues in the Nan province, Thailand. The result showed that both pristine hydrochar and activated hydrochar significantly adsorbed higher atrazine in the aqueous environment than biochar. The atrazine adsorption capacity of this biochar was low by 0.41 ± 0.1 mg/g, which was approximately 6 times lower than 10KHC. The most effective adsorbent for atrazine adsorption was 10KHC, followed by 5HHC (2.10 ± 0.0 mg/g) and HC (1.97 ± 0.1 mg/g).
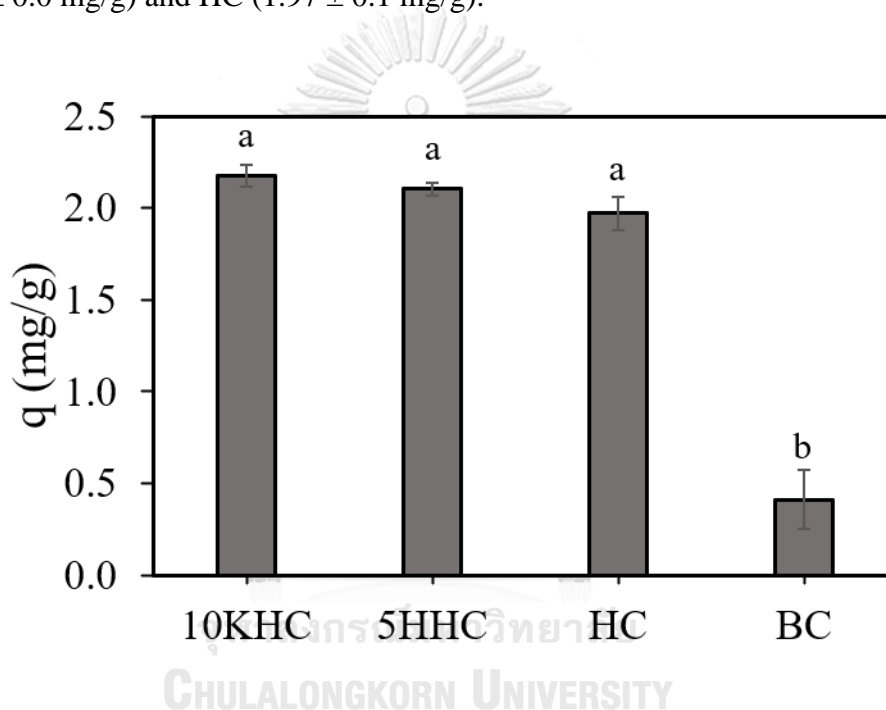
Figure 20. The atrazine adsorption capacity of studied rice husk hydrochar and commercial biochar

Means in each bar graph followed by the same letter are not significantly different ($p < 0.05$)

The physical properties of this biochar were characterized by BET analysis and presented in **Table 19**. It can be seen that the specific surface area of this biochar (31.15 m^2/g) was dramatically higher than that of 10KHC (5.16 m^2/g), 5HHC (11.51 m^2/g), and HC (13.09 m^2/g). The commercial biochar also possessed greater total pore

volume than other pristine and activated rice husk in this study. It can be deduced that the physical properties of the material such as specific surface area, pore volume, and pore size did not play a controllable role in the removal of atrazine. This finding was consistent with the study of Liu et al. corn stalk hydrochar with higher specific surface area (4.9 m^2/g) did not adsorb better atrazine than the hydrochar with lower surface area (3.8 m^2/g) [17].

Table 19. Physical properties of commercial biochar

Sample	SSA (m^2/g)	Total pore volume (cm^3/g)	Pore diameter (nm)
BC	31.15	0.068	8.72

4.9 Potential utilization of rice husk hydrochar

The sorption and characterization results revealed that rice husk hydrochar is a promising candidate for atrazine-contaminated soil remediation. When rice husk hydrochar is added to the soil, this material would fix atrazine onto its surface through the adsorption process. Such phenomenon reduces the leaching into groundwater or surface water and the surrounding areas. Nevertheless, this method cannot remove or reduce the contaminant concentration in the environment. Therefore, a material considered to be efficient and highly applicable should either be attached to atrazine-degrading bacteria or be able to hold atrazine for long periods.

Although rice husk hydrochar exhibited potentially atrazine adsorption, how it would be applied into contaminated sites is another interesting topic. The suggestion for possible rice husk hydrochar used in soils is presented in **Figure 21**. The prepared adsorbent would be applied to the topsoil of agricultural areas to prevent atrazine

leaching into groundwater or the surrounding environment. In the study of Cao et al., biochar was mixed with soils (from 0 – 20 cm) that effectively reduced atrazine concentration after extraction by 66% [54]. Moreover, Shen et al. mixed soil, biochar and compost, and then applied to the soils to immobilize contaminants and revegetation of contaminated areas [168].

In addition to its adsorption performance, rice husk hydrochar also represents cost efficiency. The ammonium releasing properties found in the rice husk hydrochar in this study should be considered the promising nitrogen source, which is regarded as the majority cost in agriculture. Therefore, it is recommended that further studies should be conducted about the effects of soil organic contents and pH on the atrazine adsorption to rice husk hydrochar as well as its nitrogen releasing behavior before full-scale application.
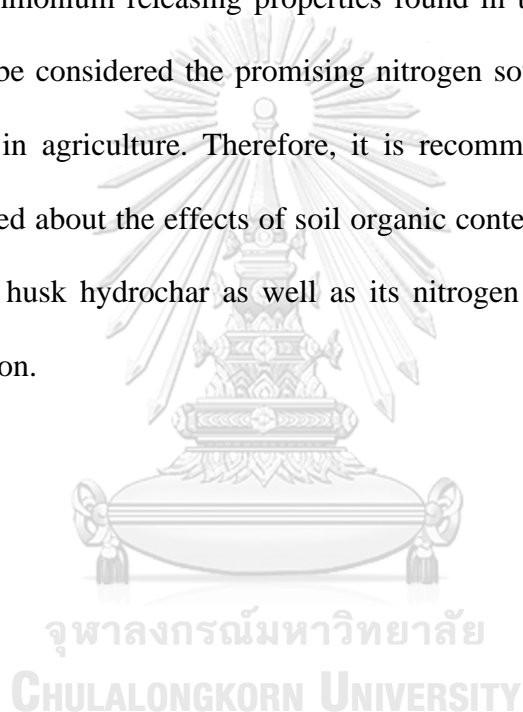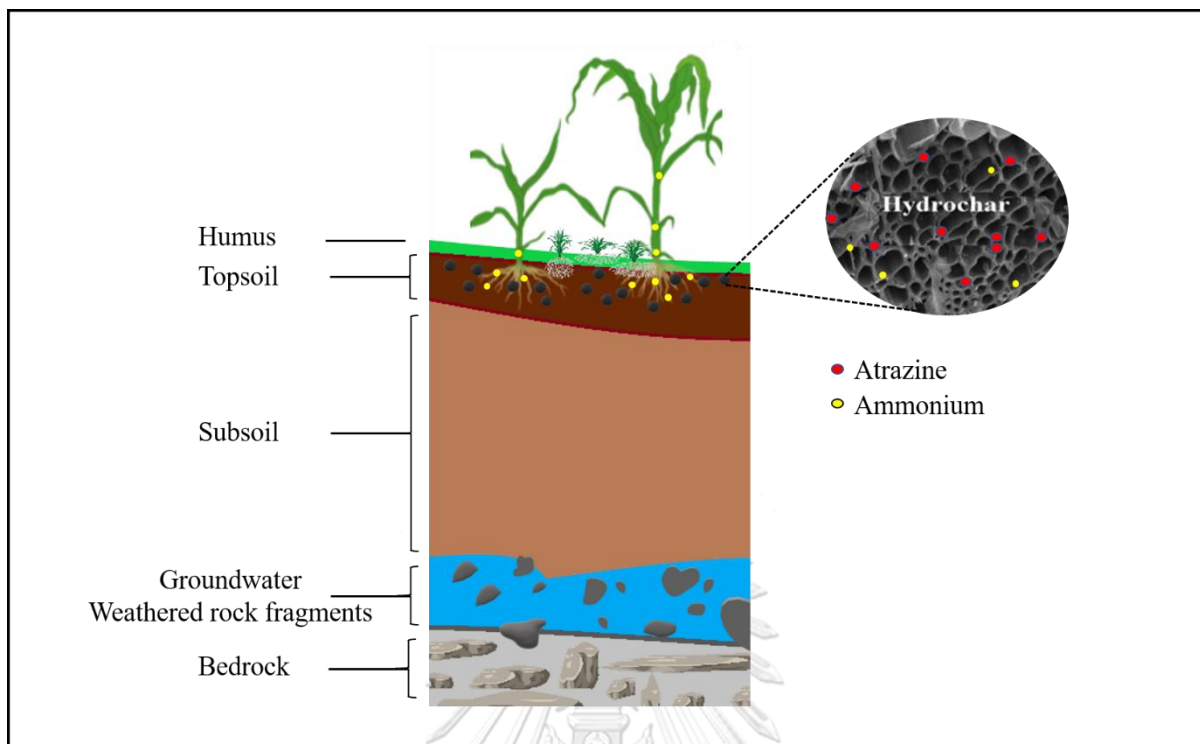
Figure 21. Suggested rice husk hydrochar application into the soils

CHAPTER V CONCLUSIONS AND RECOMMENDATIONS

5.1 Conclusions

The activation of rice husk hydrochar to enhance atrazine and ammonium adsorption was investigated in this study. Rice husk hydrochars produced under various MHTC conditions showed promising atrazine adsorption capacities, while only some of them could remove ammonium in the aqueous environment. Rice husk hydrochar produced under higher temperature (175 - 200°C) and residence time (60 min) and lower L-S ratio (5:1 to 10:1 mL/g) achieved better atrazine and ammonium adsorption capacities. Activation treatment using H_2O_2 and KOH solutions was exhibited different influences on the physicochemical properties of the rice husk hydrochar. KOH treatment increased oxygen-containing functional groups on the rice husk hydrochar, while increased aromatic compounds of H_2O_2-activated hydrochar were observed. These changes have proved the dominant role of H-bonding interaction and π-π electron donor-acceptor interaction for atrazine adsorption mechanisms of KOH-activated hydrochar and H_2O_2-activated hydrochar, respectively. The results of atrazine desorption from rice husk hydrochar demonstrated a negative hysteresis. Conversely, only KOH activation treatment effectively enhanced the ammonium adsorption of the pristine hydrochar. Although both pristine and activated hydrochars showed an increase in ammonium adsorption capacity over time, they did not present a promising performance at higher initial ammonium concentration. Moreover, several rice husk hydrochars released ammonium instead of adsorption. This might be due to the hydrolysis of lignin of rice husk during the hydrothermal process. Therefore, these novel properties of rice husk hydrochar could be used as a sustainable atrazine adsorbent to limit contaminant mobility in the environment and

simultaneously be used as a nitrogen fertilizer, which could reduce the fertilizer cost in agriculture.

5.2 Recommendations

- KOH treatment improved atrazine and ammonium adsorption capacities of rice husk hydrochar, but its effectiveness is still moderate. Further study is recommended to determine the effect of activation time and temperature.

- Rice husk hydrochar showed a promising result for atrazine adsorption in the aqueous environment. To effectively apply into the soil, the effect of pH and soil organic matter on the atrazine adsorption is recommended.

- There was a positive relation between CEC values of the adsorbent and ammonium adsorption. However, rice husk hydrochar prepared in this study was low even after the KOH activation process, so another activation treatment to enhance CEC values of rice husk hydrochar is suggested. For example, the material can be coated with positive charge chemicals (i.e., the amalgamation of iron and potassium) or activated at a higher temperature.

- In addition to increasing CEC, pH solution is also an essential factor that can affect ammonium adsorption. Thus, it is suggested to study the effect of pH in a future study to apply this material as a slow-release fertilizer.

- The release of ammonium from pristine and H_2O_2-activated rice husk hydrochar has been drawn as an interesting idea. These materials have the potential to apply as a soil conditioner by providing essential nutrients for plant development.

- Rice husk has become a green treasure in other industries by its silicon (SiO_2) contents; thus, the cost analysis for rice husk hydrochar application is needed the future study.

จุฬาลงกรณ์มหาวิทยาลัย
CHULALONGKORN UNIVERSITY

REFERENCES

[1]   United Nations. <u>World Population Projected to Reach 9.6 Billion by 2050</u> [Online]. 2013. Available from: https://www.un.org/en/development/desa/news/population/un-report-world-population-projected-to-reach-9-6-billion-by-2050.html

[2]   EPA, U. 4 - Atrazine. in Cheremisinoff, N.P. and Rosenfeld, P.E. (eds.),<u>Handbook of Pollution Prevention and Cleaner Production: Best Practices in the Agrochemical Industry</u>, pp. 215-231. Oxford: William Andrew Publishing, 2011.

[3]   de Albuquerque, F.P., de Oliveira, J.L., Moschini-Carlos, V., and Fraceto, L.F. An overview of the potential impacts of atrazine in aquatic environments: Perspectives for tailored solutions based on nanotechnology. <u>Science of the Total Environment</u> 700 (2020): 9.

[4]   Humans, I.W.G.o.t.E.o.C.R.t. and Cancer, I.A.f.R.o. <u>Some chemicals that cause tumours of the kidney or urinary bladder in rodents and some other substances</u>. International Agency for Research on Cancer, 1999.

[5]   Nodler, K., Licha, T., and Voutsa, D. Twenty years later - Atrazine concentrations in selected coastal waters of the Mediterranean and the Baltic Sea. <u>Marine Pollution Bulletin</u> 70(1-2) (2013): 112-118.

[6]   Arogo, J., Westerman, P.W., and Heber, A.J. A review of ammonia emissions from confined swine feeding operations. <u>Transactions of the Asae</u> 46(3) (2003): 805-817.

[7]   Netz, B., Davidson, O., Bosch, P., Dave, R., and Meyer, L. Climate change 2007: Mitigation. Contribution of Working Group III to the Fourth Assessment Report of the Intergovernmental Panel on Climate Change. Summary for Policymakers. <u>Climate change 2007: Mitigation. Contribution of Working Group III to the Fourth Assessment Report of the Intergovernmental Panel on Climate Change. Summary for Policymakers.</u> (2007).

[8]   Tirado, R. Nitrates in drinking water in the Philippines and Thailand. <u>Greenpeace Research Laboratories Technical Note</u> 11 (2007): 2007.

[9]   Wang, Z.H., et al. Biochar produced from oak sawdust by Lanthanum (La)-

involved pyrolysis for adsorption of ammonium (NH4+), nitrate (NO3-), and phosphate (PO43-). Chemosphere 119 (2015): 646-653.

[10] Takaya, C.A., Fletcher, L.A., Singh, S., Anyikude, K.U., and Ross, A.B. Phosphate and ammonium sorption capacity of biochar and hydrochar from different wastes. Chemosphere 145 (2016): 518-527.

[11] Naz, M.Y. and Sulaiman, S.A. Slow release coating remedy for nitrogen loss from conventional urea: a review. Journal of Controlled Release 225 (2016): 109-120.

[12] Chen, X., Lin, Q., He, R., Zhao, X., and Li, G. Hydrochar production from watermelon peel by hydrothermal carbonization. Bioresource technology 241 (2017): 236-243.

[13] Li, H., Dong, X., da Silva, E.B., de Oliveira, L.M., Chen, Y., and Ma, L.Q. Mechanisms of metal sorption by biochars: biochar characteristics and modifications. Chemosphere 178 (2017): 466-478.

[14] Yang, X., Zhang, S.Q., Ju, M.T., and Liu, L. Preparation and Modification of Biochar Materials and their Application in Soil Remediation. Applied Sciences-Basel 9(7) (2019): 25.

[15] Said, A., Tekasakul, S., and Phoungthong, K. Investigation of Hydrochar Derived from Male Oil Palm Flower: Characteristics and Application for Dye Removal. Polish Journal of Environmental Studies 29(1) (2020): 807-816.

[16] Liu, Z.G. and Zhang, F.S. Removal of lead from water using biochars prepared from hydrothermal liquefaction of biomass. Journal of Hazardous Materials 167(1-3) (2009): 933-939.

[17] Liu, Y.Y., Sohi, S.P., Jing, F.Q., and Chen, J.W. Oxidative ageing induces change in the functionality of biochar and hydrochar: Mechanistic insights from sorption of atrazine. Environmental Pollution 249 (2019): 1002-1010.

[18] Bley, H., Gianello, C., Santos, L.D., and Selau, L.P.R. Nutrient Release, Plant Nutrition, and Potassium Leaching from Polymer-Coated Fertilizer. Revista Brasileira De Ciencia Do Solo 41 (2017): 11.

[19] Chinnamuthu, C. and Boopathi, P.M. Nanotechnology and agroecosystem. Madras Agric J 96(1-6) (2009): 17-31.

[20]   Kalderis, D., Kotti, M.S., Mendez, A., and Gasco, G. Characterization of hydrochars produced by hydrothermal carbonization of rice husk. Solid Earth 5(1) (2014): 477-483.

[21]   Fang, J., Gao, B., Mosa, A., and Zhan, L. Chemical activation of hickory and peanut hull hydrochars for removal of lead and methylene blue from aqueous solutions. Chemical Speciation and Bioavailability 29(1) (2017): 197-204.

[22]   Cusioli, L.F., et al. Modified Moringa oleifera Lam. Seed husks as low-cost biosorbent for atrazine removal. Environmental technology (2019): 1-12.

[23]   Chandra, S., Medha, I., and Bhattacharya, J. Potassium-iron rice straw biochar composite for sorption of nitrate, phosphate, and ammonium ions in soil for timely and controlled release. Science of the Total Environment 712 (2020): 15.

[24]   Soltani, S.M., Yazdi, S.K., and Hosseini, S. Effects of pyrolysis conditions on the porous structure construction of mesoporous charred carbon from used cigarette filters. Applied Nanoscience 4(5) (2014): 551-569.

[25]   Liu, H., Zhang, Y.M., Huang, J., Liu, T., Xue, N.N., and Shi, Q.H. Optimization of vanadium (IV) extraction from stone coal leaching solution by emulsion liquid membrane using response surface methodology. Chemical Engineering Research & Design 123 (2017): 111-119.

[26]   Baghapour, M.A., Nasseri, S., and Derakhshan, Z. Atrazine removal from aqueous solutions using submerged biological aerated filter. Journal of Environmental Health Science and Engineering 11 (2013): 9.

[27]   Ackerman, F. The economics of atrazine. International Journal of Occupational and Environmental Health 13(4) (2007): 437-445.

[28]   Standard), T.T.T.A. Pesticide residues: Maximum residue limits. Standards, N.B.o.A.C.a.F., Editor. 2013: Ministry of Agriculture and Cooperatives, Bangkok, Thailand

[29]   EPA, U. Chemical Assessment Summary: Atrazine. (IRIS), I.R.I.S., Editor. 1993.

[30]   Singh, S., et al. Toxicity, degradation and analysis of the herbicide atrazine. Environmental Chemistry Letters 16(1) (2018): 211-237.

[31]   Jin, R. and Ke, J. Impact of atrazine disposal on the water resources of the Yang

River in Zhangjiakou area in China. <u>Bulletin of Environmental Contamination and Toxicology</u> 68(6) (2002): 893-900.

[32] Tawatsin, A. Pesticides used in Thailand and toxic effects to human health. <u>Medical Research Archives</u> (3) (2015).

[33] Wiley, J. <u>Crop protection chemicals reference</u>. 1986, CHEMICAL AND PHARMACEUTICAL PRESS.

[34] Hörmann, W., Tournayre, J., and Egli, H. Triazine herbicide residues in central European streams. <u>Pesticides monitoring journal</u> 13(3) (1979): 128-131.

[35] Muir, D.C., Yoo, J.Y., and Baker, B.E. Residues of Atrazine andN-deethylated Atrazine in water from five agricultural watersheds in Québec. <u>Archives of environmental contamination and toxicology</u> 7(1) (1978): 221-235.

[36] Correia, F.V., Macrae, A., Guilherme, L.R.G., and Langenbach, T. Atrazine sorption and fate in a Ultisol from humid tropical Brazil. <u>Chemosphere</u> 67(5) (2007): 847-854.

[37] Phewnil, O., Panichsakpatana, S., Tungkananuruk, N., and Pitiyont, B. Atrazine Transport from The Maize (Zea mays L.) Cultivated Upland Soil in Huay Kapo Watershed, Nam Nao District, Phetchabun Province, Thailand. <u>Thai Journal of Agricultural Science</u> 43(3) (2010): 119-127.

[38] Guan, Y.H., et al. Efficient degradation of atrazine by magnetic porous copper ferrite catalyzed peroxymonosulfate oxidation via the formation of hydroxyl and sulfate radicals. <u>Water Research</u> 47(14) (2013): 5431-5438.

[39] Stara, A., Kouba, A., and Velisek, J. Biochemical and histological effects of sub-chronic exposure to atrazine in crayfish Cherax destructor. <u>Chemico-Biological Interactions</u> 291 (2018): 95-102.

[40] Hayes, T.B., et al. Hermaphroditic, demasculinized frogs after exposure to the herbicide atrazine at low ecologically relevant doses. <u>Proceedings of the National Academy of Sciences of the United States of America</u> 99(8) (2002): 5476-5480.

[41] Munger, R., et al. Intrauterine growth retardation in Iowa communities with herbicide-contaminated drinking water supplies (vol 105, pg 308, 1997). <u>Environmental Health Perspectives</u> 105(6) (1997): 570-570.

[42] Arbuckle, T.E., Lin, Z.Q., and Mery, L.S. An exploratory analysis of the effect of pesticide exposure on the risk of spontaneous abortion in an Ontario farm population. Environmental Health Perspectives 109(8) (2001): 851-857.

[43] Saha, A., Bhaduri, D., Pipariya, A., and Ghosh, R.K. Linear and Nonlinear Sorption Modelling for Adsorption of Atrazine onto Activated Peanut Husk. Environmental Progress & Sustainable Energy 36(2) (2017): 348-358.

[44] Calabi-Floody, M., et al. Smart Fertilizers as a Strategy for Sustainable Agriculture. in Advances in Agronomy, Vol 147, pp. 119-157. San Diego: Elsevier Academic Press Inc, 2018.

[45] Ladha, J.K., et al. Global nitrogen budgets in cereals: A 50-year assessment for maize, rice, and wheat production systems. Scientific Reports 6 (2016): 9.

[46] Dobermann, A. and Cassman, K.G. Environmental dimensions of fertilizer nitrogen: What can be done to increase nitrogen use efficiency and ensure global food security. Agriculture and the nitrogen cycle: assessing the impacts of fertilizer use on food production and the environment 65 (2004).

[47] Donner, S.D. and Kucharik, C.J. Evaluating the impacts of land management and climate variability on crop production and nitrate export across the Upper Mississippi Basin. Global Biogeochemical Cycles 17(3) (2003): 18.

[48] Greer, F.R., Shannon, M., Comm, N., and Comm Environm, H. Infant methemoglobinemia: The role of dietary nitrate in food and water. Pediatrics 116(3) (2005): 784-786.

[49] EPA), U.S.E.P.A.U. 2018 Edition of the Drinking Water Standards and Health Advisories. 2018.

[50] Edition, F. Guidelines for drinking-water quality. WHO chronicle 38(4) (2011): 104-8.

[51] Boopathy, R., Karthikeyan, S., Mandal, A.B., and Sekaran, G. Adsorption of ammonium ion by coconut shell-activated carbon from aqueous solution: kinetic, isotherm, and thermodynamic studies. Environmental Science and Pollution Research 20(1) (2013): 533-542.

[52] Mackul'ak, T., Prousek, J., and Svorc, L. Degradation of atrazine by Fenton and modified Fenton reactions. Monatshefte Fur Chemie 142(6) (2011): 561-567.

[53]   Ahalya, N., Ramachandra, T., and Kanamadi, R. Biosorption of heavy metals. Res. J. Chem. Environ 7(4) (2003): 71-79.

[54]   Cao, X.D., Ma, L.N., Liang, Y., Gao, B., and Harris, W. Simultaneous Immobilization of Lead and Atrazine in Contaminated Soils Using Dairy-Manure Biochar. Environmental Science & Technology 45(11) (2011): 4884-4889.

[55]   Ali, I., Alothman, Z.A., and Al-Warthan, A. Sorption, kinetics and thermodynamics studies of atrazine herbicide removal from water using iron nano-composite material. International Journal of Environmental Science and Technology 13(2) (2016): 733-742.

[56]   McMillan, O. Characteristics and mechanisms of atrazine sorption to biochar for land remediation. University of Cambridge, 2018.

[57]   Ibrahim, S., Lateef, M.A., Khalifa, H., and Monem, A.A. Phytoremediation of atrazine-contaminated soil using Zea mays (maize). Annals of Agricultural Sciences 58(1) (2013): 69-75.

[58]   Zhang, J.P., et al. Biodegradation of Atrazine by the Novel Klebsiella variicola Strain FH-1. Biomed Research International 2019 (2019): 12.

[59]   Pathak, R.K. and Dikshit, A.K. Various techniques for Atrazine removal. in International Conference on Life Science and Technology IPCBEE, Singapore, pp. 19-22, 2011.

[60]   Rashed, M.N. Adsorption technique for the removal of organic pollutants from water and wastewater. Organic pollutants-monitoring, risk and treatment (2013): 167-194.

[61]   Rouquerol, J., Rouquerol, F., Llewellyn, P., Maurin, G., and Sing, K.S. Adsorption by powders and porous solids: principles, methodology and applications. Academic press, 2013.

[62]   Ali, I., Asim, M., and Khan, T.A. Low cost adsorbents for the removal of organic pollutants from wastewater. Journal of environmental management 113 (2012): 170-183.

[63]   Liu, Y.Y., Ma, S.Q., and Chen, J.W. A novel pyro-hydrochar via sequential carbonization of biomass waste: Preparation, characterization and adsorption

capacity. Journal of Cleaner Production 176 (2018): 187-195.

[64] Zhang, Y., Li, Y.M., and Zheng, X.M. Removal of atrazine by nanoscale zero valent iron supported on organobentonite. Science of the Total Environment 409(3) (2011): 625-630.

[65] Zhang, Y., et al. Biochar-supported reduced graphene oxide composite for adsorption and coadsorption of atrazine and lead ions. Applied Surface Science 427 (2018): 147-155.

[66] Liu, N., Charrua, A.B., Weng, C.H., Yuan, X.L., and Ding, F. Characterization of biochars derived from agriculture wastes and their adsorptive removal of atrazine from aqueous solution: A comparative study. Bioresource Technology 198 (2015): 55-62.

[67] Mandal, A., Singh, N., and Purakayastha, T.J. Characterization of pesticide sorption behaviour of slow pyrolysis biochars as low cost adsorbent for atrazine and imidacloprid removal. Science of the Total Environment 577 (2017): 376-385.

[68] Romero, V., et al. Efficient adsorption of endocrine-disrupting pesticides from water with a reusable magnetic covalent organic framework. Microporous and Mesoporous Materials 307 (2020): 10.

[69] Martin, E. Improving fertilizer use efficiency-controlled-release and stabilized fertilizers in agriculture. Inter. Fert. Ind. Assoc., Paris, France (1997).

[70] Manjunatha, S., Biradar, D., and Aladakatti, Y.R. Nanotechnology and its applications in agriculture: A review. J Farm Sci 29(1) (2016): 1-13.

[71] Ibrahim, A.A. and Jibril, B.Y. Controlled release of paraffin wax/rosin-coated fertilizers. Industrial & Engineering Chemistry Research 44(7) (2005): 2288-2291.

[72] Perez, J.J. and Francois, N.J. Chitosan-starch beads prepared by ionotropic gelation as potential matrices for controlled release of fertilizers. Carbohydrate Polymers 148 (2016): 134-142.

[73] Cai, Y.X., Qi, H.J.Y., Liu, Y.J., and He, X.W. Sorption/Desorption Behavior and Mechanism of NH4+ by Biochar as a Nitrogen Fertilizer Sustained-Release Material. Journal of Agricultural and Food Chemistry 64(24) (2016): 4958-4964.

[74]   Hale, S.E., Alling, V., Martinsen, V., Mulder, J., Breedveld, G.D., and Cornelissen, G. The sorption and desorption of phosphate-P, ammonium-N and nitrate-N in cacao shell and corn cob biochars. Chemosphere 91(11) (2013): 1612-1619.

[75]   Chintala, R., et al. Nitrate sorption and desorption in biochars from fast pyrolysis. Microporous and Mesoporous Materials 179 (2013): 250-257.

[76]   Hagemann, N., Kammann, C.I., Schmidt, H.P., Kappler, A., and Behrens, S. Nitrate capture and slow release in biochar amended compost and soil. Plos One 12(2) (2017): 16.

[77]   Kambo, H.S. and Dutta, A. A comparative review of biochar and hydrochar in terms of production, physico-chemical properties and applications. Renewable & Sustainable Energy Reviews 45 (2015): 359-378.

[78]   Keiluweit, M., Nico, P.S., Johnson, M.G., and Kleber, M. Dynamic Molecular Structure of Plant Biomass-Derived Black Carbon (Biochar). Environmental Science & Technology 44(4) (2010): 1247-1253.

[79]   Xing, B.S. and Pignatello, J.J. Dual-mode sorption of low-polarity compounds in glassy poly(vinyl chloride) and soil organic matter. Environmental Science & Technology 31(3) (1997): 792-799.

[80]   Kasozi, G.N., Zimmerman, A.R., Nkedi-Kizza, P., and Gao, B. Catechol and Humic Acid Sorption onto a Range of Laboratory-Produced Black Carbons (Biochars). Environmental Science & Technology 44(16) (2010): 6189-6195.

[81]   Nguyen, T.H., Cho, H.H., Poster, D.L., and Ball, W.P. Evidence for a pore-filling mechanism in the adsorption of aromatic hydrocarbons to a natural wood char. Environmental Science & Technology 41(4) (2007): 1212-1217.

[82]   Hao, F.H., et al. Molecular Structure of Corncob-Derived Biochars and the Mechanism of Atrazine Sorption. Agronomy Journal 105(3) (2013): 773-782.

[83]   Zhang, P., Sun, H.W., Yu, L., and Sun, T.H. Adsorption and catalytic hydrolysis of carbaryl and atrazine on pig manure-derived biochars: Impact of structural properties of biochars. Journal of Hazardous Materials 244 (2013): 217-224.

[84]   Sun, K., et al. Polar and aliphatic domains regulate sorption of phthalic acid esters (PAEs) to biochars. Bioresource Technology 118 (2012): 120-127.

[85]   Zhang, G.X., Zhang, Q., Sun, K., Liu, X.T., Zheng, W.J., and Zhao, Y. Sorption of simazine to corn straw biochars prepared at different pyrolytic temperatures. Environmental Pollution 159(10) (2011): 2594-2601.

[86]   Zhao, X.C., et al. Properties comparison of biochars from corn straw with different pretreatment and sorption behaviour of atrazine. Bioresource Technology 147 (2013): 338-344.

[87]   Inyang, M. and Dickenson, E. The potential role of biochar in the removal of organic and microbial contaminants from potable and reuse water: A review. Chemosphere 134 (2015): 232-240.

[88]   Abbas, Z., et al. A critical review of mechanisms involved in the adsorption of organic and inorganic contaminants through biochar. Arabian Journal of Geosciences 11(16) (2018): 23.

[89]   Fang, Q.L., Chen, B.L., Lin, Y.J., and Guan, Y.T. Aromatic and Hydrophobic Surfaces of Wood-derived Biochar Enhance Perchlorate Adsorption via Hydrogen Bonding to Oxygen-containing Organic Groups. Environmental Science & Technology 48(1) (2014): 279-288.

[90]   Xing, B., Senesi, N., and Huang, P.M. Biophysico-chemical processes of anthropogenic organic compounds in environmental systems. Vol. 4: John Wiley & Sons, 2011.

[91]   Lin, L., Zhai, S.R., Xiao, Z.Y., Song, Y., An, Q.D., and Song, X.W. Dye adsorption of mesoporous activated carbons produced from NaOH-pretreated rice husks. Bioresource Technology 136 (2013): 437-443.

[92]   Goyal, H.B., Seal, D., and Saxena, R.C. Bio-fuels from thermochemical conversion of renewable resources: A review. Renewable & Sustainable Energy Reviews 12(2) (2008): 504-517.

[93]   Saxena, R.C., Adhikari, D.K., and Goyal, H.B. Biomass-based energy fuel through biochemical routes: A review. Renewable & Sustainable Energy Reviews 13(1) (2009): 167-178.

[94]   Liu, Z., Quek, A., Hoekman, S.K., and Balasubramanian, R. Production of solid biochar fuel from waste biomass by hydrothermal carbonization. Fuel 103 (2013): 943-949.

[95]   Jiang, Q., Wang, Y.F., Gao, Y., and Zhang, Y. Fabrication and characterization of a hierarchical porous carbon from corn straw-derived hydrochar for atrazine removal: efficiency and interface mechanisms. Environmental Science and Pollution Research 26(29) (2019): 30268-30278.

[96]   Zafar, M.N., Aslam, I., Nadeem, R., Munir, S., Rana, U.A., and Khan, S.U.D. Characterization of chemically modified biosorbents from rice bran for biosorption of Ni(II). Journal of the Taiwan Institute of Chemical Engineers 46 (2015): 82-88.

[97]   Islam, M.S., Kao, N., Bhattacharya, S.N., Gupta, R., and Choi, H.J. Potential aspect of rice husk biomass in Australia for nanocrystalline cellulose production. Chinese Journal of Chemical Engineering 26(3) (2018): 465-476.

[98]   Sharma, R., et al. A Comprehensive Review on Hydrothermal Carbonization of Biomass and its Applications. Chemistry Africa (2019): 1-19.

[99]   Jain, A., Balasubramanian, R., and Srinivasan, M.P. Hydrothermal conversion of biomass waste to activated carbon with high porosity: A review. Chemical Engineering Journal 283 (2016): 789-805.

[100]   Erdogan, E., et al. Characterization of products from hydrothermal carbonization of orange pomace including anaerobic digestibility of process liquor. Bioresource Technology 196 (2015): 35-42.

[101]   Usman, M., et al. Characterization and utilization of aqueous products from hydrothermal conversion of biomass for bio-oil and hydro-char production: a review. Green Chemistry 21(7) (2019): 1553-1572.

[102]   Zhang, T., Wu, X.S., Fan, X., Tsang, D.C.W., Li, G.X., and Shen, Y.J. Corn waste valorization to generate activated hydrochar to recover ammonium nitrogen from compost leachate by hydrothermal assisted pretreatment. Journal of Environmental Management 236 (2019): 108-117.

[103]   Zhang, T., et al. Ammonium nitrogen recovery from digestate by hydrothermal pretreatment followed by activated hydrochar sorption. Chemical Engineering Journal 379 (2020): 14.

[104]   Takaya, C.A., Parmar, K.R., Fletcher, L.A., and Ross, A.B. Biomass-Derived Carbonaceous Adsorbents for Trapping Ammonia. Agriculture-Basel 9(1)

(2019): 15.

[105] IBI. Standardized product definition and product testing guidelines for biochar that is used in Soil. 2013, International Biochar Initiative.

[106] Libra, J.A., et al. Hydrothermal carbonization of biomass residuals: a comparative review of the chemistry, processes and applications of wet and dry pyrolysis. Biofuels 2(1) (2011): 71-106.

[107] Manya, J.J. Pyrolysis for Biochar Purposes: A Review to Establish Current Knowledge Gaps and Research Needs. Environmental Science & Technology 46(15) (2012): 7939-7954.

[108] Benavente, V., Calabuig, E., and Fullana, A. Upgrading of moist agro-industrial wastes by hydrothermal carbonization. Journal of Analytical and Applied Pyrolysis 113 (2015): 89-98.

[109] Liu, Z.G. and Balasubramanian, R. Upgrading of waste biomass by hydrothermal carbonization (HTC) and low temperature pyrolysis (LTP): A comparative evaluation. Applied Energy 114 (2014): 857-864.

[110] Falco, C., Baccile, N., and Titirici, M.M. Morphological and structural differences between glucose, cellulose and lignocellulosic biomass derived hydrothermal carbons. Green Chemistry 13(11) (2011): 3273-3281.

[111] Kang, S.M., Li, X.H., Fan, J., and Chang, J. Characterization of Hydrochars Produced by Hydrothermal Carbonization of Lignin, Cellulose, D-Xylose, and Wood Meal. Industrial & Engineering Chemistry Research 51(26) (2012): 9023-9031.

[112] Kruse, A. and Zevaco, T.A. Properties of Hydrochar as Function of Feedstock, Reaction Conditions and Post-Treatment. Energies 11(3) (2018): 12.

[113] Sevilla, M. and Fuertes, A.B. The production of carbon materials by hydrothermal carbonization of cellulose. Carbon 47(9) (2009): 2281-2289.

[114] He, C., Giannis, A., and Wang, J.Y. Conversion of sewage sludge to clean solid fuel using hydrothermal carbonization: Hydrochar fuel characteristics and combustion behavior. Applied Energy 111 (2013): 257-266.

[115] Elaigwu, S.E., Kyriakou, G., Prior, T.J., and Greenway, G.M. Microwave-assisted hydrothermal synthesis of carbon monolith via a soft-template method

using resorcinol and formaldehyde as carbon precursor and pluronic F127 as template. Materials Letters 123 (2014): 198-201.

[116] Nuchter, M., Ondruschka, B., Bonrath, W., and Gum, A. Microwave assisted synthesis - a critical technology overview. Green Chemistry 6(3) (2004): 128-141.

[117] Elaigwu, S.E. and Greenway, G.M. Microwave-assisted and conventional hydrothermal carbonization of lignocellulosic waste material: Comparison of the chemical and structural properties of the hydrochars. Journal of Analytical and Applied Pyrolysis 118 (2016): 1-8.

[118] Zhang, J.T., et al. Process characteristics for microwave assisted hydrothermal carbonization of cellulose. Bioresource Technology 259 (2018): 91-98.

[119] Nizamuddin, S., et al. Microwave Hydrothermal Carbonization of Rice Straw: Optimization of Process Parameters and Upgrading of Chemical, Fuel, Structural and Thermal Properties. Materials 12(3) (2019): 19.

[120] Kannan, S., Gariepy, Y., and Raghavan, G.S.V. Optimization and Characterization of Hydrochar Derived from Shrimp Waste. Energy & Fuels 31(4) (2017): 4068-4077.

[121] Zhang, T.Y., Walawender, W.P., Fan, L.T., Fan, M.H., Daugaard, D., and Brown, R.C. Preparation of activated carbon from forest and agricultural residues through CO2 activation (vol 105, pg 53, 2004). Chemical Engineering Journal 106(2) (2005): 185-185.

[122] Puccini, M., Stefanelli, E., Hiltz, M., Seggiani, M., and Vitolo, S. Activated carbon from hydrochar produced by hydrothermal carbonization of wastes. Chemical Engineering Transactions 57 (2017): 169-174.

[123] Tan, G.C., Sun, W.L., Xu, Y.R., Wang, H.Y., and Xu, N. Sorption of mercury (II) and atrazine by biochar, modified biochars and biochar based activated carbon in aqueous solution. Bioresource Technology 211 (2016): 727-735.

[124] Sajjadi, B., Zubatiuk, T., Leszczynska, D., Leszczynski, J., and Chen, W.Y. Chemical activation of biochar for energy and environmental applications: a comprehensive review. Reviews in Chemical Engineering 35(7) (2019): 777-815.

[125] Liu, Z.G., Xue, Y.W., Gao, F., Cheng, X.R., and Yang, K. Removal of ammonium from aqueous solutions using alkali-modified biochars. Chemical Speciation and Bioavailability 28(1-4) (2016): 26-32.

[126] Huang, Y., Huang, Y., Wang, W., and Zheng, K. Characterization of hydrogen peroxide (H2O2) modified hydrochars from walnut shell for enhanced adsorption performance of methylene blue from aqueous solution. Desalination and Water Treatment 109 (2018): 221-230.

[127] Petrovic, J.T., et al. Alkali modified hydrochar of grape pomace as a perspective adsorbent of Pb2+ from aqueous solution. Journal of Environmental Management 182 (2016): 292-300.

[128] Xue, Y.W., et al. Hydrogen peroxide modification enhances the ability of biochar (hydrochar) produced from hydrothermal carbonization of peanut hull to remove aqueous heavy metals: Batch and column tests. Chemical Engineering Journal 200 (2012): 673-680.

[129] Wang, Z.W., et al. Characterization of Acid-Aged Biochar and Its Ammonium Adsorption in an Aqueous Solution. Materials 13(10) (2020): 17.

[130] Regmi, P., Moscoso, J.L.G., Kumar, S., Cao, X.Y., Mao, J.D., and Schafran, G. Removal of copper and cadmium from aqueous solution using switchgrass biochar produced via hydrothermal carbonization process. Journal of Environmental Management 109 (2012): 61-69.

[131] Sun, K., Tang, J., Gong, Y., and Zhang, H. Characterization of potassium hydroxide (KOH) modified hydrochars from different feedstocks for enhanced removal of heavy metals from water. Environmental Science and Pollution Research 22(21) (2015): 16640-16651.

[132] Menya, E., Olupot, P.W., Storz, H., Lubwama, M., Kiros, Y., and John, M.J. Optimization of pyrolysis conditions for char production from rice husks and its characterization as a precursor for production of activated carbon. Biomass Conversion and Biorefinery 10(1) (2020): 57-72.

[133] Nizamuddin, S., Mubarak, N.M., Tiripathi, M., Jayakumar, N.S., Sahu, J.N., and Ganesan, P. Chemical, dielectric and structural characterization of optimized hydrochar produced from hydrothermal carbonization of palm shell. Fuel 163

(2016): 88-97.

[134] Shao, Y.C., Long, Y.Y., Wang, H.Y., Liu, D.Y., Shen, D.S., and Chen, T. Hydrochar derived from green waste by microwave hydrothermal carbonization. Renewable Energy 135 (2019): 1327-1334.

[135] Yue, L., Ge, C.J., Feng, D., Yu, H.M., Deng, H., and Fu, B.M. Adsorption-desorption behavior of atrazine on agricultural soils in China. Journal of Environmental Sciences 57 (2017): 180-189.

[136] Chapman, H. Cation-exchange capacity. Methods of Soil Analysis: Part 2 Chemical and Microbiological Properties 9 (1965): 891-901.

[137] Cao, X.D., Ma, L.N., Gao, B., and Harris, W. Dairy-Manure Derived Biochar Effectively Sorbs Lead and Atrazine. Environmental Science & Technology 43(9) (2009): 3285-3291.

[138] Chen, B.L., Zhou, D.D., and Zhu, L.Z. Transitional adsorption and partition of nonpolar and polar aromatic contaminants by biochars of pine needles with different pyrolytic temperatures. Environmental Science & Technology 42(14) (2008): 5137-5143.

[139] Yao, Y., Gao, B., Zhang, M., Inyang, M., and Zimmerman, A.R. Effect of biochar amendment on sorption and leaching of nitrate, ammonium, and phosphate in a sandy soil. Chemosphere 89(11) (2012): 1467-1471.

[140] Qu, J.H., et al. Simultaneously enhanced removal and stepwise recovery of atrazine and Pb (II) from water using beta-cyclodextrin functionalized cellulose: Characterization, adsorptive performance and mechanism exploration. Journal of Hazardous Materials 400 (2020): 10.

[141] Teng, F.Y., Zhang, Y.X., Wang, D.Q., Shen, M.C., and Hu, D.F. Iron-modified rice husk hydrochar and its immobilization effect for Pb and Sb in contaminated soil. Journal of Hazardous Materials 398 (2020): 7.

[142] Huff, M.D. and Lee, J.W. Biochar-surface oxygenation with hydrogen peroxide. Journal of Environmental Management 165 (2016): 17-21.

[143] Salihi, E.C. and Mahramanlioglu, M. Equilibrium and kinetic adsorption of drugs on bentonite: Presence of surface active agents effect. Applied Clay Science 101 (2014): 381-389.

[144] Suo, F.Y., You, X.W., Ma, Y.Q., and Li, Y.Q. Rapid removal of triazine pesticides by P doped biochar and the adsorption mechanism. Chemosphere 235 (2019): 918-925.

[145] Yang, Q.F., et al. Interface engineering of metal organic framework on graphene oxide with enhanced adsorption capacity for organophosphorus pesticide. Chemical Engineering Journal 313 (2017): 19-26.

[146] Rajabi, M., et al. Adsorption of malachite green from aqueous solution by carboxylate group functionalized multi-walled carbon nanotubes: Determination of equilibrium and kinetics parameters. Journal of Industrial and Engineering Chemistry 34 (2016): 130-138.

[147] Yang, H.I., Lou, K., Rajapaksha, A.U., Ok, Y.S., Anyia, A.O., and Chang, S.X. Adsorption of ammonium in aqueous solutions by pine sawdust and wheat straw biochars. Environmental Science and Pollution Research 25(26) (2018): 25638-25647.

[148] Gai, X.P., et al. Effects of Feedstock and Pyrolysis Temperature on Biochar Adsorption of Ammonium and Nitrate. Plos One 9(12) (2014): 19.

[149] Nazari, M.A., Mohaddes, F, Pramanik, B.K., Othman, M., Muster, T., and Bhuiyan, M.A. Application of Victorian brown coal for removal of ammonium and organics from wastewater. Environmental Technology 39(8) (2018): 1041-1051.

[150] Ho, Y.S. Review of second-order models for adsorption systems. Journal of Hazardous Materials 136(3) (2006): 681-689.

[151] Wang, X.L., Guo, X.Y., Yang, Y., Tao, S., and Xing, B.S. Sorption Mechanisms of Phenanthrene, Lindane, and Atrazine with Various Humic Acid Fractions from a Single Soil Sample. Environmental Science & Technology 45(6) (2011): 2124-2130.

[152] Ren, X.H., Sun, H.W., Wang, F., and Cao, F.M. The changes in biochar properties and sorption capacities after being cultured with wheat for 3 months. Chemosphere 144 (2016): 2257-2263.

[153] Dai, Y.J., Wang, W.S., Lu, L., Yan, L.L., and Yu, D.Y. Utilization of biochar for the removal of nitrogen and phosphorus. Journal of Cleaner Production 257

(2020): 15.

[154] Kizito, S., et al. Evaluation of slow pyrolyzed wood and rice husks biochar for adsorption of ammonium nitrogen from piggery manure anaerobic digestate slurry. Science of the Total Environment 505 (2015): 102-112.

[155] Huang, H.M., Xiao, X.M., Yan, B., and Yang, L.P. Ammonium removal from aqueous solutions by using natural Chinese (Chende) zeolite as adsorbent. Journal of Hazardous Materials 175(1-3) (2010): 247-252.

[156] Shin, J., Choi, E., Jang, E., Hong, S.G., Lee, S., and Ravindran, B. Adsorption Characteristics of Ammonium Nitrogen and Plant Responses to Biochar Pellet. Sustainability 10(5) (2018): 11.

[157] Moussavi, G., Talebi, S., Farrokhi, M., and Sabouti, R.M. The investigation of mechanism, kinetic and isotherm of ammonia and humic acid co-adsorption onto natural zeolite. Chemical Engineering Journal 171(3) (2011): 1159-1169.

[158] Jaramillo, J., Alvarez, P.M., and Gomez-Serrano, V. Oxidation of activated carbon by dry and wet methods Surface chemistry and textural modifications. Fuel Processing Technology 91(11) (2010): 1768-1775.

[159] Harwood, L.M. and Claridge, T.D. Introduction to organic spectroscopy. Oxford University Press New York, 1997.

[160] Hossain, N., Nizamuddin, S., Griffin, G., Selvakannan, P., Mubarak, N.M., and Mahlia, T.M.I. Synthesis and characterization of rice husk biochar via hydrothermal carbonization for wastewater treatment and biofuel production. Scientific Reports 10(1) (2020): 15.

[161] Correa, C.R., Otto, T., and Kruse, A. Influence of the biomass components on the pore formation of activated carbon. Biomass & Bioenergy 97 (2017): 53-64.

[162] Traore, M., Kaal, J., and Cortizas, A.M. Application of FTIR spectroscopy to the characterization of archeological wood. Spectrochimica Acta Part a-Molecular and Biomolecular Spectroscopy 153 (2016): 63-70.

[163] Wang, Y.F., Xiao, X., and Chen, B.L. Biochar Impacts on Soil Silicon Dissolution Kinetics and their Interaction Mechanisms. Scientific Reports 8 (2018): 11.

[164] Xia, Y., et al. Enhanced adsorption of Pb(II) onto modified hydrochar: Modeling

and mechanism analysis. <u>Bioresource Technology</u> 288 (2019): 8.

[165] Tan, X., et al. Application of biochar for the removal of pollutants from aqueous solutions. <u>Chemosphere</u> 125 (2015): 70-85.

[166] Bhandari, A., Novak, J.T., and Berry, D.F. Binding of 4-monochlorophenol to soil. <u>Environmental Science & Technology</u> 30(7) (1996): 2305-2311.

[167] Carroll, K.M., Harkness, M.R., Bracco, A.A., and Balcarcel, R.R. Application of a permeant polymer diffusional model to the desorption of polychlorinated-biphenyls from Hudson river sediments. <u>Environmental Science & Technology</u> 28(2) (1994): 253-258.

[168] Shen, Z.T., Som, A.M., Wang, F., Jin, F., McMillan, O., and Al-Tabba, A. Long-term impact of biochar on the immobilisation of nickel (II) and zinc (II) and the revegetation of a contaminated site. <u>Science of the Total Environment</u> 542 (2016): 771-776.
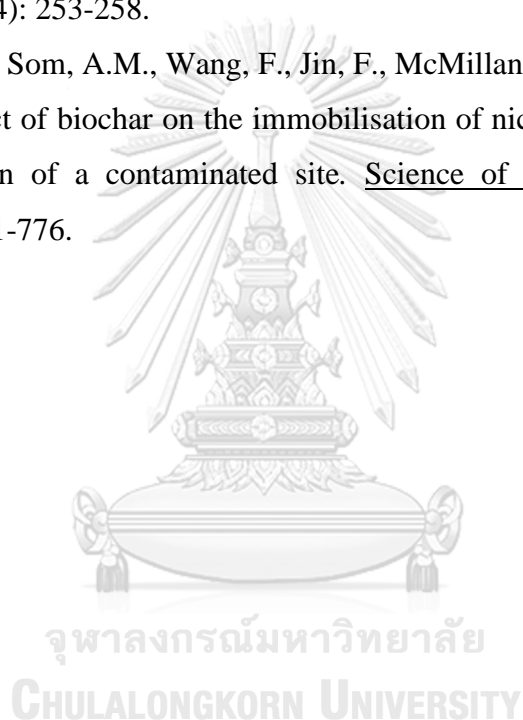
APPENDICES

Appendix A. Rice husk hydrochar produced under different MHTC conditions

Table A1. Hydrochar yield produced under different MHTC conditions

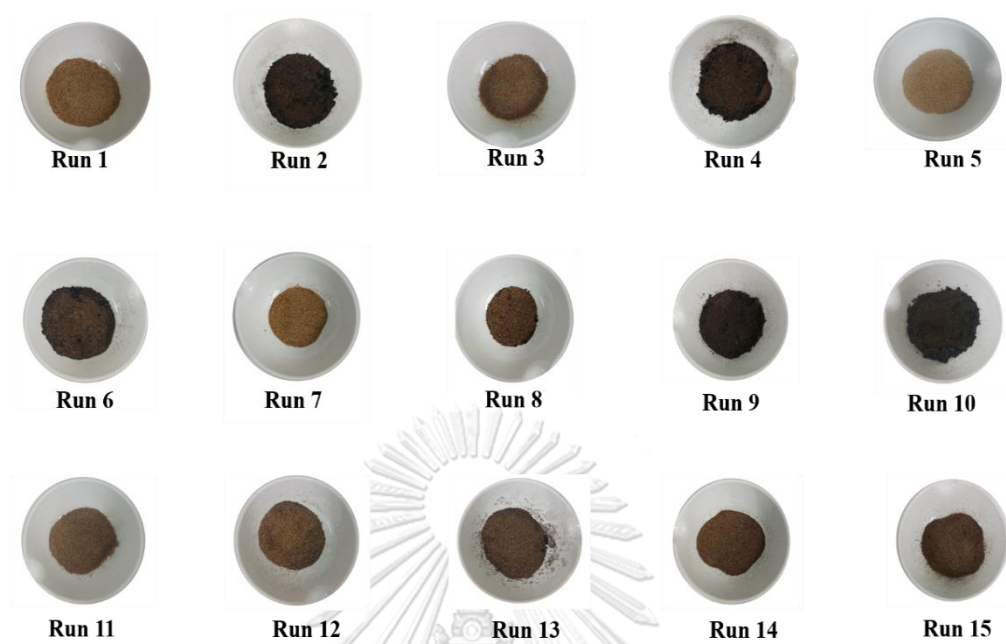| Treatment	Temperature (ºC)	Time (min)	L-S ratio (mL/g)	Hydrochar yield (%)
1	150	20	10:1	88.25
2	200	20	10:1	66.60
3	150	60	10:1	83.69
4	200	60	10:1	65.15
5	150	40	5:1	91.13
6	200	40	5:1	73.19
7	150	40	15:1	89.36
8	200	40	15:1	72.32
9	175	20	5:1	69.66
10	175	60	5:1	67.82
11	175	20	15:1	82.84
12	175	60	15:1	72.99
13	175	40	10:1	66.13
14	175	40	10:1	72.42
15	175	40	10:1	69.50

Figure A1. Rice husk hydrochar produced under different MHTC conditions

Appendix B Optimization of MHTC condition

Table B1. Regression analysis of the atrazine adsorption capacity

Factor	Regression coefficient	Std. Error	t(2)	p	-95% Cnf. Limt	+95% Cnf.Limt
Mean/Intercept	-53.6971	17.54861	-3.05991	0.092	-129.203	21.80849
(1) Temperature (L)	0.6085	0.19940	3.05142	0.093	-0.249	1.46641
Temperature (Q)	-0.0016	0.00057	-2.89820	02101	-0.004	0.0008
(2) Time (L)	-0.2029	0.34139	-0.59423	0.612	-1.672	1.26603
Time (Q)	-0.0015	0.00213	-0.72161	0.545	-0.011	0.00764
(3) L-S ratio (L)	5.8773	1.18483	4.96047	0.038	0.779	10.97524
L-S ratio (Q)	0.0011	0.00357	0.31309	0.783	-0.014	0.01647
1L by 2L	0.0029	0.00353	0.82430	0.496	-0.012	0.01812
1L by 2Q	0.0000	0.00001	0.96845	0.434	0.00	0.00006
1Q by 2L	0.0000	0.00001	-1.13109	0.375	0.00	0.00003
1L by 3L	-0.0684	0.0136	-5.03414	0.037	-0.127	-0.00995
1Q by 3L	0.0002	0.00004	5.01762	0.038	0.00	0.000366
2L by 3L	-0.0002	0.00086	-0.26077	0.819	-0.004	0.00347

จุฬาลงกรณ์มหาวิทยาลัย

CHULALONGKORN UNIVERSITY

Table B2. Regression analysis of the ammonium adsorption capacity

Factor	Regression coefficient	Std. Error	t(2)	p	-95% Cnf. Limt	+95% Cnf.Limt
Mean/Intercept	-74.4054	28.8762	-2.57671	0.123	-198.650	49.83878
(1) Temperature (L)	0.9106	0.3281	2.77537	0.109	-0.501	2.32241
Temperature (Q)	-0.0027	0.0009	-2.89546	0.101	-0.007	0.00131
(2) Time (L)	1.4083	0.5618	2.50695	0.129	-1.009	3.82536
Time (Q)	0.0024	0.0035	0.69245	0.560	-0.013	0.01754
(3) L-S ratio (L)	4.8211	1.9464	2.4728	0.131	-3.568	13.20972
L-S ratio (Q)	0.0011	0.00587	0.1812	0.873	-0.024	0.02633
1L by 2L	-0.0178	0.00582	-3.0523	0.092	-0.043	0.00727
1L by 2Q	0.0000	0.00002	-0.4116	0.721	0.0	0.00008
1Q by 2L	0.0001	0.00002	3.3157	0.080	0.0	0.0012
1L by 3L	-0.0585	0.02237	-2.6147	0.120	-0.155	0.03776
1Q by 3L	0.0002	0.00006	2.7393	0.111	0.0	0.00045
2Q by 3L	-0.0023	0.00141	-1.6113	0.248	-0.008	0.0038

จุฬาลงกรณ์มหาวิทยาลัย

CHULALONGKORN UNIVERSITY

Table B3. The results of observed and predicted adsorption capacity onto different

Run	Atrazine adsorption capacity (mg/g)		Ammonium adsorption capacity (mg N/g)	
	Observed	Predicted	Observed	Predicted
1	0.41	0.41	0.08	0.08
2	1.23	1.23	0.30	0.30
3	0.53	0.53	0.45	0.45
4	1.37	1.37	0.89	0.89
5	0.39	0.39	0.25	0.25
6	1.07	1.07	0.07	0.07
7	0.43	0.43	-0.63	-0.63
8	0.95	0.95	0.54	0.54
9	1.40	1.40	0.57	0.57
10	1.85	1.85	0.18	0.18
11	0.19	0.19	-0.27	-0.27
12	0.55	0.55	-1.57	-1.57
13	0.95	0.76	-1.02	-0.69
14	0.60	0.76	-0.53	-0.69
15	0.74	0.76	-0.54	-0.69

Appendix C Statistical analysis between pristine and activated hydrochars

Table C1. Atrazine adsorption between pristine and KOH-activated hydrochars

Duncan

Samples	N	Subset for alpha = 0.05	
		1	2
HC	3	1.5122	
5KHC	3	1.5170	
10KHC	3	1.5778	1.5778
20KHC	3		1.6820
Sig.		.349	.138

Means for groups in homogeneous subsets are displayed.

a. Uses Harmonic Mean Sample Size = 3.000.

Table C2. Atrazine adsorption between pristine and H_2O_2-activated hydrochars

Duncan

Samples	N	Subset for alpha = 0.05	
		1	2
HC	3	1.5122	
20HHC	3	1.6142	1.6142
5HHC	3		1.6226
10HHC	3		1.6281
Sig.		.057	.779

Means for groups in homogeneous subsets are displayed.

a. Uses Harmonic Mean Sample Size = 3.000.

Table C3. Atrazine adsorption between studied materials and commercial biochar

Atrazine adsorption capacity

Duncan

Adsorbent	N	Subset for alpha = 0.05	
		1	2
BC	2	.4123	
HC	2		1.9705
5HHC	2		2.1028
10KHC	2		2.1773
Sig.		1.000	.106

Means for groups in homogeneous subsets are displayed.

a. Uses Harmonic Mean Sample Size = 2.000.

จุฬาลงกรณ์มหาวิทยาลัย

CHULALONGKORN UNIVERSITY

Appendix D. Atrazine adsorption results

Table D1. Activation effects of rice husk hydrochar on atrazine adsorption capacity

	Sample	Mean (mg/g)	SD
No activation	HC	1.51	0.05
H_2O_2 treatment	5HHC	1.62	0.06
	10HHC	1.63	0.06
	20HHC	1.61	0.06
KOH treatment	5KHC	1.52	0.07
	10KHC	1.58	0.10
	20KHC	1.68	0.08

จุฬาลงกรณ์มหาวิทยาลัย

CHULALONGKORN UNIVERSITY
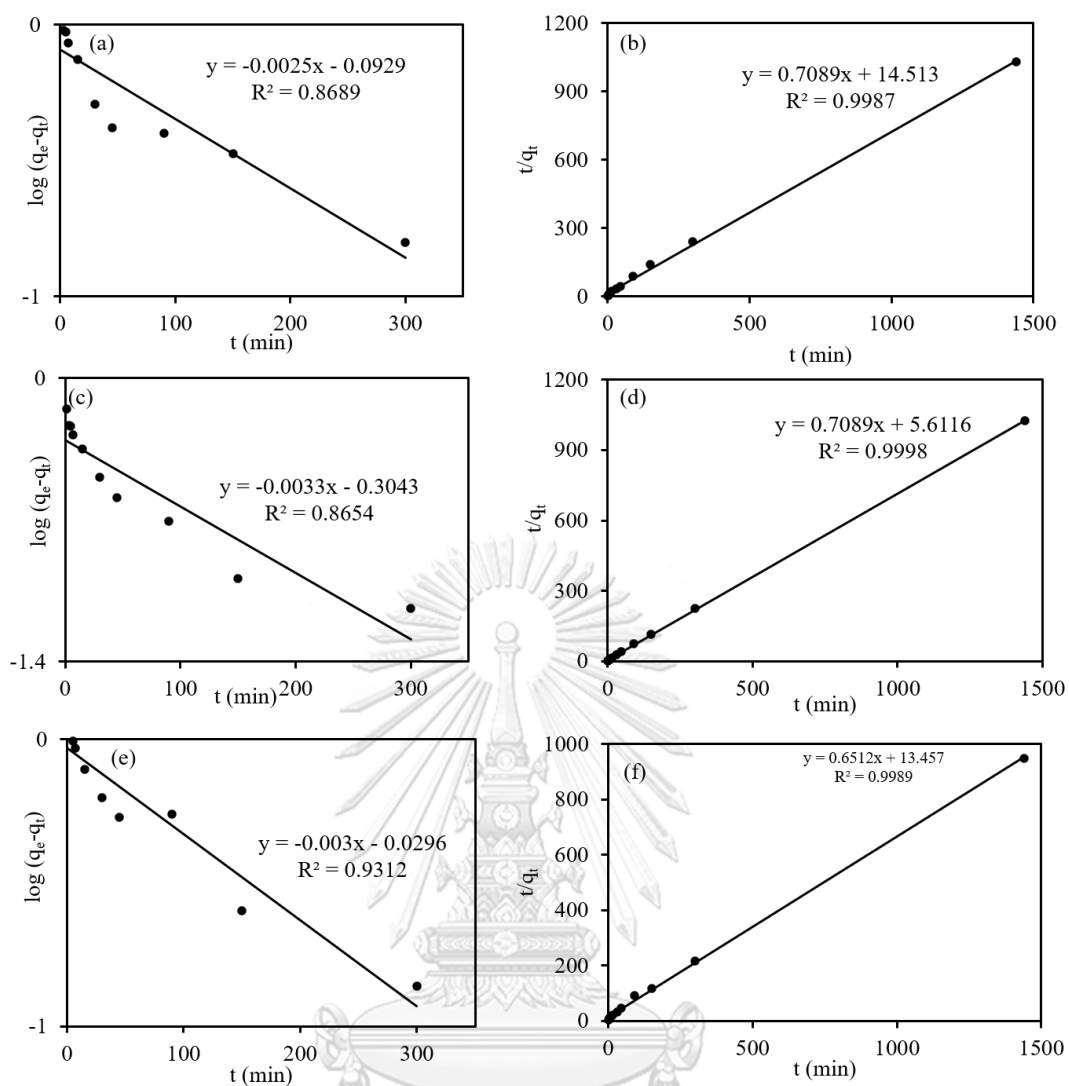
Figure D1. Linear plots for atrazine adsorption fitting to pseudo-first-order and

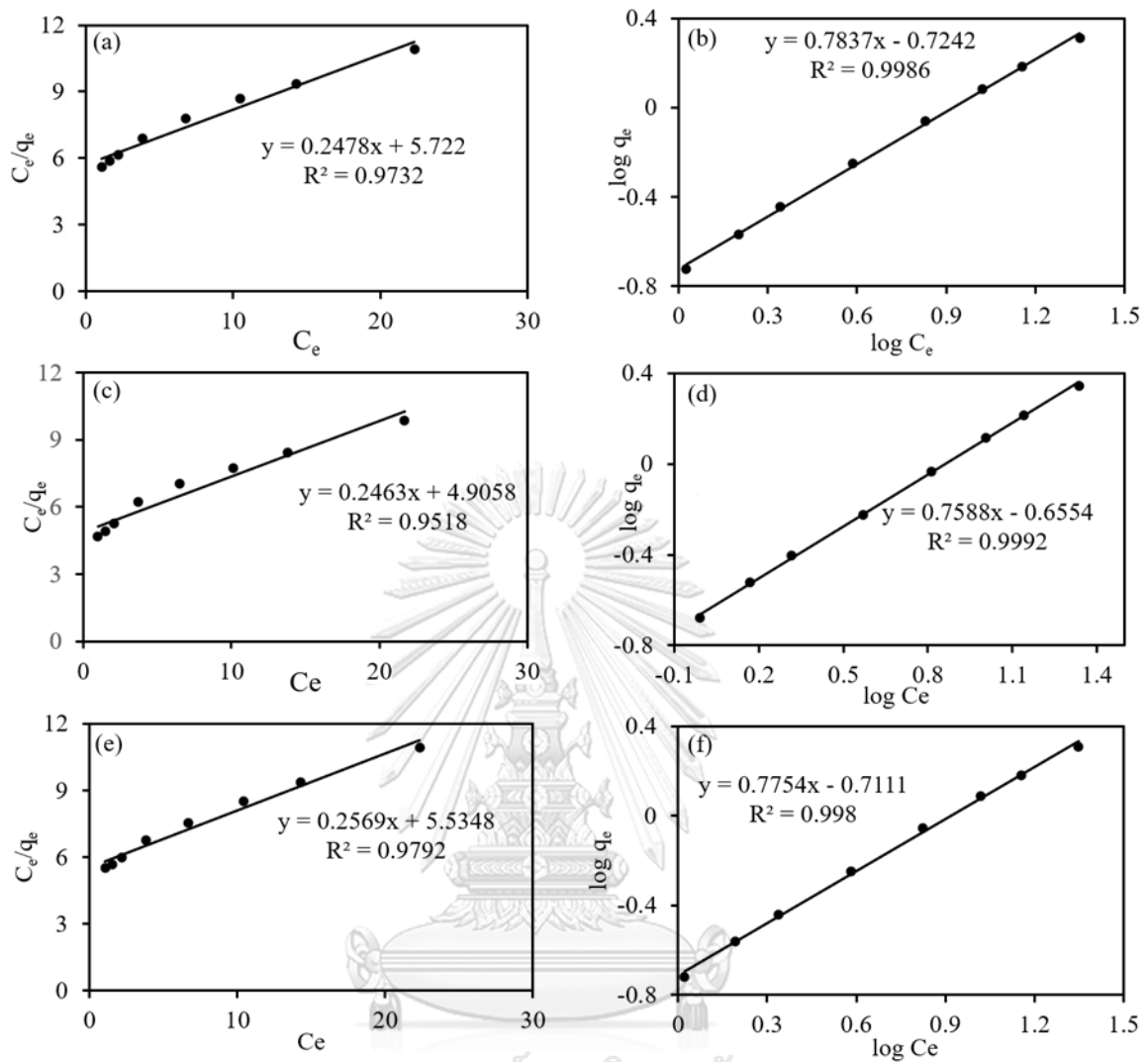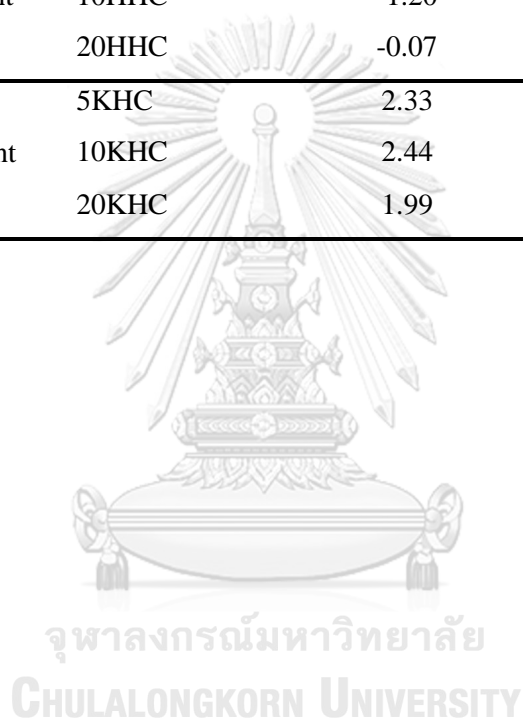pseudo-second-order models of (a,b) hydrochar, (c,d) 10KHC, and (e,f) 5HHC

Figure D2. Linear plots for atrazine adsorption fitting to Langmuir and Freundlich

models of (a,b) hydrochar, (c,d) 10KHC, and (e,f) 5HHC

Appendix E. Ammonium adsorption results

Table E1. Activation effects of rice husk hydrochar on ammonium adsorption capacity

		Adsorption capacity (mg/g)	SD
No activation	HC	0.10	0.01
H_2O_2 treatment	5HHC	0.03	1.34
	10HHC	-1.20	1.06
	20HHC	-0.07	0.50
KOH treatment	5KHC	2.33	0.18
	10KHC	2.44	0.20
	20KHC	1.99	0.59

จุฬาลงกรณ์มหาวิทยาลัย
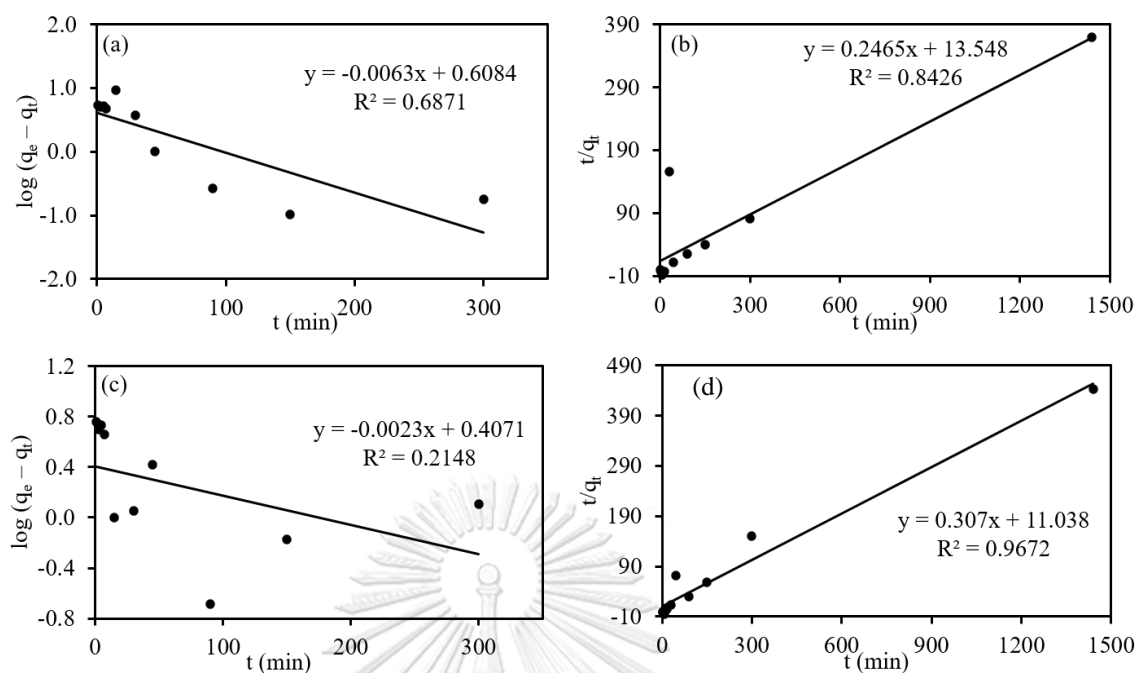
CHULALONGKORN UNIVERSITY

Figure E1. Linear plots for ammonium adsorption fitting to pseudo-first-order and

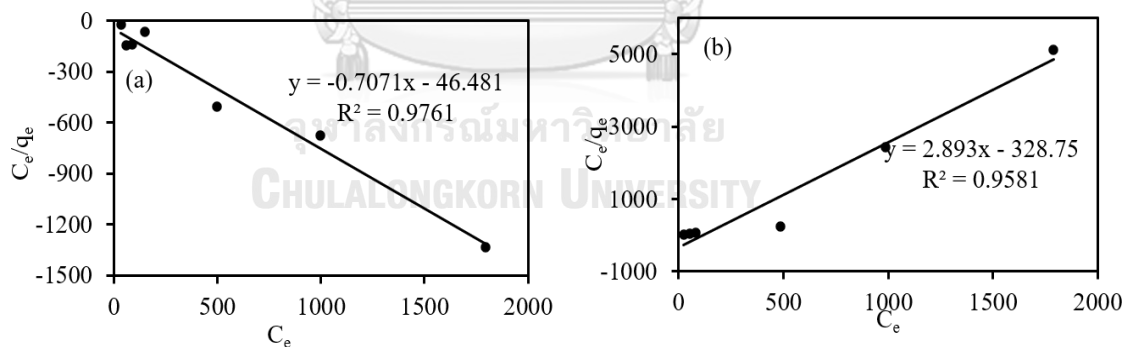pseudo-second-order models of (a,b) hydrochar and (c,d) 10KHC

Figure E2. Linear plots for ammonium adsorption fitting to Langmuir model of (a)
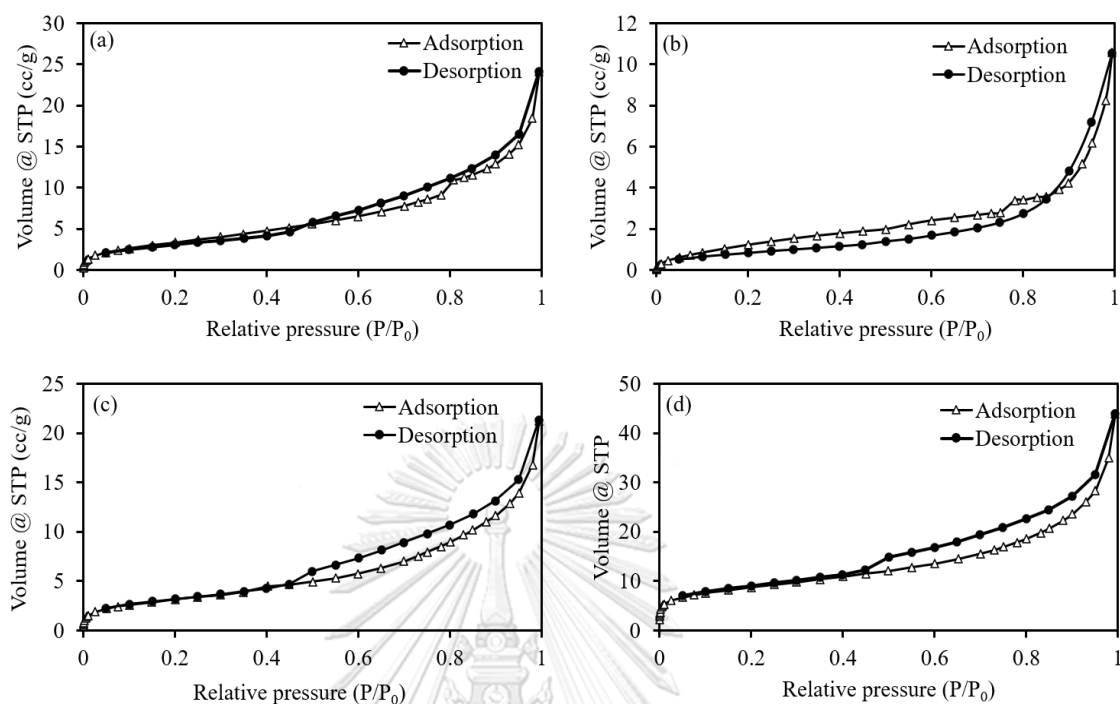
hydrochar and (b) 10KHC

Appendix F Characterization of rice husk hydrochar

Figure F1. BET surface analysis of N$_2$ adsorption – desorption isotherm of (a) HC, (b) 10KHC, (c) 5HHC, (d) BC

VITA

NAME	Kim Anh Phan
DATE OF BIRTH	13 January 1996
PLACE OF BIRTH	Kien Giang province, Vietnam
INSTITUTIONS ATTENDED	Bachelor's degree: Can Tho University Master's degree: International Program in Hazardous Substance and Environmental Management, Graduate School, Chulalongkorn University
HOME ADDRESS	Tho Son commune, Hon Dat district, Kien Giang province, Vietnam
PUBLICATION	Phan, K.A., Phihusut, D., and Tuntiwiwattanapun, N. Optimization of Microwave Hydrothermal Carbonization Conditions of Hydrochar for Ammonium Adsorption. in 2020 International Conference and Utility Exhibition on Energy, Environment and Climate Change (ICUE), pp. 1-5: IEEE, 2020. Phan, K.A. and Nguyen, T.G. Groundwater quality and human health risk assessment related to groundwater consumption in An Giang province, Viet Nam. Journal of Vietnamese Environment 10(2) (2018): 85-91.

จุฬาลงกรณ์มหาวิทยาลัย
CHULALONGKORN UNIVERSITY